Title
Hotspots of Dendritic Spine Dynamics Facilitate Learning and Memory

Author
Huang, Shan

Publication Date
2017

Peer reviewed|Thesis/dissertation

UNIVERSITY OF CALIFORNIA

Los Angeles

Hotspots of Dendritic Spine Dynamics Facilitate Learning and Memory

A dissertation submitted in partial satisfaction of the

requirements for the degree Doctor of Philosophy

in Neuroscience

by

Shan Huang

2017

ABSTRACT OF THE DISSERTATION

Hotspots of Dendritic Spine Dynamics Facilitate Learning and Memory

by

Shan Huang

Doctor of Philosophy in Neuroscience

University of California, Los Angeles, 2017

Professor Alcino Jose Silva, Chair

Structural plasticity mediated by addition and elimination of dendritic spines is thought to underlie the formation of long-term memory. However, the spatial relationship of those structural activities during learning and memory remains unclear. Using *in vivo* two-photon microscopy, I track spine dynamics in mouse retrosplenial cortex (RSC) during contextual and spatial learning. I report that learning leads to addition of new spines that are spatially clustered, and the amount of clustering is predicted by spine turnover prior to learning. Both spine measures are correlated with learning and memory performance. Accordingly, a genetic manipulation by heterozygous mutation of *Ccr5* that enhances pre-learning spine turnover also enhances learning-related spine clustering, as well as future learning and memory performance. New spines related to one memory do not form cluster with spines related to a distinct memory. In contrast, spines gained

from one repetitive task tend to cluster with each other. Remarkably, clustered new spines are usually added on dendritic segments with rapid spine turnover, revealing the presence of hotspots on dendritic tree where elevated rates of spine turnover facilitate clustered spine addition associated with memory. One implication of these findings is that increased spine turnover may allow neurons to more efficiently sample the synaptic space during learning in order to optimize information acquisition. Once acquired, spine clustering may stabilize this information, thus strengthening memory circuits.

The dissertation of Shan Huang is approved.

Dean Buonomano

Michael S Fanselow

David L Glanzman

Joshua Trachtenberg

Alcino Jose Silva, Committee Chair

University of California, Los Angeles

2017

Table of Contents

LIST OF FIGURES

LIST OF ABBREVIATIONS

RSC: retrosplenial cortex

CREB: cAMP response element-binding protein

SOM: somatostatin

STC: synaptic tagging and capture

LTP: long-term potentiation

PRPs: plasticity related proteins

ASD: Autism spectrum disorder

FRET: fluorescence resonance energy transfer

CCR5: C-C chemokine receptor type 5

CFC: contextual fear conditioning

MWM: Morris water maze

WT: wild type

ACKNOWLEDGEMENTS

Figure 1.1 was originally published on Lu J, and Zuo Y. Clustered structural and functional plasticity of dendritic spines. Brain Research Bulletin. 2017; 129, 18-22. DOI: 10.1016/j.brainresbull.2016.09.008. © 2016 Elsevier Inc.

Figure 1.2a was originally published on Kleindienst T, Winnubst J, Roth-Alpermann C, Bonhoeffer T, and Lohmann C. Activity-dependent clustering of functional synaptic inputs on developing hippocampal dendrites. Neuron. 2011; 72, 1012-1024. DOI: 10.1016/j.neuron.2011.10.015. © 2011 Elsevier Inc.

Figure 1.2b was originally published on Takahashi N, Kitamura K, Matsuo N, Mayford M, Kano M, Matsuki N, and Ikegaya Y. Locally synchronized synaptic inputs. Science. 2012; 335, 353-356. DOI: 10.1126/science.1210362. © The Authors

Chapter 2.1 was originally published as *Zhou M, *Greenhill S (*co-first author), **Huang S**, Silva TK, Sano Y, Wu S, Cai Y, Nagaoka Y, Sehgal M, Cai DJ, Lee YS, Fox K, Silva AJ. CCR5 is a suppressor for cortical plasticity and hippocampal learning and memory. eLife. 2016; 5: e20985. DOI: 10.7554/eLife.20985 (PMID: 27996938). ©eLife

Chapter 3, 4, 6, 7 are a modified version of submitted manuscript *Frank AC, ***Huang S** (*co-first author, alphabetically listed), Zhou M, Gdalyahu A, Silva TK, Lu E, Wen X, Trachtenberg JT, Silva AJ. Hotspots of dendritic spine turnover facilitate learning-related clustered spine addition.

The work presented herein would not have been possible without the support of my advisor, Dr. Alcino Silva, who has provided me with not only tremendous support and guidance, but also a lot of inspiration and enthusiasm for science which motivates me to move forward. His deep love for human life and obligation to benefit society greatly influenced me as a graduate student, and a human being. I would also like to thank my thesis committee Dr. Dean Buonomano, Dr. Michael Fanselow, Dr. David Glanzman, and Dr. Joshua Trachtenberg for their insightful advice and guidance. The committee not only support and inspire me at the annual committee meeting, but also through numerous individual discussions whenever I need them. I also received invaluable advice from Dr. Carlos Portera-Cailliau for spine dynamics, and Dr. Nicholas Wisniewski for statistical analysis. I am grateful to the entire Silva lab who have given me encouragement and inspiration, especially to Miou Zhou, Adam Frank, Katie Cai, Tawnie Silva, Denise Cai and Megha Sehgal. Finally, I would not be where I am today without the tremendous love and support from my parents, Xianghua Liu and Yaoli Huang, my grandparents Guizhen Wu and Wenrui Liu, my family and friends, and most of all, my husband Ximiao Wen.

For funding, this work was supported by grants NIH R37 AG013622, and the Dr. Miriam and Sheldon G. Adelson Medical Research Foundation to my mentor Alcino J. Silva, and China Scholarship Council Scholarship and UCLA Dissertation Year Fellowship to me.

VITA

Education

Nankai University (NKU), B.S. in Biological Technology — 2007-2011

Research Experience

Advisor:

- The role of CCR5 in dendritic spine dynamics in retrosplenial cortex during learning (Dissertation) — Alcino Silva, Ph.D. — 2013-Present **UCLA**
- Mechanisms of memory allocation and linking
- The function of CCR5 in hippocampus-dependent learning and memory

Undergraduate Student

- The effects of mTOR inhibition on cognitive and affective deficits caused by Disc1 knockdown in adult-born dentate granule neurons — Alcino Silva, Ph.D. — 2010-2012 **UCLA**

Publications

- *Frank AC, ***Huang** S (*co-first author, alphabetically listed), Zhou M, Gdalyahu A, Silva TK, Wen X, Trachtenberg JT, Silva AJ. Hotspots of dendritic spine turnover facilitate learning-related clustered spine addition (*Submitted*)
- Joy MT, Ben Assayag E, Shabashov-Stone D, Zhou M, Arenas M, Kliper E, Korczyn AD, Liraz-Zaltsman S, Kesner EL, **Huang** S, Silva TK, Bornstein NM, Silva AJ, Shohami E, Carmichael ST. CCR5 is a therapeutic target to stimulate recovery in stroke and traumatic brain injury (*Science* under revision)
- Zhou M, Greenhill S, **Huang** S, Silva TK, Sano Y, Wu S, Cai Y, Nagaoka Y, Sehgal M, Cai DJ, Lee YS, Fox K, Silva AJ. CCR5 is a suppressor for cortical plasticity and hippocampal learning and memory. eLife. 2016 Dec; 10.7554/eLife.20985. (PMID: 27996938)
- Sehgal M., Zhou M., Cai DJ, Lavi A, **Huang** S, Silva AJ. Mechanisms for Allocating, Tagging, and Linking Memories. Invited book chapter in Learning and Memory: A Comprehensive Reference 2E. 2016.
- Sano Y, Shobe JL, Zhou M, **Huang** S, Shuman T, Cai DJ, Golshani P, Kamata M, Silva AJ. CREB regulates memory allocation in the insular cortex. Current Biology. 2014 Dec 1;24(23):2833-7. (PMID: 23439118)
- Zhou M, Li W, **Huang** S, Song J, Kim JY, Tian X, Kang E, Sano Y, Liu C, Balaji J, Wu S, Zhou Y, Zhou Y, Parivash SN, Ehninger D, He L, Song H, Ming GL, Silva AJ. mTOR Inhibition ameliorates cognitive and affective deficits caused by Disc1 knockdown in adult-born dentate granule neurons. Neuron. 2013 Feb 20;77(4):647-54. (PMID: 25454591)

Professional Societies

Society for Neuroscience — 2013-Present

Molecular and Cellular Cognition Society — 2014-Present

Teaching Experience

- M205- Systems Neuroscience — Teaching Assistant — 2017
- M101C- Behavioral and Cognitive Neuroscience — Teaching Assistant — 2016

Invited Talks

- Icahn School of Medicine at Mount Sinai, Seminar Talk — 2017
  Hotspots of dendritic spine turnover facilitate learning-related clustered spine addition — Mount Sinai
- Integrative Center for Learning and Memory, Young Investigator Lecture — 2017
  Increased dendritic spine turnover and clustering accompany memory enhancement — UCLA
- Neuroscience Interdepartmental Program Retreat — 2016
  Dendritic spine clustering in retrosplenial cortex during contextual learning — UCLA

Scholarships & Awards

- Brain Research Institute/Semel Institute Neuroscience Graduate Travel Award — 2017
- Dissertation Year Fellowship — 2016-2017
- UCLA Doctoral Student Travel Grant — 2016
- Top 3 Neuroscience IDP retreat data blitz presenters — 2016
- Brain Research Institute/Semel Institute Neuroscience Graduate Travel Award — 2016
- Graduate Programs in Bioscience fellowship — 2013-2015
- China Scholarship Council(CSC) scholarship — 2012-2016
- Cross-disciplinary Scholars in Science and Technology (CSST) Award. — 2010
- First Prize of Excellent Undergraduate Scholarship of NKU — 2010
- Innovative Scientific Research Awards of NKU. — 2010
- First Prize of Excellent Undergraduate Scholarship of NKU. — 2009
- Excellent Student Leader in the Department of Organization of NKU — 2008

Conference Presentations

- **Huang** S, Frank AC, Zhou M, Silva TK, Wen X, Trachtenberg JT, Silva AJ. (2016) *Memory enhancement increases dendritic spine turnover and clustering in retrosplenial cortex*. Poster at *Society for Neuroscience*, San Diego, CA.
- **Huang** S, Frank AC, Zhou M, Silva TK, Wen X, Trachtenberg JT, Silva AJ. (2016) *Memory enhancement increases dendritic spine turnover and clustering in retrosplenial cortex*. Poster at *Molecular and Cellular Cognition Society*, San Diego, CA.
- **Huang** S, Frank AC, Zhou M, Silva TK, Wen X, Trachtenberg JT, Silva AJ. (2016) *Memory enhancement increases dendritic spine turnover and clustering in retrosplenial cortex*. Poster at *Brain Research Institute's Neuroscience Poster Session*, Los Angeles, CA.

Chapter 1 Introduction

One of the most fascinating questions in neuroscience is where memory is stored in the brain. Much progress has been made toward elucidating the functions of a variety of brain regions and their networks in specific types of memory. For example, retrosplenial cortex (RSC) is required for spatial learning and memory; primary motor cortex stores motor memory. However, little is known about the mechanisms of how memory is allocated to particular neurons, dendritic branches and synapses, and not their neighbors in the same region. What is even less explored is how allocation of memory to certain neurons, dendrites and synapses will stabilize the acquired information (or prevent the memory from disappearing), thus enhancing learning rates and memory performance. This dissertation will focus on addressing these two questions, particularly the relationship between spine dynamics in dendritic hotspots and learning and memory. I hypothesize that there are certain dendritic hotspots where higher rates of pre-learning spine turnover facilitate the formation of learning and memory-related clustered spines, and that clustering serves as a structural mechanism to stabilize structural plasticity and memory.

1.1 Memory allocation in neurons, dendrites and synapses

Neuronal level:

Growing evidence suggest that memory is not randomly allocated to neurons within a neural network, but instead allocated to particular neurons by some specific mechanisms. One of these mechanisms is through cAMP response element-binding protein (CREB), which is a

transcription factor and has a well-known role in long-term memory formation and synaptic potentiation (Silva et al., 1998; Silva et al., 2009). Compelling evidence also demonstrate that CREB activated during learning triggers cellular changes, which affect the probability that a given neuron will be involved in subsequent memory encoding (Han et al., 2007; Sano et al., 2014; Silva et al., 2009; Zhou et al., 2009). One of these studies is to overexpress CREB in lateral amygdala with viral vectors. Higher CREB levels increase the probability that amygdala neurons participate in memory for tone conditioning (Han et al., 2007). Specific inactivation of the cells with the virally delivered CREB disrupts memory for tone conditioning. This amnesia can be reversed after the inactivation disappeared (Zhou et al., 2009), further confirming that those cells with higher CREB levels are more likely being involved in storing the fear memory. Importantly, CREB's role in memory allocation is not only limited to amygdala, but also has been proven to be true in the insular cortex for a conditioned taste memory (Sano et al., 2014). All of these findings indicate that CREB levels determine where information is stored within a neural network, and this process could probably be true in other cortical regions, such as RSC during encoding a spatial memory. Another recent study shows that two distinct contextual memories encoded within 5 hours share an overlap neuronal ensemble in hippocampal CA1, compared to two encoded across a week (Cai et al., 2016). The first memory strengthens the second memory probably through this shared neuronal ensemble. Why the second memory is preferentially encoded by the same neurons that are responsible for another recent memory? This is consistent with the memory allocation hypothesis that, learning triggers a temporary increase in neuronal excitability that biases the representation of the second memory to the ensemble encoding the first memory (McKay et al., 2009; Moyer et al., 1996; Oh et al., 2010).

Dendritic level:

Not only at the neuronal level, memory also allocate at dendritic level. There are 100 billion (10^{11}) neurons and 100 trillion (10^{14}) synapses in human brain. If memories were only encoded at neuronal level, our memory capacity would be limited by finite neuron combinations. In addition, memories can share neuronal ensemble to strengthen each other, but they are still distinct. Extinction of one memory does not affect recall of another memory (Cai et al., 2016). Synapses on different dendrites greatly expand the synaptic area of a post-synaptic neuron, where pre-synaptic neuron can build connections with. Such that, a post-synaptic neuron could receive thousands of different pre-synaptic inputs, which dramatically expands the memory storage capacity, and memories do not interfere with each other. Evidence supporting this hypothesis is done by *in vivo* imaging of calcium spikes on dendritic branches. Different motor learning tasks induce dendritic Ca^{2+} on different apical tuft branches of individual layer V pyramidal neurons in the mouse motor cortex (Cichon and Gan, 2015). There is an increase of overlapping branches at apical trunks, which is deeper below pia and closer to cell body. The regulation of memory allocation on distinct dendritic branches is by somatostatin (SOM)-expressing interneurons. When SOM interneurons are inactivated, different motor tasks frequently induce Ca^{2+} spikes on the same branches, disrupting increased neuronal activity and performance improvement of previously learned task (Cichon and Gan, 2015). However, little is known about how memory is encoded by particular dendritic ensemble at the initial learning stage.

Synaptic level:

So far, we have discussed plasticity mechanisms that regulate which neurons are recruited to encode memory, and a phenomenon that distinct memories, although may involve the same neurons, are encoded by distinct dendritic branches. However, it is widely conceived that

memories are encoded and stored at the synaptic level. Circuit changes mediated by structural plasticity (formation and elimination of synapses) are thought to underlie the formation of long-term memory (Bailey and Kandel, 1993). Recently, a photoactivatable construct (AsPaRac1) labeling active spines enables manipulation of those spines. The study shows that the shrinkage of task-specific spines disrupts performance of the learned task (Hayashi-Takagi et al., 2015), providing the first causal evidence that memory is stored in synapses. Next, a mechanism that regulates which synapses are recruited to form an engram is needed. Such mechanisms may include hypotheses such as *synaptic tagging and capture (STC) model*, *clustered plasticity hypothesis*, and a very new model that this dissertation will focus on: *dendritic hotspots of turnover model*.

Synaptic tagging and capture model: Long-term potentiation (LTP) induction sets a short-term "tag" (less than 3 hours), which is protein synthesis independent, and allows the tagged synapses to capture newly synthesized plasticity related proteins (PRPs), thus lowering the LTP induction threshold (Frey and Morris, 1997). Late-phase LTP (L-LTP) is the natural extension of early-phase LTP (E-LTP). E-LTP is independent of protein synthesis, so it is short lasting (less than 3 hours), while L-LTP requires gene transcription and protein synthesis, so it is long lasting. Both E-LTP and L-LTP are able to set tags, while only L-LTP is able to induce PRPs synthesis at the soma and transporting the products to tagged synapses. Therefore, a weakly stimulated set of synapses that have access to the PRPs will also succeed in maintaining L-LTP (Redondo and Morris, 2011).

PRPs that have been implicated in learning and plasticity include activity-regulated cytoskeleton-associated protein (ARC), Homer1a and the AMPAR (α-amino-3-hydroxyl-5-methyl-4-

isoxazole-propionate receptor) subunit GluR1 (Lanahan and Worley, 1998; Miyashita et al., 2008; Redondo and Morris, 2011).

Clustered plasticity hypothesis: *STC* is more likely to facilitate LTP at nearby synapses, because there are local protein synthesis which are more available to nearby synapses (Govindarajan et al., 2011). More introductions about clustered plasticity hypothesis are continued in the next section.

The two hypotheses are conceptually related. One is not conflict with the other. *Clustered plasticity hypothesis* is based on *STC*, but involve the fact of diffusion of local PRPs between nearby synapses. Nearby synapses are thereby easier to be potentiated together and being recruited in encoding a memory. The initial *STC* only talk about PRPs that are synthesized in the neuronal soma and transported through the dendrites by non-specific mechanisms. In an elegant study, LTP is measured as a change in spine volume using two-photon microscopy and validated using perforated-patch clamp electrophysiology (Govindarajan et al., 2011). It shows that the efficacy of *STC* is dependent upon the distance between the spines: spines that are farther away (on different dendritic branches, or more than 70 μm away on the same branch) are not likely to benefit from *STC*. L-LTP formation is itself biased toward occurring on spines within a branch, because rescue of E-LTP to L-LTP is much less efficient if the two stimulated spines are on sister branches of the same dendrite.

The third hypothesis is *dendritic hotspots of turnover model*. Dendritic spines are the postsynaptic sites of excitatory synaptic connections on pyramidal neurons and are thus good indicators of synapses (Fu et al., 2012). Recent technical advances have allowed scientists to image and follow the structure of spines over time periods of months in living animals by

utilizing two-photon laser scanning microscopy (Trachtenberg et al., 2002). *In vivo* imaging studies on a variety of organisms have made a consensus that spines are dynamic structures, which can be modified by long-term potentiation (LTP), sensory experience and learning (Fu et al., 2012; Holtmaat et al., 2009; Toni et al., 1999; Trachtenberg et al., 2002). Importantly, spine imaging of juvenile zebra finches suggests that spine turnover prior to song imitation correlates with future song performance (Roberts et al., 2010), which suggests that baseline spine turnover may indicate the ability of the brain to adapt neural circuits to new information. Individuals with faster spine turnover prior to learning may have better ability to capture the new information during learning, and integrate the information to the memory circuit by stabilization of functional synapses that have successfully stored the information. There is a huge variability of dendritic spine turnover across individuals, and across dendritic branches within same individual. It may suggest that there are certain hotspots on dendritic branches where higher spine turnover ratio may allow neurons to more efficiently sample the synaptic space during learning to optimize information acquisition. Therefore, spines within the hotspots have a higher probability being recruited to encode a memory. However, there is no evidence so far in supporting this hypothesis.

A lot of studies using mouse model of Autism spectrum disorder (ASD), such as *fmr1* knockout mice, have shown that dendritic spines are highly dynamic in the *fmr1* knockout mice (Padmashri et al., 2013; Pan et al., 2010), and those mice have impairment in learning and memory. These findings suggest that excessive spine turnover is problematic, because the newly encoded information is not able to be stabilized: newly formed spines are usually lost in a short time. Therefore, a structural stabilization mechanism is needed after learning to retain the newly acquired information.

1.2 Evidence for clustered plasticity hypothesis

One mechanism of such stabilization is probably through the clustered addition of spines. Interesting emerging phenomenon of spine structural dynamics (De Roo et al., 2008; Fu et al., 2012; Harvey and Svoboda, 2007; Toni et al., 1999; Yang et al., 2016) and functional plasticity (Wilson et al., 2016) is that these events occur in clusters on dendrites. Fu et al. trained mice to learn a motor task, which led to rapid spine formation in clusters (less than 5 μm) (Fu et al., 2012). The second new spine formed in a close distance with the first new spine (Fig. 1.1a). In contrast, under baseline conditions, new spines appear to avoid existing stable spines on the same dendritic branch, rather than form uniformly (Lu and Zuo, 2017). In addition to the clustered formation and elimination of spines, morphological and functional alterations in spines also show correlation between nearby spines. These findings support the hypothesis that clustering of plasticity events within dendrites is a means to efficiently store information (DeBello et al., 2014; Govindarajan et al., 2006; Kastellakis et al., 2015; Poirazi and Mel, 2001). The following chapter will focus on the evidence that support the *clustered plasticity hypothesis*.

1.2.1 Local protein resources within dendritic branch

LTP is input-specific at individual synapses, but the interactions between plasticity at nearby synapses exist. Pairing a train of two-photon glutamate uncaging stimuli with postsynaptic depolarization induces LTP at individual spines. Subthreshold stimuli, which by themselves are too weak to induce LTP, result in robust LTP and spine enlargement at neighboring spines. The

reduction in LTP induction threshold last 10 min and spread over 10 μm along dendrites (Fig. 1.1b); (Harvey and Svoboda, 2007). In another study, high-frequency glutamate uncaging at individual spines leads to input-specific synaptic potentiation, and induces shrinkage of nearby unstimulated synapses. To be more specific, if more than 6 neighboring spines are potentiated simultaneously, the inactive synapse within the cluster weakens and shrinks (Fig. 1.1c); (Lu and Zuo, 2017; Oh et al., 2015).

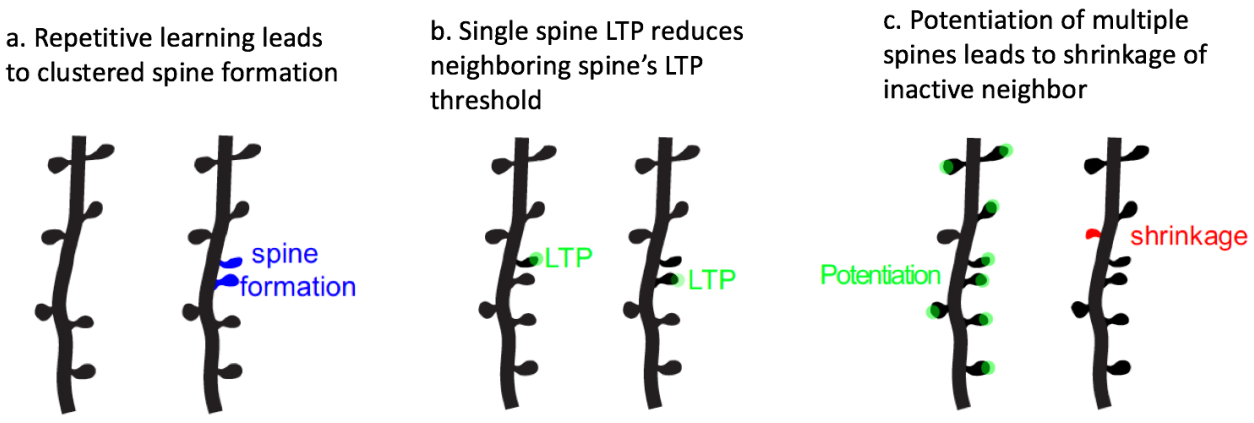

Figure 1.1. Schematic illustration of clustered synaptic alterations under various experimental conditions (from review by Lu and Zuo, Brain Research Bulletin, 2017). **(a)** Repetitive learning of the same task leads to clustered dendritic spine formation. **(b)** LTP induced at a single spine decreases the threshold for LTP at its neighboring spine. **(c)** Simultaneous potentiation of multiple dendritic spines in a cluster leads to the shrinkage of the inactive spine in the cluster.

What could be the reason for this reduction of LTP induction threshold at neighboring synapses? On the postsynaptic side, clustering could be due to the diffusion of intracellular signaling molecules, such as small guanosine triphosphatase (GTPase) (Harvey et al., 2008; Lu and Zuo, 2017). In this study, the authors used two-photon imaging of a fluorescence resonance energy transfer (FRET)-based indicator of Ras activation. The authors demonstrated that following LTP induction by glutamate uncaging, Ca^{2+} entry led to Ras activation that persisted up to 5 min. Activated Ras could diffuse out of the stimulated spine, traveled approximately 10 μm along the dendritic shaft, and diffused into neighboring spines. Using a MEK (downstream target of Ras signaling) inhibitor prevented the induction of LTP at a neighboring spine with a subsequent sub-threshold induction protocol. Therefore, diffusion of activated signaling molecules is a key component of interactions between nearby spines, providing biochemical support for the *clustered plasticity model*.

Another study shows that, in addition to Ras, another GTPase named RhoA is also able to diffuse between spines (Murakoshi et al., 2011). In this study, the authors used a similar method, FRET-based sensors optimized for imaging under 2 photon imaging combined with 2 photon glutamate uncaging, and demonstrated that two Rho GTPases, RhoA and Cdc42, were activated in the stimulated spines. Their activation lasted about 5 min, and were then followed by a phase of persistent activation lasting over 30 min. The two Rho GTPases were different in regulating spine plasticity from many perspectives. First, RhoA activation diffused out of the stimulated spines and spread over 5 μm along the dendrite, whereas Cdc42 activation was limited within stimulated spine. Second, inhibition of Rho-Rock pathway preferentially inhibited the initial spine growth, whereas the inhibition of the Cdc42-Pak pathway disrupted the maintenance of sustained structural plasticity. Both Rho GTPases required CaMKII. But CaMKII activation was

restricted to spines, and decayed rapidly with a time constant of 10 s. Therefore, in order to have long-lasting spine plasticity, the authors proposed that RhoA and Cdc42 relayed transient CaMKII activation to synapse-specific and long-lasting signaling.

The diffusion of activated GTPases may be one of the mechanisms that regulate spine clustering. Govindarajan et al. suggest that locally synthesized protein resources maybe another important mechanism involved in clustered plasticity (Govindarajan et al., 2011). They modified the *STC* model by including time and location factors that should be taken into consideration for synaptic plasticity. The original *STC* model stated that the efficacy of L-LTP induced at some synapses facilitated L-LTP expression at other synapses receiving stimulation that were too weak to induce L-LTP by itself. By using glutamate uncaging and two-photon imaging, Govindarajan et al. found that this facilitation decreased as time interval increased between two stimulations, and decreased as distance increased between stimulated spines on same branches (no facilitation if >70 μm) or sister branches (no facilitation if >50 μm), indicating that *STC* is likely to be more efficient on a single branch, compared to spines at sister branches. Second, stimulated spines competed for L-LTP expression if stimulated too closely in time. One explanation of the observed spatial restriction of *STC*, and the competition between spines for L-LTP expression is that the rate-limiting PRPs are synthesized locally (Martin and Kosik, 2002; Steward and Schuman, 2001), and passively diffuses or is actively transported to create a gradient, away from the synthesis site (Govindarajan et al., 2006). This does not exclude the possibility that rate-nonlimiting PRPs synthesized in the soma contribute to L-LTP formation.

The findings by Govindarajan et al. (*STC*) and by Harvey et al. (*Synaptic crosstalk*) both contribute to the clustered plasticity hypothesis, but are clearly two different mechanisms. First,

STC is protein synthesis-dependent, whereas *crosstalk* is not; second, *STC* can operate over a larger time window of 90 min, compared to 5 min for *crosstalk*; third, *STC* operates over a larger distance around 70 μm, compared to 10 μm for *crosstalk*; Fourth, *STC* occurs both regardless of E-LTP is induced before or after L-LTP induced at a nearby spine, while this is not shown in *crosstalk*. Importantly, it is also observed that in *STC*, distance is not the only factor governing the sharing of PRPs, but that the branch point between dendrites acts as a filter to further limit diffusion of newly synthesized proteins. These data indicate that *STC* and *synaptic crosstalk* are different phenomena, but both may contribute to *clustered plasticity hypothesis* (Govindarajan et al., 2011).

1.2.2 Similar activity patterns of clustered synapses

There are numerous electrophysiological interactions within dendrites that support *clustered plasticity hypothesis*. The main finding is that adjacent spines may receive locally convergent inputs from axons of the same neuronal ensemble and exhibit similar activity patterns (Kleindienst et al., 2011; Lu and Zuo, 2017; Takahashi et al., 2012; Wilms and Hausser, 2015). First, Kleindienst et al. monitored the spontaneous synaptic activation in developing hippocampal CA3 pyramidal neurons by patch-clamp recordings and calcium imaging (Kleindienst et al., 2011). Voltage-clamp was used to record spontaneously occurring synaptic currents, representing both unitary synaptic events and bursts of synaptic inputs. Calcium imaging was used to reveal spontaneous local calcium transients. The authors next wanted to investigate the possibility that calcium transients at the dendritic shaft that occurred simultaneously with synaptic currents represent synaptic transmission at the respective dendritic

locations. They found that synaptic currents and simultaneous local calcium transients triggered by electrical stimulation were indistinguishable from those of the spontaneous transients that coincided with synaptic currents, indicating that the spontaneous local calcium transients and the synaptic currents were not accidental. Importantly, the authors frequently observed that neighboring synapses were coactive (Fig. 1.2a). In contrast, the percentage of co-activation was very small in pairs of synapses that were separated by more than 16 μm. The relationship between distance and input correlation was entirely blocked in cells that developed in the absence of neuronal spiking by tetrodotoxin (sodium channel blocker) treatment during incubation. Interestingly, the authors also found that minimal stimulation of presynaptic axons never triggered responses at more than one synapse within 16 μm along the dendrite. Therefore, the functional clustering observed was unlikely due to spill-over of glutamate or diffusion of intra- or extracellular signaling factors caused by activation of one synapse. Therefore, the authors concluded that the co-activation of neighboring synapses was due to clustering of functionally related axons. However, this may just be a special case for developing hippocampal CA3 neurons.

Takahashi et al. found a similar phenomenon through *in vivo* whole cell patch clamp recordings and two-photon calcium imaging from spines of layer 2/3 pyramidal cells in the barrel cortex of anesthetized young adult mice. Spontaneous activities frequently occurred in neighboring spines; the probability of observing the coactive spines significantly increased within 6 μm along the dendrites (Fig. 1.2b); (Takahashi et al., 2012). It is very rigorous that the authors tried to differentiate the 5 possible mechanisms for this synchronization of adjacent spines: “ (i) convergent afferents from a population of spontaneously synchronized presynaptic neurons (cell assembly); (ii) multiple innervations of a single presynaptic axon; (iii) spillover of diffusible

molecules (such as glutamate) to neighboring synapses; (iv) spatial segregation of spine excitation by local dendritic inhibition; or (v) local depolarization-induced increase in a chance of calcium influx in neighboring spines." They applied electrical field stimulation to the CA3 stratum radiatum and induced synchronized network activity. However, this cell-assembly irrelevant artificial synchronization did not trigger spatially clustered spine activation, which was inconsistent with ii, iii and v. ii can also be ruled out by the evidence from biocytin reconstructions of neurons that were synaptically connected. 51 of 55 putative synapses arising from 12 presynaptic neurons contacted single spines. iv can be ruled out by showing nearby spines were still coactive in dendrites that were disinhibited by the local application of picrotoxin. Therefore, mechanism i becomes the most plausible mechanism: clustered synaptic activation is due to connecting to convergent afferents from a population of spontaneously synchronized presynaptic neurons (Takahashi et al., 2012).

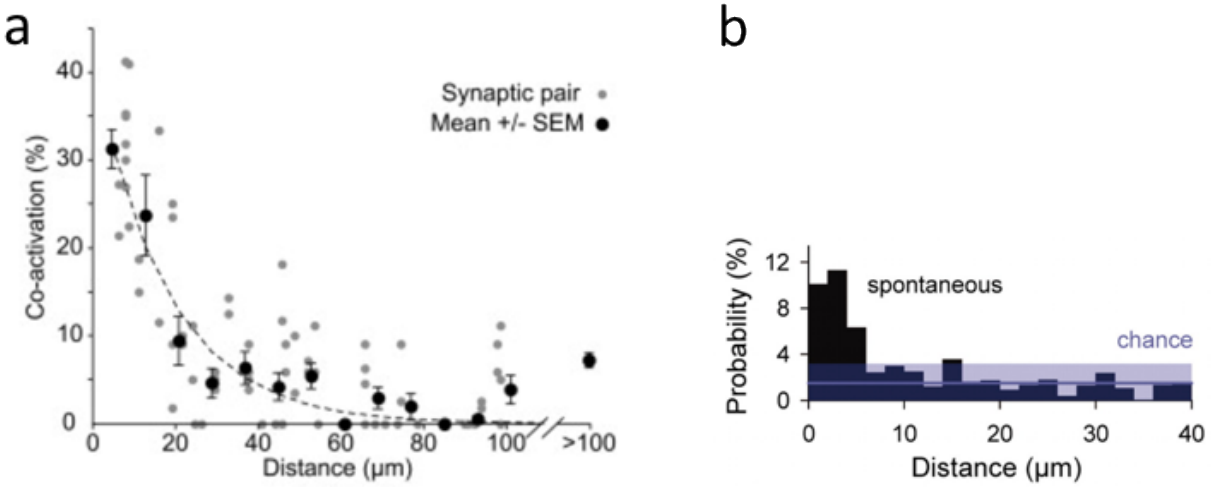

Figure 1.2. Co-activation of neighboring synapses *ex vivo* and *in vivo*. (a) *ex vivo* relationship between inter-synaptic distance and prevalence of co-activation for all synapse pairs of one cell.

Manual analysis. Dotted line: nonlinear fit (Nelder-Mead) (from Kleindienst et al., Neuron, 2011). **(b)** *in vivo* recordings show the probability of observing co-activated spines as a function of the inter-spine path distance (n = 10 dendritic segments in four cells). The chance level and its 95% confidence intervals (purple) were estimated from the distribution of distances of more than 10 μm (from Takahashi et al., Science, 2012).

Wilms and Hausser used *in vivo* calcium imaging of multiple neighboring cerebellar parallel fiber axons, and found that parallel fibers active during sensory processing (airpuffs) exhibited spatially clustering pattern (Wilms and Hausser, 2015). All of these findings indicate that the functional clustering of spine activation is probably due to the close vicinity of function-related axons.

Besides receiving inputs from functionally related axons, clustered spines may also share input from the exact same axons due to close vicinity (Yang et al., 2016). Yang et al. applied dual-color *in vivo* two-photon imaging of mouse auditory cortex, so both pre- and postsynaptic structures were labeled by GFP and YFP, respectively. GFP and YFP signals were separated using bandpass filters. Unexpectedly, they discovered that essentially all new synaptic contacts were made by adding new partners to existing synaptic elements: either a new spine was added on an existing bouton (43.5%) or a new bouton was added on an existing spine (55%), while the *de novo* synapse formation was rare (1.5%, 4 out of 262 new pairs). This add-on fashion of new synapse formation strengthens the connections between existing neuronal partners. This finding is also consistent with a previous electron microscopy study that, LTP induced formation of

multiple spines from the same dendrite contacting with a single axon bouton, duplicating activated synapses (Toni et al., 1999).

The nearby synapses are not always receiving similar inputs. In some cases, nearby spines receive functionally diverse inputs (Chen et al., 2011; Jia et al., 2010; Varga et al., 2011). These studies used high-resolution two-photon imaging to detect sensory-evoked calcium transients in single dendritic spines of mouse cortical neurons *in vivo*. Spines tuned for different sound frequencies, visual orientations, or whisker combinations were highly interspersed on the same dendrites. Neighboring spines were mostly responsive to distinct stimulations. These findings are not conflict with clustered plasticity hypothesis; instead they support the model by indicating that diverse synaptic inputs that are integrated by the postsynaptic cell through clustering of spines to generate highly specific output (Kleindienst et al., 2011). In addition, it is also possible that apical tuft dendrites have more clustered sensory inputs to the same dendrite, so that they are able to generate large amplitude dendritic spikes, while basal dendrites are more heterogeneous.

In such a scenario, clustered spines may receive 1) shared input by same axon from the same pre-synaptic neuron or 2) different but related inputs from the same neuronal ensemble, or 3) diverse inputs that need summation to generate a dendritic spike.

1.2.3 Amplification of inputs by clustered spines

A large amount of evidence has shown that dendritic integration in pyramidal neurons is supra-linear. Therefore, the simultaneous activation of synapses that are spatially clustered on the same dendritic branch exhibit a stronger influence on firing action potentials, compared to the

activation of the same number of synapses on different dendritic branches (Branco and Hausser, 2010; Kleindienst et al., 2011; Larkum and Nevian, 2008; Losonczy and Magee, 2006; Polsky et al., 2004). Further, theoretical studies suggest that this local integration structure can dramatically boost the information processing or computing capacities of neurons, thus optimizing learning and memory capacities (Hausser and Mel, 2003; Poirazi and Mel, 2001; Spruston, 2008).

1.2.4 Learning-induced formation of clustered spines

Learning triggers formation of clustered spines on dendrites (Fu et al., 2012). Specifically, the authors trained mice to learn a motor task (use forelimb to grab a seed through a narrow window). By performing two-photon imaging of Thy1-YFP mice, which express YFP in a subset of layer 5 cortical pyramidal cells, the authors were able to collect time-lapse spine images before, during and after training. They found that spines added during training had 35% formed within 5 μm with each other on the same dendrites, while spines added in untrained group had only 10%. In other words, learning-induced new spines tended to form clusters. This is the first study showing that learning induces clustered spine formation *in vivo*. The newly added clustered spines were more stable than those dispersed new spines, further suggesting that the clustered spines maybe involved in long-term memory storage. Importantly, clustered spine formation is task-specific. The authors added another group of mice that received training of one motor task for a day, and another task for the subsequent 3 days. Both tasks by itself induced clustered spine formation. However, the second task-induced new spines did not cluster with first task-induced new spines,

suggesting that clustered spine addition is task-specific, so the memories for different tasks do not interfere with each other.

However, although this study shows that learning induces spine clustering, it does not have a causal relationship between clustered spine and memory, or correlational evidence supporting this relationship.

1.3 Goals of the dissertation

Our understanding of how memories are formed and stored in the brain has advanced significantly over the past several decades (Dudai and Morris, 2013; Kandel et al., 2014). It is now accepted that memory storage processes operate conjointly at the level of neurons, dendrites, and dendritic spines (Bailey and Kandel, 1993; Holtmaat and Caroni, 2016; Kandel et al., 2014; Kastellakis et al., 2015). Further, dendritic spines are dynamic structures whose formation and elimination is postulated to expand memory storage capacity beyond that permissible solely from synaptic weight changes of existing synapses (Chklovskii et al., 2004; Kandel et al., 2014; Poirazi and Mel, 2001).

A variety of studies in varying preparations and organisms have shown that spine turnover is modified by electrical activity, sensory experience, and learning (Fu et al., 2012; Holtmaat and Svoboda, 2009; Lai et al., 2012; Toni et al., 1999; Xu et al., 2009; Yang et al., 2009). Additionally, results from juvenile zebra finch show that endogenously higher levels of spine turnover before tutoring correlate with a greater capacity for subsequent song learning during the

critical period (Roberts et al., 2010). Another interesting emerging phenomenon of spine structural dynamics (De Roo et al., 2008; Fu et al., 2012; Harvey and Svoboda, 2007; Toni et al., 1999; Yang et al., 2016) and activity (Wilson et al., 2016) is that these events occur in clusters on dendrites. These findings support the hypothesis that clustering of plasticity events within dendrites is a means to efficiently store information (DeBello et al., 2014; Govindarajan et al., 2006; Kastellakis et al., 2015; Poirazi and Mel, 2001).

However, although both spine turnover and spine clustering have been shown to impact learning and memory, it remains unclear how spine turnover and clustered spine addition relate to one and other and how does clustered spines contribute to memory storage. According to the *clustered plasticity model*, a stronger memory is hypothesized to consist of higher percentage of clustered spines within the circuit, to efficiently reactivate the engram. Therefore, a correlation and manipulation of spine turnover, clustering or memory is in need to strengthen the causal link between spine turnover, clustering and learning and memory.

In this dissertation, I used transcranial two-photon microscopy to track spine dynamics, and examined the relation between basal spine turnover, contextual and spatial learning and memory, and subsequent spine clustering in the mouse retrosplenial cortex (RSC). RSC is important for spatial learning and amenable to long-term *in vivo* imaging. RSC (Brodmann areas 29 and 30) resides within the posterior cingulate cortex. From an anatomical perspective, this region has dense reciprocal connections with three notable regions that have been significantly implicated in cognitive functions: hippocampus, entorhinal cortex, and anterior thalamic nuclei. These strong connections immediately point RSC to a role in learning and memory (Vann et al., 2009). Indeed, a large number of rodent studies have shown that RSC lesions impair spatial memory (Aggleton

and Vann, 2004; Harker and Whishaw, 2004). In addition, human fMRI studies suggest that RSC is active during learning of new environments and navigation in recently learned environments (Epstein, 2008; Maguire, 2001). More recently, optogenetical reactivation of a specific ensemble of RSC neurons engaged by contextual fear conditioning is sufficient to produce context-specific behavior (Cowansage et al., 2014). Elevated expression of immediate early genes in RSC is detected by *in vivo* imaging during spatial learning in the Morris water maze (Czajkowski et al., 2014). All of these results indicate that RSC neurons actually encode and store spatial memory. Overexpression of CREB in RSC results in spatial memory enhancements in the Morris water maze (Czajkowski et al., 2014). Also, RSC is amenable to long-term *in vivo* imaging, which allows us to image the dendritic spine turnover across time. Therefore, RSC is an ideal cortical structure to examine the effects of contextual and spatial learning and memory on spine dynamics.

In this dissertation, I report that pre-learning spine turnover predicts both learning and memory performance and learning and memory-related spine clustering. Accordingly, a genetic manipulation ($Ccr5^{+/-}$) that enhances pre-learning spine turnover also enhances clustering and learning and memory, strengthening the causal relationship between spine dynamics and learning and memory. Further, I also report that pre-learning spine turnover and learning-related clustering are related processes that themselves exhibit spatial clustering within the dendritic tree. This dissertation posits a hotspot model of memory storage in which higher rates of pre-learning spine turnover facilitate the formation of learning and memory-related clustered spines near regions of turnover, and that clustering serves as a structural mechanism to stabilize structural plasticity.

Chapter 2 CCR5 is a suppressor for learning and memory

In this Chapter, I will firstly report the findings of CCR5 protein function in hippocampal learning and memory, and in barrel cortex synaptic plasticity. This is an important component of this dissertation, because I will adopt *Ccr5* heterozygous mutation as a genetic manipulation of learning and memory in the following chapters, to investigate the causal relationship between hotspots of dendritic spine dynamics and learning and memory. This is the first spine imaging study using the 'gain of function' manipulation. Therefore, it is important to confirm 1) memory enhancement phenotype of *Ccr5*$^{+/-}$ mice that have fluorescence labeled spines; 2) that RSC is an important region for memory enhancement by *Ccr5* mutation, so that it is likely for me to observe a structural plasticity phenotype in RSC.

2.1 CCR5 is a suppressor for cortical plasticity and hippocampal learning and memory

The following content was originally published in eLife:

*Zhou M, *Greenhill S, **Huang S**, Silva TK, Sano Y, Wu S, Cai Y, Nagaoka Y, Sehgal M, Cai DJ, Lee YS, Fox K, Silva AJ. CCR5 is a suppressor for cortical plasticity and hippocampal learning and memory. eLife. 2016; 5: e20985. DOI: 10.7554/eLife.20985 (PMID: 27996938)

eLIFE elifesciences.org

RESEARCH ARTICLE

CCR5 is a suppressor for cortical plasticity and hippocampal learning and memory

Miou Zhou[1†], Stuart Greenhill[2,3†], Shan Huang[1], Tawnie K Silva[1], Yoshitake Sano[1,4], Shumin Wu[5], Ying Cai[1], Yoshiko Nagaoka[5], Megha Sehgal[1], Denise J Cai[1], Yong-Seok Lee[1,6], Kevin Fox[2]*, Alcino J Silva[1]*

[1]Departments of Neurobiology, Psychology, Psychiatry, Integrative Center for Learning and Memory and Brain Research Institute, University of California, Los Angeles, Los Angeles, United States; [2]Cardiff School of Biosciences, Cardiff University, Cardiff, United Kingdom; [3]School of Life and Health Sciences, Aston University, Birmingham, United Kingdom; [4]Department of Applied Biological Science, Tokyo University of Science, Chiba, Japan; [5]Department of Molecular and Medical Pharmacology, University of California, Los Angeles, Los Angeles, United States; [6]Department of Physiology, Seoul National University College of Medicine, Seoul, Republic of Korea

Abstract Although the role of CCR5 in immunity and in HIV infection has been studied widely, its role in neuronal plasticity, learning and memory is not understood. Here, we report that decreasing the function of CCR5 increases MAPK/CREB signaling, long-term potentiation (LTP), and hippocampus-dependent memory in mice, while neuronal CCR5 overexpression caused memory deficits. Decreasing CCR5 function in mouse barrel cortex also resulted in enhanced spike timing dependent plasticity and consequently, dramatically accelerated experience-dependent plasticity. These results suggest that CCR5 is a powerful suppressor for plasticity and memory, and CCR5 over-activation by viral proteins may contribute to HIV-associated cognitive deficits. Consistent with this hypothesis, the HIV V3 peptide caused LTP, signaling and memory deficits that were prevented by Ccr5 knockout or knockdown. Overall, our results demonstrate that CCR5 plays an important role in neuroplasticity, learning and memory, and indicate that CCR5 has a role in the cognitive deficits caused by HIV.
DOI: 10.7554/eLife.20985.001

***For correspondence:** foxkd@cardiff.ac.uk (KF); silvaa@mednet.ucla.edu (AJS)

[†]These authors contributed equally to this work

Competing interests: The authors declare that no competing interests exist.

Funding: See page 26

Received: 26 August 2016
Accepted: 19 December 2016
Published: 20 December 2016

Reviewing editor: Moses V Chao, New York University Langone Medical Center, United States

Introduction

C-C chemokine receptor 5 (CCR5) is a seven-transmembrane G protein-coupled receptor (GPCR) involved in recruiting leukocytes to sites of tissue damage during inflammatory responses. CCR5 is highly expressed in T cells and macrophages in the immune system (***Sorce et al., 2011***). In the central nervous system, CCR5 is expressed in microglia, astrocytes and neurons in multiple brain regions (***Cartier et al., 2005***; ***Meucci et al., 1998***; ***Tran et al., 2007***; ***Westmoreland et al., 2002***), including the CA1 region of the hippocampus (***Torres-Muñoz et al., 2004***).

Ligand binding to CCR5 is known to modulate several parallel signaling cascades implicated in learning and memory, including the suppression of adenylyl cyclase (AC), as well as the activation of the PI3K/AKT and p44/42 MAPK signaling (***Cartier et al., 2005***; ***Paruch et al., 2007***; ***Tyner et al., 2005***). The CCR5 endogenous ligand RANTES (also known as CCL5) is reported to block neuronal $[Ca^{2+}]_i$ oscillations (***Meucci et al., 1998***) and to modulate glutamate release (***Musante et al., 2008***), suggesting a role for CCR5 in the regulation of neuronal function.

CCR5 has a key role in HIV infection by mediating virus cellular entry. *Ccr5* knockdown inhibits HIV-1 infection in macrophages (***Liang et al., 2010***) and CCR5 antagonists effectively reduce HIV-1

expression in AIDS patients (**Hunt and Romanelli, 2009**). Treatment with the CCR5 antagonist maraviroc has been reported to improve neurocognitive test performance among patients with moderate cognitive impairment (**Ndhlovu et al., 2014**), supposedly by reducing monocytes and inflammation. Cognitive deficits affect approximately 30% of HIV-positive adults and 50% of HIV-positive infants (**Galicia et al., 2002**), and are a significant clinical problem associated with HIV infection. Although CCR5 plays a crucial role in HIV infection in the central nervous system (CNS) (**Ellis et al., 2007**; **Zhou and Saksena, 2013**), little is known about its role in neuronal plasticity or learning and memory, or whether this receptor plays a direct role in HIV-associated cognitive disorders.

Here, we demonstrate that manipulations that decrease CCR5 function result in elevated MAPK and CREB levels during learning, enhance synaptic plasticity and improve both cortical sensory plasticity and hippocampal learning and memory, while the transgenic overexpression of this receptor causes learning and memory deficits. Thus, our studies reveal an important suppressor role for CCR5 in neuroplasticity, learning and memory, independent of the proposed roles of CCR5 in neuroinflammation and neurodegeneration. Since our results and other studies (**Cormier and Dragic, 2002**; **Morikis et al., 2007**; **Shen et al., 2000**) show that HIV coat proteins can bind and activate CCR5, thus activating its memory suppressor functions, our results suggest that besides the neuroinflammation induced neurodegeneration that can cause HIV-associated cognitive deficits, CCR5 activation by HIV coat proteins also contributes to the cognitive deficits caused by HIV.

Results

Identification of *Ccr5* knockout mice in a reverse genetic memory screen

Our first indication that CCR5 was involved in plasticity and memory came from a reverse genetic memory screen. In total, 148 transgenic and knockout mutant mouse strains with controlled genetic backgrounds were chosen at random from the inventories of commercial vendors (Jackson Laboratories and Taconic Farms) as well as individual laboratories, and screened for contextual memory phenotypes (**Figure 1—figure supplement 1** and **Figure 1—source data 1**). Interestingly, 6 out of the 8 chemokine or chemokine receptor mutant strains screened (# labeling, **Figure 1—figure supplement 1**) showed positive Z scores (see Materials and methods), including three mutant strains with scores above 1, suggesting enhanced memory for contextual conditioning. $HRas^{G12V}$ mice were used for comparison, since they were previously reported (**Kushner et al., 2005**) to show enhanced memory for contextual fear conditioning. Like $HRas^{G12V}$ mice, mice homozygous for a null-mutation of the *Ccr5* gene ($Ccr5^{-/-}$) showed average Z scores above 1. The *CCR5* knockout resulted in memory enhancements for contextual conditioning when tested 24 hr after training (**Figure 1—figure supplement 2A**, $t_{(14)} = 2.43$ $p<0.05$, Student's *t*-test) and 2-weeks after training (**Figure 1—figure supplement 2B**, $t_{(14)} = 3.07$ $p<0.01$, Student's *t*-test). These results show that the *Ccr5* knockout results in enhanced long-term (24 hr) and remote (2-weeks) memory. Importantly, activity levels including baseline activity and activity bursts during shock-exposure were normal (**Figure 1—figure supplement 2C,D**), a result demonstrating that the enhanced freezing of $Ccr5^{-/-}$ mice is not due to either decreases in activity or increased sensitivity to the unconditioning stimulus (i.e., the footshock). In contrast to contextual conditioning, tone conditioning (**Hall et al., 2001**) was unaltered in the $Ccr5^{-/-}$ mice (**Figure 1—figure supplement 2E**), confirming that the contextual conditioning enhancement of these mutants is not due to non-specific behavioral changes that alter conditioning responses.

Ccr5$^{+/-}$ mice show enhanced memory in multiple memory tasks

To test whether the heterozygous deletion mutation ($Ccr5^{+/-}$) also results in enhanced memory, $Ccr5^{+/-}$ mice were trained in the contextual fear conditioning task and were tested 2-weeks after training. Compared to WT littermates, $Ccr5^{+/-}$ mice showed increased freezing levels (**Figure 1A**, $t_{(20)} = 2.37$ $p<0.05$, Student's *t*-test); in contrast, baseline activity and shock sensitivity were normal in these mutants (**Figure 1—figure supplement 3A**), demonstrating that both the *Ccr5* heterozygous and homozygous mutations result in enhanced contextual memory.

To determine whether the $Ccr5^{+/-}$ mutation also affects other forms of hippocampal-dependent memory (**Kogan et al., 2000**; **Riedel et al., 1999**), the mice were tested in the Morris water maze and social recognition tasks. In the hidden-platform version of the Morris water maze, mice were

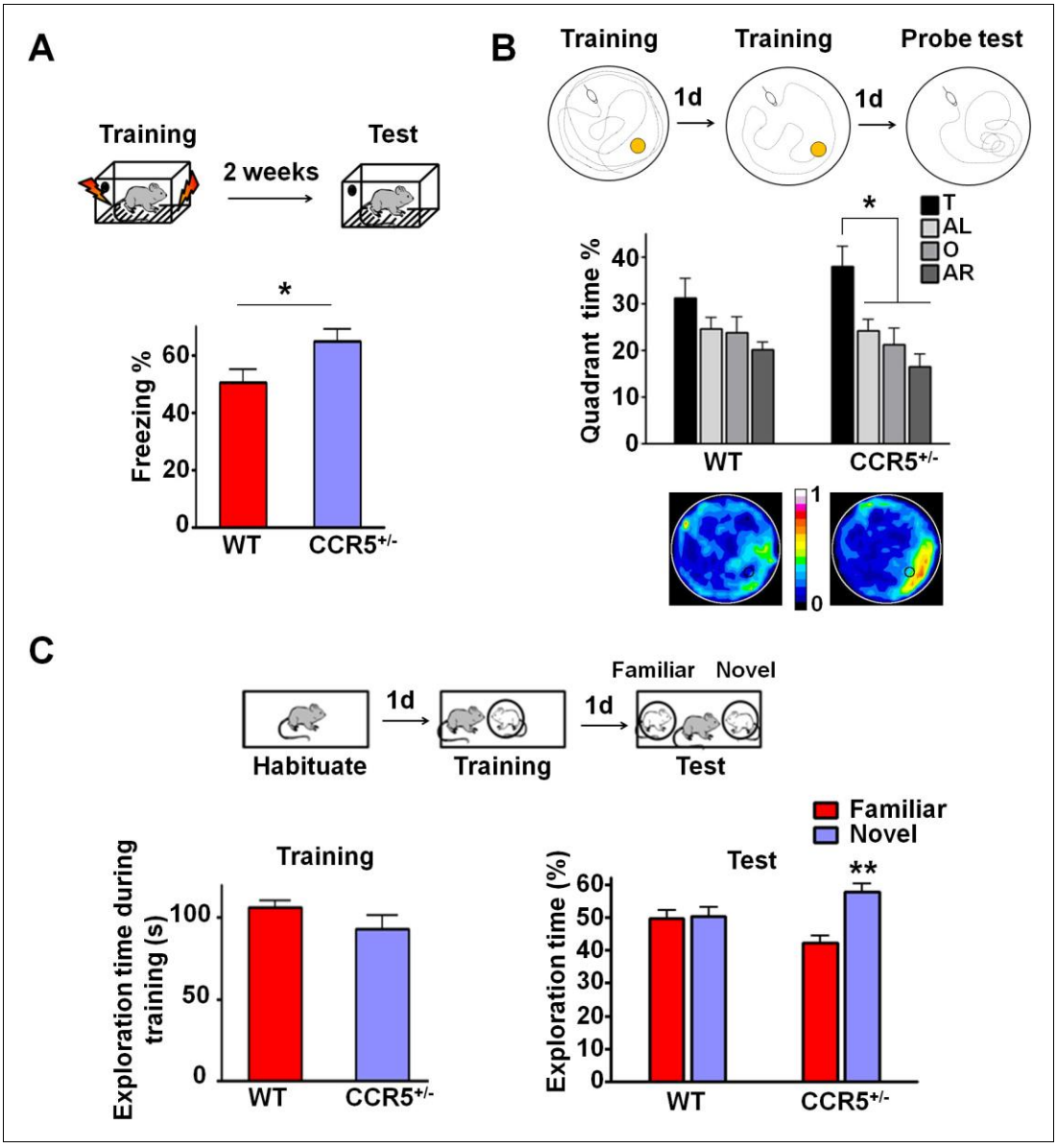

Figure 1. *Ccr5*$^{+/-}$ mice show enhanced memory in multiple memory tasks. (**A**) In a fear conditioning test given two weeks after training, *Ccr5*$^{+/-}$ mice showed enhanced contextual memory (WT n = 11, *Ccr5*$^{+/-}$ n = 11; *p<0.05, Student's *t*-test). (**B**) In a water maze probe test given after two days of training, *Ccr5*$^{+/-}$ mice spent significantly more time in the target quadrant than in the other three quadrants of the water maze. In contrast, WT mice did not search selectively for the platform (WT n = 14, *Ccr5*$^{+/-}$ n = 16; *p<0.05, Two-way ANOVA with repeated measure). Heat maps below the bar graphs show the combined traces of the mice from each group during the probe test. (**C**) There was no difference between WT mice and *Ccr5*$^{+/-}$ mice in social

Figure 1 continued on next page

Figure 1 continued

training. In the social recognition test given 24 hr after training (7 min, a training time chosen to undertrain WT mice), *Ccr5*$^{+/-}$ mice, but not WT mice, spent more time exploring the novel OVX mouse (WT n = 14, *Ccr5*$^{+/-}$ n = 19; **p<0.01, one sample *t*-test compared to 50%). Error bars indicate SEM.

DOI: 10.7554/eLife.20985.002

The following source data and figure supplements are available for figure 1:

Source data 1. Full names and MGI accession # of the 148 mutant strains in the reverse genetic memory screen (*Jax stock#: 370200; **Jax stock#: 370202).

DOI: 10.7554/eLife.20985.003

Figure supplement 1. Identification of *Ccr5* knockout mice in a reverse genetic memory screen.

DOI: 10.7554/eLife.20985.004

Figure supplement 2. *Ccr5*$^{-/-}$ mice show enhanced contextual memory.

DOI: 10.7554/eLife.20985.005

Figure supplement 3. Behavioral tasks to test the baseline activity and activity burst during fear conditioning, and anxiety and locomotive levels in WT and *Ccr5*$^{+/-}$ mice.

DOI: 10.7554/eLife.20985.006

Figure supplement 4. WT and *Ccr5*$^{+/-}$ mice show similar GFAP and TUNEL immunostaining and similar spine density.

DOI: 10.7554/eLife.20985.007

tested for their ability to use spatial cues around a pool to find an escape platform hidden just beneath the water surface. Following 2-days of training, memory was assessed by a probe test wherein the mice search for 60 s with the platform removed from the pool. Since this probe test was administered early in training, the WT mice did not search selectively for the platform. In contrast, even with this limited amount of training, *Ccr5*$^{+/-}$ mice spent significantly more time in the quadrant where the platform had been during training (target quadrant) than the other three quadrants, demonstrating that the *Ccr5*$^{+/-}$ mutation not only enhances learning and memory for contextual conditioning, but also results in enhanced spatial learning and memory [***Figure 1B***; Two-way ANOVA with repeated measure, overall (genotype × percentage of time in each quadrant) interaction: $F_{(3,84)}$ = 0.81; Main effect of quadrant%: $F_{(3,84)}$ = 6.99. Between the target quadrant and all other quadrants for *Ccr5*$^{+/-}$ mice: p<0.05, Bonferroni post-tests]. Heat maps, derived from the combined swimming traces of the mice in each group during the probe test, also illustrate the spatial learning and memory enhancement of *Ccr5*$^{+/-}$ mice (***Figure 1B***).

The social recognition task takes advantage of mice's preference for novel stimuli and tests their ability to distinguish familiar versus novel conspecifics (***Kogan et al., 2000***). For this task, mice were first habituated to the testing chamber on day 1; on day 2, they were placed in the same chamber and allowed to interact for 7 min with an ovariectomized (OVX) female mouse placed under a wired cylinder (training session). On day 3, individual mice were placed back into the same chamber (test session), and allowed to interact with two OVX females (one familiar and one novel) (***Figure 1C***). In the test session, compared to WT mice, *Ccr5*$^{+/-}$ mice spent significantly more time exploring the novel OVX mouse, indicating that the *Ccr5*$^{+/-}$ mutation also enhanced learning and memory in the social recognition test (***Figure 1C***, $t_{(18)}$ = 3.39 p<0.01, one sample paired *t*-test compared to 50%). Importantly, the *Ccr5*$^{+/-}$ mutation did not affect the total interaction time during training, demonstrating that their learning and memory enhancement is not due to increased social interaction.

Since anxiety and activity levels could confound the results of the memory tests described above, we tested the *Ccr5*$^{+/-}$ mice and their WT littermate controls in the elevated plus maze and open field tasks. *Ccr5*$^{+/-}$ mice were similar to WT littermates in both open arm entries and percentage time spent in the open arms of the elevated plus-maze, two well-known measures of anxiety (***Figure 1—figure supplement 3B***); Analyses of the open field (e.g., measures of total distance traveled and percentage time in center zone) also revealed no differences between the *Ccr5*$^{+/-}$ mice and their WT controls (***Figure 1—figure supplement 3C***). A previous study reported that CCR5 deficiency results in the activation of astrocytes, which leads to neurodegeneration in aged mice (***Lee et al., 2009***). We measured astrocyte numbers and apoptosis with GFAP and TUNEL staining in the hippocampus of 3-month old mice, and found that in our genetic background there is no difference between WT and *Ccr5*$^{+/-}$ mice (***Figure 1—figure supplement 4A–C***). Measurements of spine density in the hippocampal CA1 subregion revealed no differences between YFP/WT and YFP/*Ccr5*$^{+/-}$ mice (***Figure 1—figure supplement 4D***). Altogether, these results indicate that the learning and memory

enhancements of the *Ccr5*$^{+/-}$ mice are not confounded by abnormal anxiety, changes in locomotor activity, astrogliosis, apoptosis, or spine density.

Enhanced MAPK and CREB signaling and long-term potentiation in *Ccr5*$^{+/-}$ mice

Mitogen-activated protein kinases p44/42 (MAPKs) (***Atkins et al., 1998***; ***Kushner et al., 2005***; ***Schafe et al., 2000***) and cAMP-responsive element-binding protein (CREB) (***Bourtchuladze et al., 1994***; ***Dash et al., 1990***; ***Yin et al., 1994***) are known to have a central role in hippocampal learning and memory and in cortical plasticity (***Barth et al., 2000***; ***Glazewski et al., 1999***). We focused our signaling studies at two different time points (1 hr and 3 hr) following training (***Chwang et al., 2006***; ***Stanciu et al., 2001***). Prior to learning (measurements in home cage controls), there were no differences between WT and *Ccr5*$^{+/-}$ mice in either hippocampal MAPK or CREB activation measured with phospho-specific antibodies (***Figure 2A***). In contrast, *Ccr5*$^{+/-}$ mice showed enhanced phosphorylated MAPK (***Figure 2B***, $t_{(10)}$ = 4.45 p<0.01, Student's *t*-test) and enhanced phosphorylated CREB levels (***Figure 2C***, $t_{(12)}$ = 2.21 p<0.05, Student's *t*-test) at 1 and 3 hr after fear conditioning, respectively (see ***Figure 2—figure supplements 1***, ***2*** and ***3*** for MAPK and CREB levels at both 1 hr and 3 hr).

Since MAPK/CREB signaling in neurons is known to affect synaptic plasticity, we tested whether the *Ccr5*$^{+/-}$ mice show enhanced long-term potentiation (LTP), a cellular mechanism underlying learning and memory (***Bliss and Collingridge, 1993***; ***Lee and Silva, 2009***). Field EPSPs (fEPSPs) evoked by Schaffer collateral stimulation were recorded in the CA1 region of acute hippocampal slices prepared from WT and *Ccr5*$^{+/-}$ mice. Analyses of the fEPSPs between 50 and 60 min post-tetanus revealed enhanced LTP in *Ccr5*$^{+/-}$ mice (***Figure 2D***, $t_{(12)}$ = 2.61 p<0.05, Student's *t*-test). Our results suggest that the enhancement in MAPK/CREB signaling causes the hippocampal enhancements in LTP that likely underlies the hippocampal-dependent learning and memory enhancements of *Ccr5*$^{+/-}$ mice. More importantly, these signaling, electrophysiological and behavioral results of *Ccr5*$^{+/-}$ mice suggest that CCR5 is a plasticity and memory suppressor (***Abel et al., 1998***).

Knockdown of *Ccr5* in adult hippocampus results in enhanced memory

The *Ccr5* knockout we studied is neither restricted to the hippocampus nor specific to adult brain neurons, leaving open a number of other alternative explanations for the results described above. Therefore, we used Adeno-Associated Viral vectors (AAV5) to restrict a shRNA-mediated *Ccr5* knockdown to the adult hippocampus. AAV5 vectors containing either shRNA-CCR5 or shRNA-dsRed (shRNA-Cont) (***Figure 3A***) were injected into the hippocampal pyramidal fields of 3 month-old C57BL/6N mice. One month after shRNA-CCR5 virus injection, *Ccr5* mRNA was markedly reduced in the hippocampus compared to shRNA-Cont virus (***Figure 3B***, $t_{(7)}$ = 7.54 p<0.001, Student's *t*-test). Similarly, in cultured HEK293 cells, infection of shRNA-CCR5, but not shRNA-Cont reduced *Ccr5* expression (***Figure 3—figure supplement 1A***). Additionally, one-month after shRNA-Cont or shRNA-CCR5 AAV injection, GFP expression (indicating AAV transfection) was observed widely in the hippocampal pyramidal fields (including CA1 and CA2) of both groups (***Figure 3C***). Most GFP-positive cells were recognized by the NeuN antibody (neuronal marker), but not by the Iba1 antibody (microglia marker) (***Figure 3D*** and ***Figure 3—figure supplement 1B***) or the GFAP antibody (astrocyte marker) (***Figure 3—figure supplement 1C***), demonstrating that the viral vectors we used mainly transfected neurons, a result that we also confirmed in the barrel cortex (see results below).

To test the impact of *Ccr5* knockdown in hippocampal pyramidal fields, we trained the transfected mice with contextual fear conditioning one-month after virus injection. When tested 2-weeks after training, the shRNA-CCR5 mice showed enhanced contextual memory compared to shRNA-Cont mice (***Figure 3E***, $t_{(15)}$ = 3.46 p<0.01, Student's *t*-test). Mice transfected with shRNA-CCR5 showed similar enhancements in spatial learning and memory in the Morris water maze. Specifically, we utilized the paradigm used for our knockout studies where a probe test was given after 2 days training, when most control mice (transfected with shRNA-Cont virus) still failed to learn the task (e.g., spent similar times in all four quadrants of the maze). Strikingly, mice transfected with the shRNA-CCR5 virus spent significantly more time in the target quadrant than the other three quadrants [***Figure 3F***; Two-way ANOVA with repeated measure, overall (virus × percentage of time in each quadrant) interaction: $F_{(3,120)}$ = 4.18; Main effect of quadrant%: $F_{(3,120)}$ = 9.45. Between the

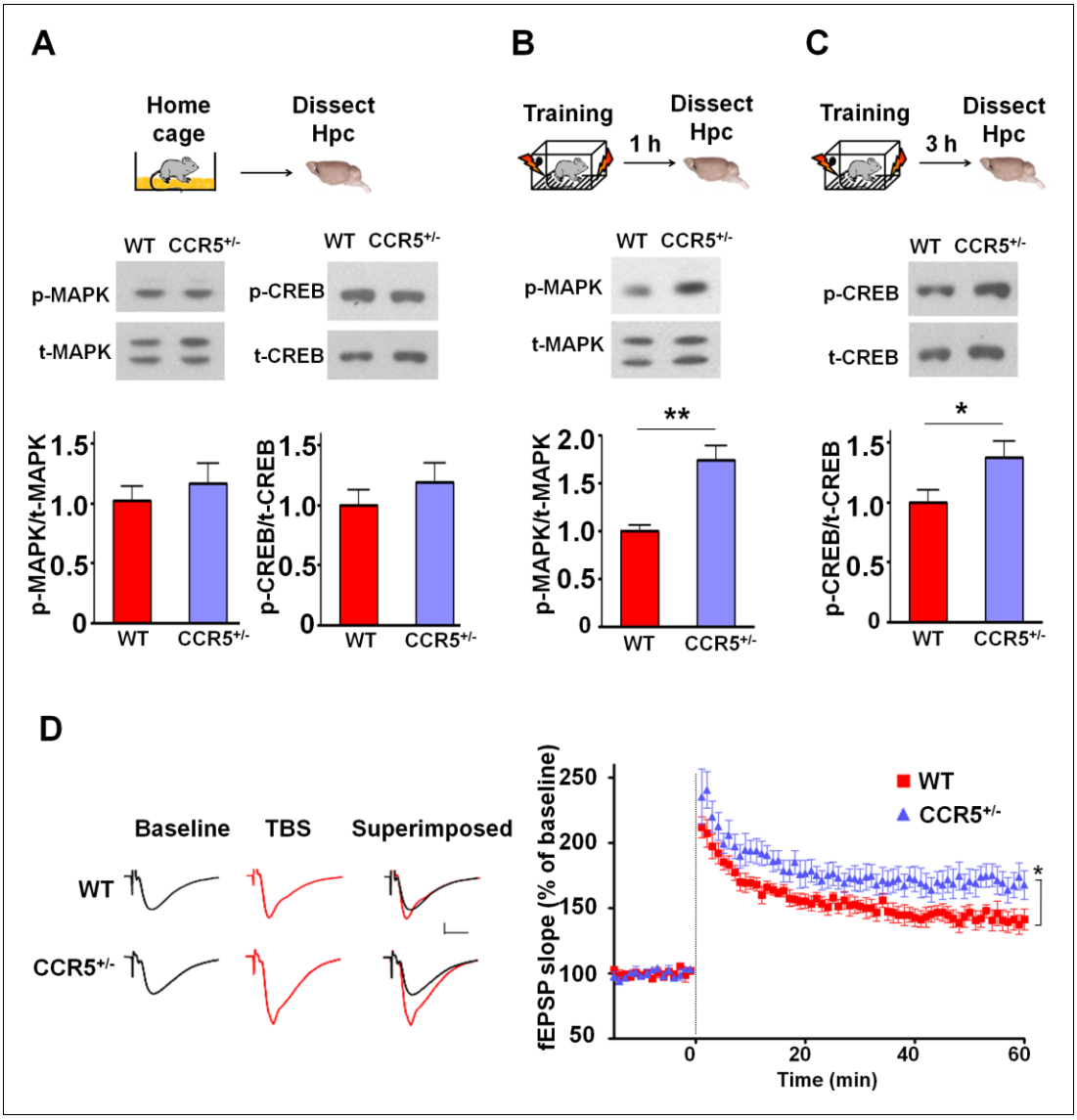

Figure 2. *Ccr5*$^{+/-}$ mice show post-training increases in MAPK and CREB signaling and enhanced hippocampal LTP. (**A**) Hippocampus collected from home cage WT and *Ccr5*$^{+/-}$ mice had similar levels of phosphorylated p44/42 MAPK and CREB (MAPK: WT n = 4, *Ccr5*$^{+/-}$ n = 4; CREB: WT n = 6, *Ccr5*$^{+/-}$ n = 7). (**B**) *Ccr5*$^{+/-}$ mice showed enhanced levels of phosphorylated p44/42 MAPK (normalized with total MAPK) in hippocampal samples collected one hour after fear conditioning training (WT n = 6, *Ccr5*$^{+/-}$ n = 6; **p<0.01, Student's *t*-test). (**C**) *Ccr5*$^{+/-}$ mice showed enhanced levels of phosphorylated CREB (normalized with total CREB) in hippocampal samples collected 3 hr after fear conditioning training (WT n = 7, *Ccr5*$^{+/-}$ n = 7; *p<0.05, Student's *t*-test). (**D**) CA1 fEPSPs were recorded in hippocampal slices before (baseline) and after 5 TBS (theta bursts stimulation, each burst consists of four stimuli at 100 Hz, 200 ms inter-burst interval). *Ccr5*$^{+/-}$ slices show a significant LTP enhancement in the fEPSP measured during the last 10 min of recordings following the tetanus (n = 7 mice for both WT and *Ccr5*$^{+/-}$; *p<0.05, Student's *t*-test). Error bars indicate SEM.

Figure 2 continued on next page

Figure 2 continued

DOI: 10.7554/eLife.20985.008

The following figure supplements are available for figure 2:

Figure supplement 1. Hippocampal MAPK/CREB signaling of WT, *Ccr5*$^{+/-}$ and *Ccr5*$^{-/-}$ mice.

DOI: 10.7554/eLife.20985.009

Figure supplement 2. Hippocampal MAPK/CREB signaling of WT, *Ccr5*$^{+/-}$ and *Ccr5*$^{-/-}$ mice after fear conditioning.

DOI: 10.7554/eLife.20985.010

Figure supplement 3. Hippocampal MAPK/CREB signaling of WT, *Ccr5*$^{+/-}$ and *Ccr5*$^{-/-}$ mice after fear conditioning.

DOI: 10.7554/eLife.20985.011

target quadrant and all other quadrants for shRNA-CCR5 mice: p<0.001, Bonferroni post-tests; Target quadrant percentage between shRNA-Cont and shRNA-CCR5 group: $t_{(40)}$ = 2.53 p<0.05, Student's *t*-test]. Similar results were also obtained for other measures of probe trial performance including proximity to the target platform and platform crossings (data not shown). Heat maps, derived from the combined swimming traces of the mice in each group during the probe test, also illustrate the spatial learning and memory enhancement of the shRNA-CCR5 group (***Figure 3F***). To test whether with more extended training shRNA-Cont mice could also learn the water maze task, a second probe test was given after 5 days of training. In this probe test, both shRNA-Cont and shRNA-CCR5 mice spent more time in the target quadrant (***Figure 3—figure supplement 1D***), demonstrating that with additional training the shRNA-Cont mice are able to show spatial learning in the water maze task.

Altogether, these results demonstrate that CCR5 is a memory suppressor and that knocking-down *Ccr5* specifically in the adult CA1/CA2 is sufficient to enhance hippocampus-dependent learning and memory.

CCR5 overexpression leads to learning and memory deficits

Our CCR5 knockout and knockdown results demonstrate that CCR5 is a plasticity and memory suppressor, and therefore predict that increases in CCR5 function lead to memory deficits. To test this hypothesis, we generated transgenic (Tg) mice overexpressing *Ccr5* under the *Camk2a* promoter (***Mayford et al., 1996***). Compared to WT mice, CCR5 Tg mice show increases in hippocampal *Ccr5* mRNA expression (***Figure 4A***). To test the impact of CCR5 overexpression on learning and memory, WT and CCR5 Tg mice were tested in three hippocampal-dependent learning tasks, including two contextual fear conditioning paradigms that are sensitive to changes in hippocampal function (***Cui et al., 2008***; ***Matus-Amat et al., 2004***). Analyses of a context pre-exposure fear-conditioning paradigm (***Matus-Amat et al., 2004***) demonstrated that CCR5 Tg mice showed robust memory deficits (***Figure 4B***, $t_{(26)}$ = 3.71 p=0.001, Student's *t*-test). Similar results were also obtained with a multi-day fear conditioning training procedure (***Figure 4—figure supplement 1A***).

WT and CCR5 Tg mice were also trained in the Morris water maze, and probe tests were given after 3 days of training. In the probe test only WT mice, but not CCR5 Tg mice spent more time in the target quadrant than the other three quadrants [***Figure 4C***, Two-way ANOVA with repeated measure, Overall (genotype × quadrant%) interaction: $F_{(3,102)}$ = 3.42; Main effect of quadrant%: $F_{(3,102)}$ = 21.44; Between the target quadrant and all other quadrants for WT mice: ***p<0.001, Bonferroni post-tests; Target quadrant percentage between WT and *Ccr5* transgenic group: $t_{(34)}$ = 2.33 *p<0.05, Student's *t*-test]. CCR5 Tg mice also had higher average proximity from the platform and less target platform crossing compared to WT mice (***Figure 4—figure supplement 1B***), indicating that CCR5 overexpression results in spatial memory deficits. When a second probe test was given after extended training, both WT and CCR5 Tg mice spent more time in the target quadrant than the other three quadrants (***Figure 4—figure supplement 1C***), demonstrating that with extended training CCR5 Tg mice also learned the water maze task. Altogether, the results presented demonstrate a critical role for CCR5 in learning and memory.

We tested whether CCR5 overexpression changes either MAPK or CREB signaling in CCR5 Tg mice after fear conditioning. Compared to their WT controls, CCR5 Tg mice show similar phosphorylated p44/42 MAPK levels at baseline or after fear conditioning training (***Figure 4—figure supplement 2A, B and C***). Although CCR5 Tg mice and their WT controls have similar phosphorylated

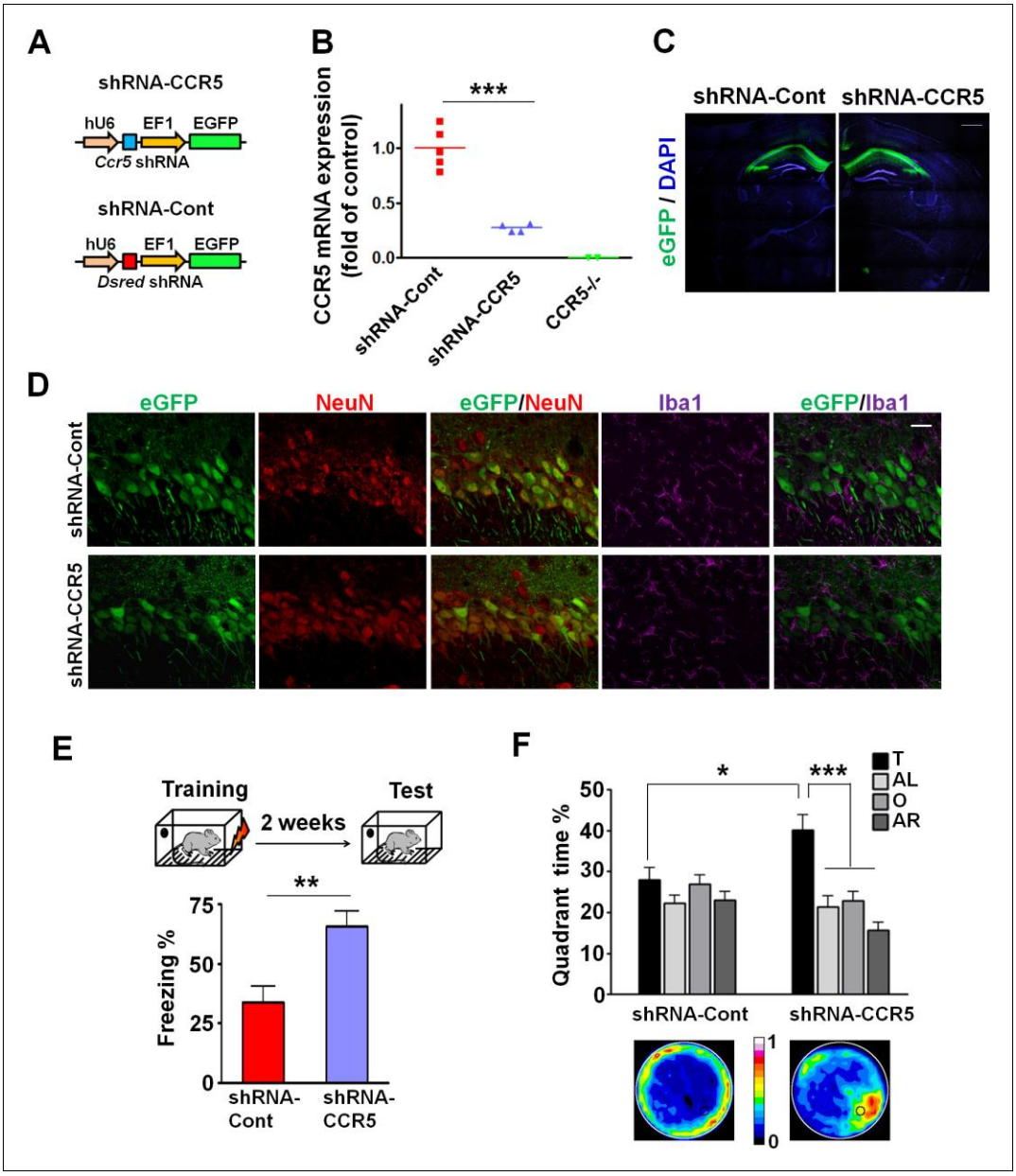

Figure 3. *Ccr5* knockdown in the adult hippocampus results in enhanced memory. (**A**) Schematics of the shRNA-CCR5 and shRNA-dsRed (shRNA-Cont) plasmids. (**B**) AAV containing shRNA-CCR5 or shRNA-Cont was injected into the hippocampus CA1/CA2 region, and dorsal CA1/CA2 *Ccr5* mRNA was measured one-month after virus injection. Compared to shRNA-Cont, shRNA-CCR5 triggered a significant reduction in *Ccr5* mRNA expression (***p<0.001, student's *t*-test). Also, $Ccr5^{-/-}$ mice showed no *Ccr5* mRNA expression in hippocampus. (**C**) AAV containing shRNA-CCR5 or shRNA-Cont

Figure 3 continued on next page

Figure 3 continued

was injected into the hippocampus. One month after virus injection, brain slices were stained with DAPI (nuclear labeling) and GFP (virus infection). Scale bar, 500 μm. (**D**) AAV containing shRNA-CCR5 or shRNA-Cont was injected into the hippocampus. One month after virus injection, brain slices were stained with GFP (virus infection), NeuN (neurons), and Iba1 (microglia). GFP was exclusively expressed in neurons. Scale bar, 20 μm. (**E**) AAV containing shRNA-CCR5 or shRNA-Cont was injected into the hippocampus, and mice were subjected to behavioral testing one month after virus injection. In the fear conditioning test, shRNA-CCR5 mice showed enhanced contextual memory when compared to those injected with shRNA-Cont virus (shRNA-cont n = 7, shRNA-CCR5 n = 10; **p<0.01, Student's *t*-test). (**F**) In the probe test given after two days of water maze training, only shRNA-CCR5 mice but not shRNA-Cont mice spent significantly more time in the target quadrant than the other three quadrants (shRNA-cont n = 22; shRNA-CCR5 n = 20; *p<0.05, Student's *t*-test; ***p<0.001, Two-way ANOVA with repeated measure). Heat maps below the bar graphs show the combined traces of the mice from each group during the probe test. shRNA-Cont mice showed a pattern of wall-hugging swim after two days training, but they learned the water maze task with extended training (***Figure 3—figure supplement 1D***). Error bars indicate SEM.

DOI: 10.7554/eLife.20985.012

The following figure supplement is available for figure 3:

Figure supplement 1. shRNA-CCR5 knockdown efficiency in HEK 293 cells, AAV infection specificity, and mice performance in the water maze probe test 2.

DOI: 10.7554/eLife.20985.013

CREB levels at baseline (***Figure 4—figure supplement 3A***), CCR5 Tg mice show decreased phospho-CREB levels at 3 hr after fear conditioning training (***Figure 4—figure supplement 3C***). Because of the critical role of CREB in memory consolidation (***Bourtchuladze et al., 1994***; ***Guzowski and McGaugh, 1997***), these results suggest that the memory deficits caused by CCR5 overexpression in excitatory neurons are due to deficits in memory consolidation processes mediated by CREB (***Silva et al., 1998***).

Ccr5$^{+/-}$ mice display faster experience-dependent plasticity in the barrel cortex

To test the hypothesis that CCR5 may also be a neuronal suppressor of neocortical sensory plasticity, we studied experience-dependent plasticity in the barrel cortex. Trimming all of whiskers except for D1 produces both an increase in the responses of layer 2/3 (L2/3) cells located in deprived barrel-columns to stimulation of the spared D1 whisker, and an increase in the size of the spared whisker's representation in the barrel cortex (***Fox, 1992***). Experience-dependent plasticity was assayed by measuring the single unit spike responses to the spared D1 whisker of single L2/3 neurons located in the deprived barrels surrounding the D1 barrel (***Figure 5A***). Although 7-days of single whisker experience is insufficient to produce experience-dependent potentiation in WT barrel cortex (***Glazewski and Fox, 1996***), three measures indicated faster potentiation in *Ccr5*$^{+/-}$ mice. First, penetrations in barrels surrounding D1 revealed potentiated responses to D1 stimulation in *Ccr5*$^{+/-}$ but not WT mice (***Figure 5A***). Second, a comparison of each cell's response to the spared versus deprived principal whisker response (vibrissae dominance) showed plasticity in *Ccr5*$^{+/-}$ (***Figure 5C***, deprived versus undeprived $t_{(21)}$ = 3.222 p<0.01, Student's *t*-test) but not in WT mice (***Figure 5B***, deprived versus undeprived, $t_{(11)}$ = 1.663, p>0.05). Third, a plot of D1 response versus principal whisker (PW) response showed points above the identity line (D1>PW) only for *Ccr5*$^{+/-}$ but not WT mice (***Figure 5D***). Comparison of the time course of vibrissae dominance also showed a significant increase in WVDI in *Ccr5*$^{+/-}$ mice (0.396 ± 0.051), but not in WT mice (0.111 ± 0.011) after 7 days deprivation [***Figure 5E***; Interaction: $F_{(2,41)}$ = 1.398, genotype, $F_{(1,41)}$ = 8.919, days deprived $F_{(2,41)}$ = 10.20, genotype and deprivation period are significant: t = 3.05, p<0.05, Bonferroni post-tests]. These results demonstrate that *Ccr5*$^{+/-}$ mice show faster plasticity in the barrel cortex.

Ccr5$^{+/-}$ mice display greater probability and magnitude of LTP in barrel cortical neurons

To investigate whether *Ccr5*$^{+/-}$ mice also show enhanced synaptic plasticity in the barrel cortex, a spike-timing dependent protocol was used to induce low levels of LTP in L2/3 cells of WT mice. Whole cell recordings were performed in L2/3 and field stimulation was applied to L4 in the same cortical column (***Figure 6A***), and LTP was induced using a 5 ms pre-post interval as described previously (***Kaneko et al., 2010***). In WT mice, L2/3 cells showed significant LTP in just 20% of cases while in *Ccr5*$^{+/-}$ and *Ccr5*$^{-/-}$ mice the same protocol produced LTP in 70% of cases (***Figure 6B***, χ^2 = 15.63,

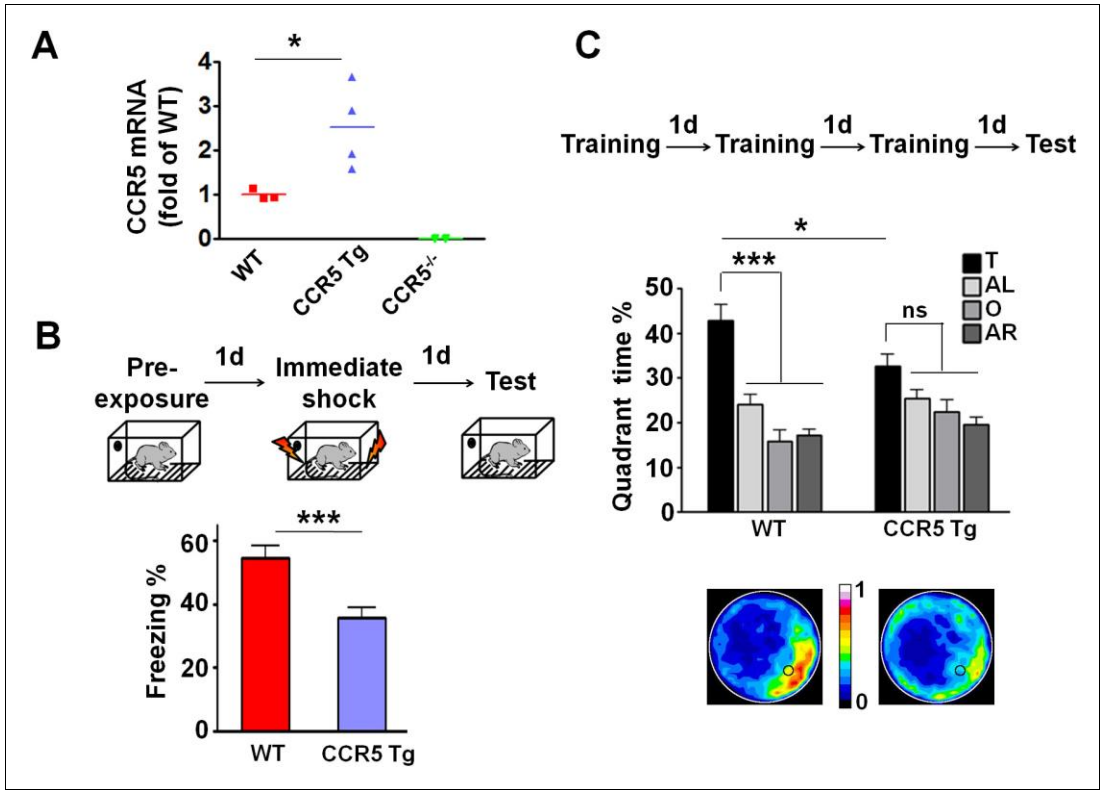

Figure 4. CCR5 overexpression leads to learning and memory deficits. (**A**) Compared to WT mice, CCR5-overexpressing transgenic (Tg) mice showed enhanced *Ccr5* mRNA expression in the hippocampus. (**B**) In a context pre-exposure fear-conditioning paradigm, CCR5 Tg mice showed contextual memory deficits compared to WT mice (WT n = 13, CCR5 Tg n = 15; ***p<0.001, Student's *t*-test). (**C**) In the probe test given after 3 days of training in water maze, only WT mice but not CCR5 Tg mice, spent significantly more time in the target quadrant than the other three quadrants; CCR5 Tg mice also had lower searching times in the target quadrant than WT mice, indicating a learning and memory deficit (WT n = 18, CCR5 Tg n = 18; *p<0.05, Student's *t*-test; ***p<0.001, Bonferroni post-tests, Two-way ANOVA with repeated measure). Error bars indicate SEM.

DOI: 10.7554/eLife.20985.014

The following figure supplements are available for figure 4:

Figure supplement 1. CCR5 overexpression leads to learning and memory deficits.

DOI: 10.7554/eLife.20985.015

Figure supplement 2. Hippocampal p44/42 MAPK signaling of WT and CCR5 transgenic (Tg) mice.

DOI: 10.7554/eLife.20985.016

Figure supplement 3. Hippocampal CREB signaling of WT and CCR5 transgenic (Tg) mice.

DOI: 10.7554/eLife.20985.017

p<0.001, χ-squared test). On average, the WT mice did not show LTP, while the *Ccr5*$^{+/-}$ and *Ccr5*$^{-/-}$ mice showed 188.1 ± 1.45% and 164.5 ± 22.5% potentiation, respectively (***Figure 6C***).

Ccr5$^{+/-}$ mice display lower release probability, and smaller and less frequent mEPSPs in barrel cortical neurons

Previous studies with HRas^{G12V} mice suggest that an increase in ocular dominance plasticity, as well as in learning and memory, is accompanied by a lower synaptic release probability in the cortex

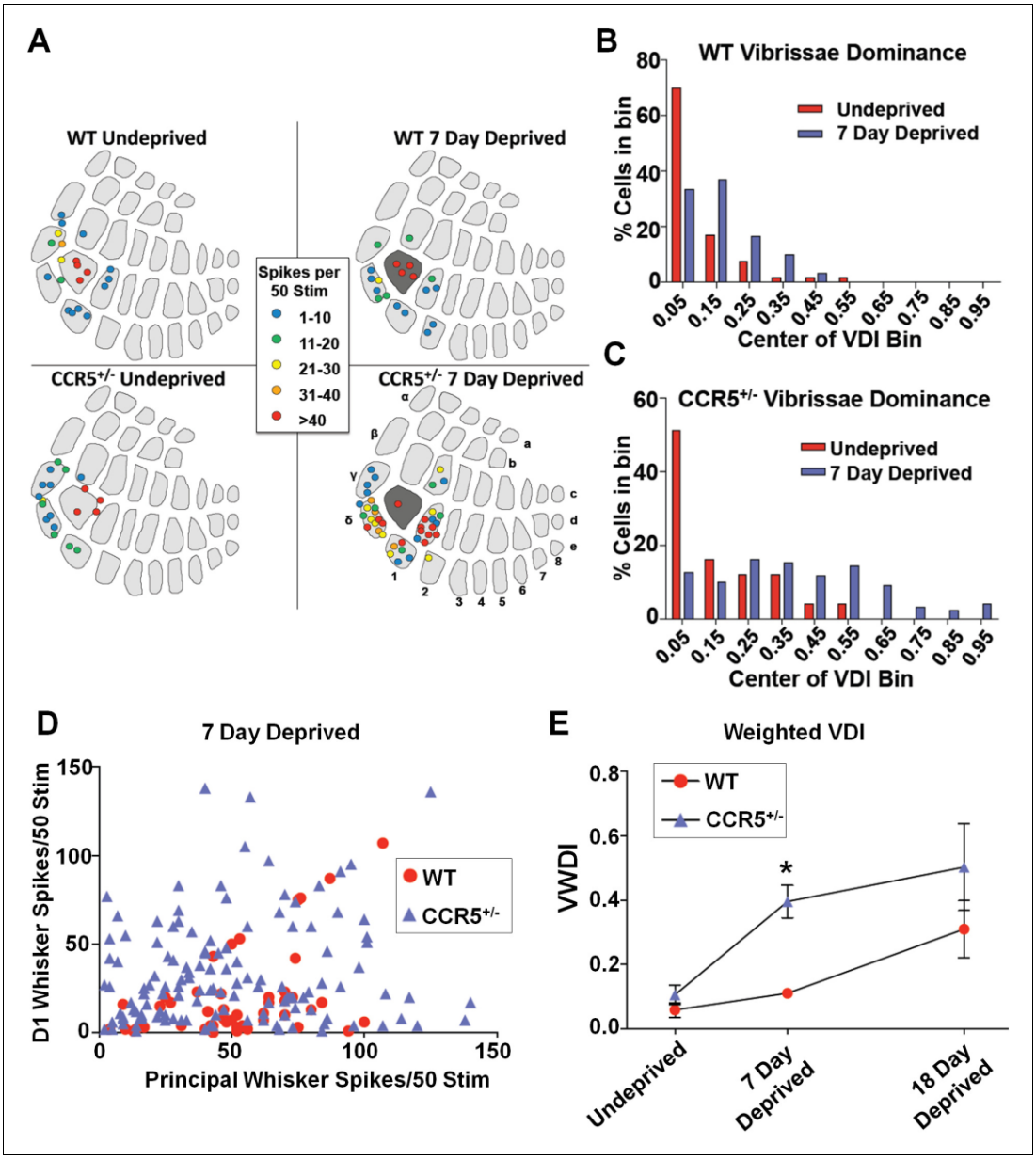

Figure 5. *Ccr5*$^{+/-}$ mice display accelerated experience dependent plasticity. (**A**) Recording locations plotted on a standard barrel field map. The barrel shaded dark grey indicates the principal barrel for the spared whisker. The color of each circle represents the average response to D1 whisker stimulation (spikes per 50 stimulations) for cells in L2/3. Deprived *Ccr5*$^{+/-}$ mice showed greater proportion of penetrations responding strongly to D1 stimulation (WT: control vs deprived, p>0.99;*Ccr5*$^{+/-}$: control vs deprived, p=0.0019, binomial test). (**B**) Vibrissae dominance histograms. Vibrissae

Figure 5 continued on next page

Figure 5 continued

dominance is calculated as D1/(PW + D1) and sorted into 10 bins (see Materials and methods). In WT mice, there is very little shift in the dominance histogram after 7 days of deprivation (n = 14). (**C**) The vibrissae dominance histogram shows a substantial shift right toward D1 dominance in the D1-spared *Ccr5*$^{+/-}$ mice (blue) compared with undeprived *Ccr5*$^{+/-}$ mice (red) (n = 24; p<0.01, Student's *t*-test). (**D**) The value of the response to D1 stimulation is plotted against the same L2/3 cell's response to principal whisker (PW) stimulation for mice subject to 7 days deprivation. A large number of *Ccr5*$^{+/-}$ (but not WT) cells lie above the unity line. (**E**) The average weighted vibrissae dominance index (WVDI) is plotted against deprivation period for WT and *Ccr5*$^{+/-}$ mice. Naïve WT and *Ccr5*$^{+/-}$ mice do not exhibit differences in their vibrissae dominance, however after 7 days deprivation there is an increase in WVDI in *Ccr5*$^{+/-}$ mice but not in WT mice (7-day WT vs *Ccr5*$^{+/-}$ mice: p=0.0030, ANOVA, Bonferroni post-tests). Error bars indicate SEM.
DOI: 10.7554/eLife.20985.018

(***Kaneko et al., 2010***; ***Kushner et al., 2005***). Therefore, we investigated the release probability in the barrel cortex of WT, *Ccr5*$^{+/-}$ and *Ccr5*$^{-/-}$ mice, by measuring the attenuation rate of NMDA receptor mediated evoked EPSPs (***Figure 7A***) in the presence of the activity-dependent NMDA receptor

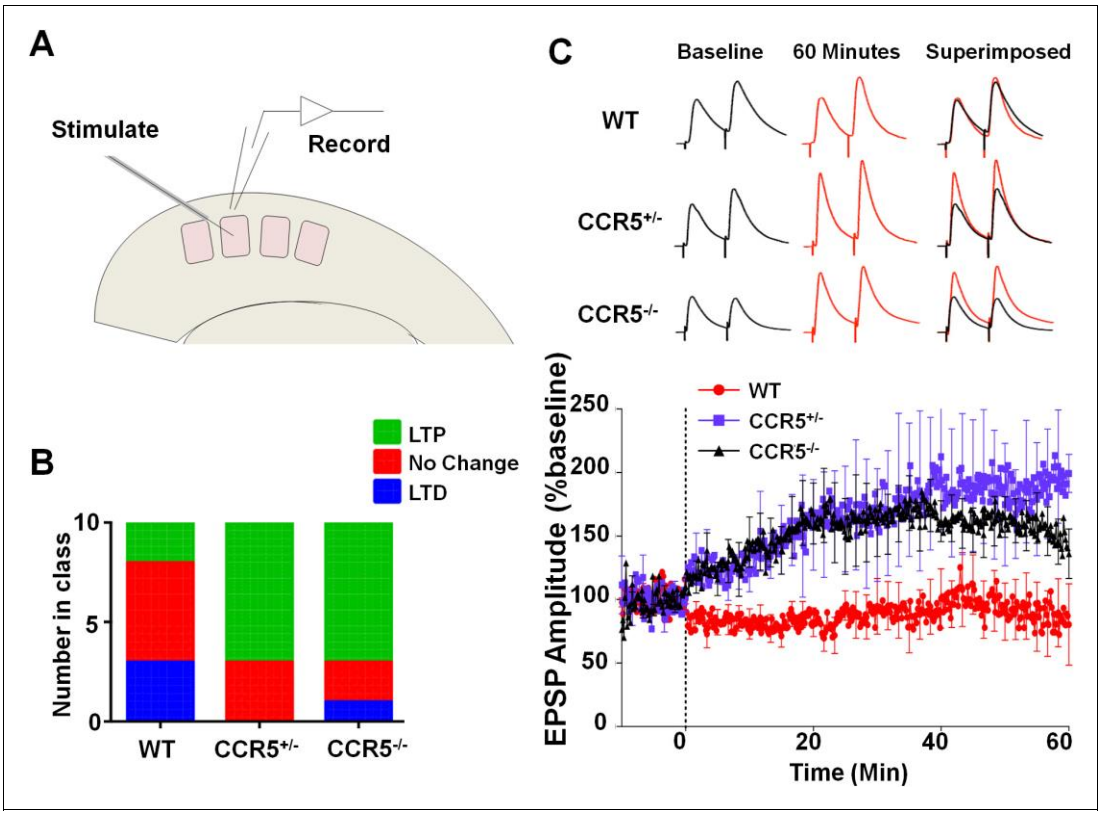

Figure 6. *Ccr5* knockout mice exhibit a higher probability of LTP than WT Mice. (**A**) Schematic of LTP in vitro recordings. Whole-cell patch clamp recordings were made from pyramidal cells in L2/3 of the barrel cortex. A stimulating electrode was placed in the center of the barrel immediately below the recording site and the columnar projection from L4 to L2/3 was stimulated. (**B**) When LTP was induced with a spike-timing dependent protocol with a low probability of potentiation in WT mice, *Ccr5*$^{+/-}$ and *Ccr5*$^{-/-}$ mice showed a higher incidence of LTP (70% LTP in *Ccr5*$^{+/-}$ and *Ccr5*$^{-/-}$ mice vs 20% in WT, p<0.001, χ-squared test). (**C**) Mean amplitude of LTP. Failures and successes are averaged together to give an overall average of all recordings. *Ccr5*$^{+/-}$ and *Ccr5*$^{-/-}$ cells had larger LTP than WT cells which on average did not potentiate (n = 10 per group).
DOI: 10.7554/eLife.20985.019

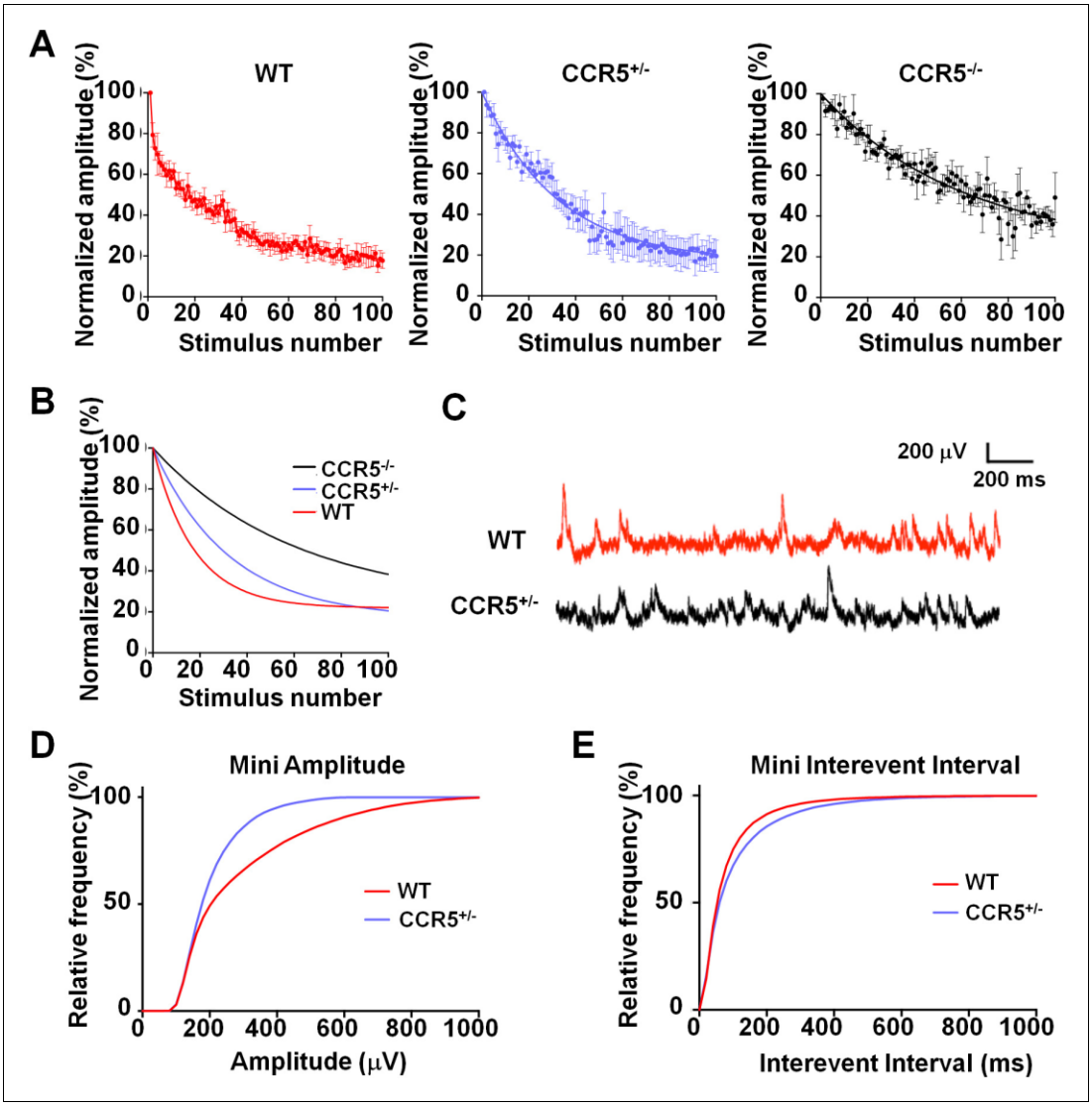

Figure 7. *Ccr5* knockout mice exhibit lower release probability, and smaller, less frequent mEPSPs than WT mice. (**A**) Cells from *Ccr5*$^{+/-}$and *Ccr5*$^{-/-}$ mice exhibited lower release probability than cells from WT mice. Traces represent normalized amplitude of NMDA-receptor mediated evoked EPSPs in the presence of the use-dependent antagonist MK-801. A faster decrease in the peak EPSP amplitude is indicative of a higher release probability. (**B**) Single exponential curves were fitted for the data presented in panel **A**, and *Ccr5*$^{+/-}$ and *Ccr5*$^{-/-}$ mice demonstrated lower P_r than WT mice (n = 10 per group; p<0.01, Kruskal-Wallis test). (**C**) Example miniature EPSPs recordings from WT and *Ccr5*$^{+/-}$ mice. (**D**) Cells from *Ccr5*$^{+/-}$ mice displayed smaller mEPSPs than WT (WT n = 10, *Ccr5*$^{+/-}$ n = 10; p<0.001, K-S test). (**E**) Cells from *Ccr5*$^{+/-}$ mice displayed less frequent mEPSPs than WT and therefore greater inter-event intervals (WT n = 10, *Ccr5*$^{+/-}$ n = 10;p<0.001, K-S test).

DOI: 10.7554/eLife.20985.020

antagonist MK-801 (**Hessler et al., 1993**). The release probability was significantly lower in *Ccr5*$^{+/-}$ and *Ccr5*$^{-/-}$ mice (**Figure 7B**, p<0.01, Kruskal-Wallis test). Consistent with this finding, mEPSPs (**Figure 7C**) in L2/3 cells of *Ccr5*$^{+/-}$ mice were smaller (**Figure 7D**, $D_{(52)}$ = 0.6154 p<0.001, K-S test) and occurred at a lower frequency compared to WT mice (**Figure 7E**, $D_{(21)}$ = 0.9524 p<0.001, K-S test). Both effects could create greater 'headroom' for LTP and experience-dependent potentiation in *Ccr5* knockout mice.

Viral knockdown of *Ccr5* expression in adult barrel cortex results in enhanced experience dependent plasticity

To check whether the *Ccr5*$^{+/-}$ plasticity phenotype in the barrel cortex was dependent on a developmental effect, we also injected shRNA-CCR5 or shRNA-Cont AAV into the barrel cortex of adult C57BL/6N mice. Immuno-histochemistry confirmed that the virus exclusively infected neurons (**Figure 8A** and **Figure 8—figure supplement 1**, 35% infection rate and 100% co-localization of NeuN and GFP). Only shRNA-CCR5 mice, but not shRNA-Cont mice, exhibited a shifted vibrissae dominance histogram after 7 days of single whisker experience (**Figure 8B**, $t_{(10)}$ = 6.485 p<0.001, Student's *t*-test). Knockdown of *Ccr5* in the adult barrel cortex resulted in an experience-dependent plasticity phenotype that closely mirrored that of the *Ccr5*$^{+/-}$ mice (**Figure 8C**, *Ccr5*$^{+/-}$ mice $t_{(20)}$ = 2.939 p<0.01, Student's *t*-test; viral knockdown: $t_{(10)}$ = 6.485 p<0.001, Student's *t*-test), demonstrating that CCR5 is a suppressor of neocortical plasticity acting directly on neurons in the adult brain.

Ccr5 knockout prevents V3 peptide-induced signaling, plasticity and memory deficits

Our molecular, electrophysiological, sensory plasticity and behavioral results demonstrate that CCR5 is a suppressor for plasticity and learning and memory. Therefore, it is possible that acute activation of CCR5 by HIV coat proteins could contribute to deficits in neuroplasticity and thereby learning and memory. To explore this hypothesis, we tested whether the HIV gp120 V3 loop peptide results in plasticity and learning deficits, and whether CCR5 is responsible for these deficits. The HIV gp120 V3 loop peptide contains the gp120 domain that binds to and activates CCR5 (**Cormier and Dragic, 2002**; **Galanakis et al., 2009**; **Morikis et al., 2007**; **Sirois et al., 2005**). Immunoprecipitation with anti-HA-agarose, to co-precipitate V3-HA peptide and CCR5 in mouse hippocampal lysates, demonstrated that V3 peptide binds to mouse hippocampal CCR5 (**Figure 10—figure supplement 1**).

To examine the effects of V3 peptide on neuroplasticity and the possible role of CCR5 in this, we repeated the cortical LTP study shown in **Figure 6** after pre-incubation for one hour with either 200 pM V3 peptide fragment or saline (control). In cells from WT mice, V3 treatment had a strong effect on the magnitude and probability of LTP (**Figure 9A,B**), completely abolishing any instance of LTP and producing an average depression of 27.8% ($t_{(120)}$ = 26.6, p<0.001, Student's *t*-test). Cells from *Ccr5*$^{+/-}$ mice still displayed a similar proportion of LTP (75% V3-treated vs 62.5% control, **Figure 9D**) but showed significantly lower potentiation than in control conditions (127% V3 vs 208% control, **Figure 9C**, $t_{(120)}$ = 42.2, p<0.001, Student's *t*-test). In contrast, cells from mice lacking CCR5 (*Ccr5*$^{-/-}$ mice) were not affected by V3 treatment at all, with higher probability of LTP (86% V3 vs 66% control, **Figure 9F**) and a similar magnitude of potentiation (186% V3 vs 182% control, **Figure 9E**). Similar effects of V3 treatment on plasticity were observed in hippocampal slices from WT mice and *Ccr5* knockout mice. Analyses of hippocampal slices, that had been pre-incubated 1 hr with 200 pM V3 peptide, revealed Schaffer collateral fEPSPs LTP deficits between 50 and 60 min post-TBS (theta burst stimulation) in WT (**Figure 9G**, $t_{(14)}$ = 2.53, p<0.05, Student's *t*-test), but not from *Ccr5*$^{+/-}$ (**Figure 9H**, $t_{(13)}$ = 1.74, p=0.105, Student's *t*-test) and *Ccr5*$^{-/-}$ mice (**Figure 9I**, $t_{(12)}$ = 0.994, p=0.340, Student's *t*-test). These results demonstrate that V3 peptide causes LTP deficits both in barrel cortex and hippocampus.

To examine the effect of V3 peptide on learning and memory, mice received a single hippocampal V3 peptide infusion (concentration 2 µg/µl, 1 µl peptide to each hemisphere with the infusion speed of 0.1 µl/min) either 30 min before or immediately after contextual fear conditioning (**Figure 10A**). When injected 30 min before fear conditioning, V3 peptide caused contextual memory deficits in C57BL/6N mice (**Figure 10B**, $t_{(10)}$ = 4.04, p<0.01, Student's *t*-test). In contrast, V3 peptide infusions following training did not affect contextual fear memory (**Figure 10C**, $t_{(18)}$ = 0.92, p=0.37,

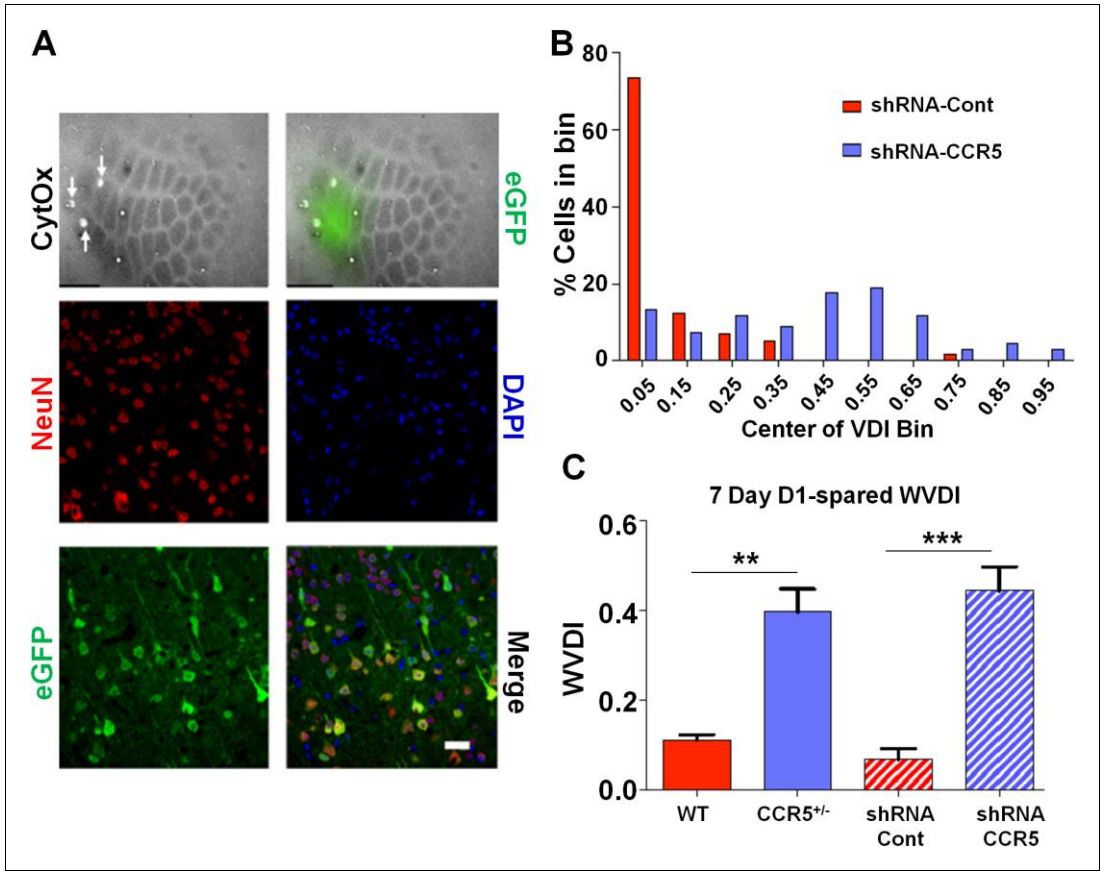

Figure 8. Viral knockdown of *Ccr5* in barrel cortex enhances experience-dependent plasticity. (**A**) Specificity and spread of viral infection. Interleaved slices processed for cytochrome oxidase (CytOx) confirmed viral location (GFP) over the recorded area of the barrel cortex. Arrows show lesions marking recording penetrations. Confocal images of the neuronal marker (NeuN) and viral expression (GFP) suggest that the shRNA is expressed exclusively in neurons. Scale bar = 20 μm. (**B**) Vibrissae dominance histogram after 7 days D1-spared single-whisker experience. Compared to control group, knockdown of *Ccr5* leads to a shifted histogram (shRNA-cont n = 6; shRNA-CCR5 n = 6; p<0.001, Student's *t*-test). (**C**) Weighted VDI values comparing $Ccr5^{+/-}$ mice with viral knockdowns. Viral knockdown has a similar effect to that of constitutive mutants after 7 days deprivation. Error bars indicate SEM.

DOI: 10.7554/eLife.20985.021

The following figure supplement is available for figure 8:

Figure supplement 1. Specificity of viral infection in the barrel cortex.

DOI: 10.7554/eLife.20985.022

Student's *t*-test), indicating that the V3 peptide must be present during training to disrupt learning and memory.

When V3 peptide was infused into the hippocampus of WT, $Ccr5^{+/-}$ or $Ccr5^{-/-}$ mice 30 min before training (***Figure 10D***), the V3-induced memory deficit was prevented by the $Ccr5^{+/-}$ or $Ccr5^{-/-}$ mutation [***Figure 10E***; Two-way ANOVA, overall (genotype × treatment) interaction: $F_{(2,50)} = 1.0$; Main effect of treatment: $F_{(1,50)} = 11.10$, Post hoc linear contrast: WT/Cont versus WT/V3, $t_{(50)} = 3.25$ p<0.01, Bonferroni post-tests]. To examine whether decreasing *Ccr5* expression specifically in

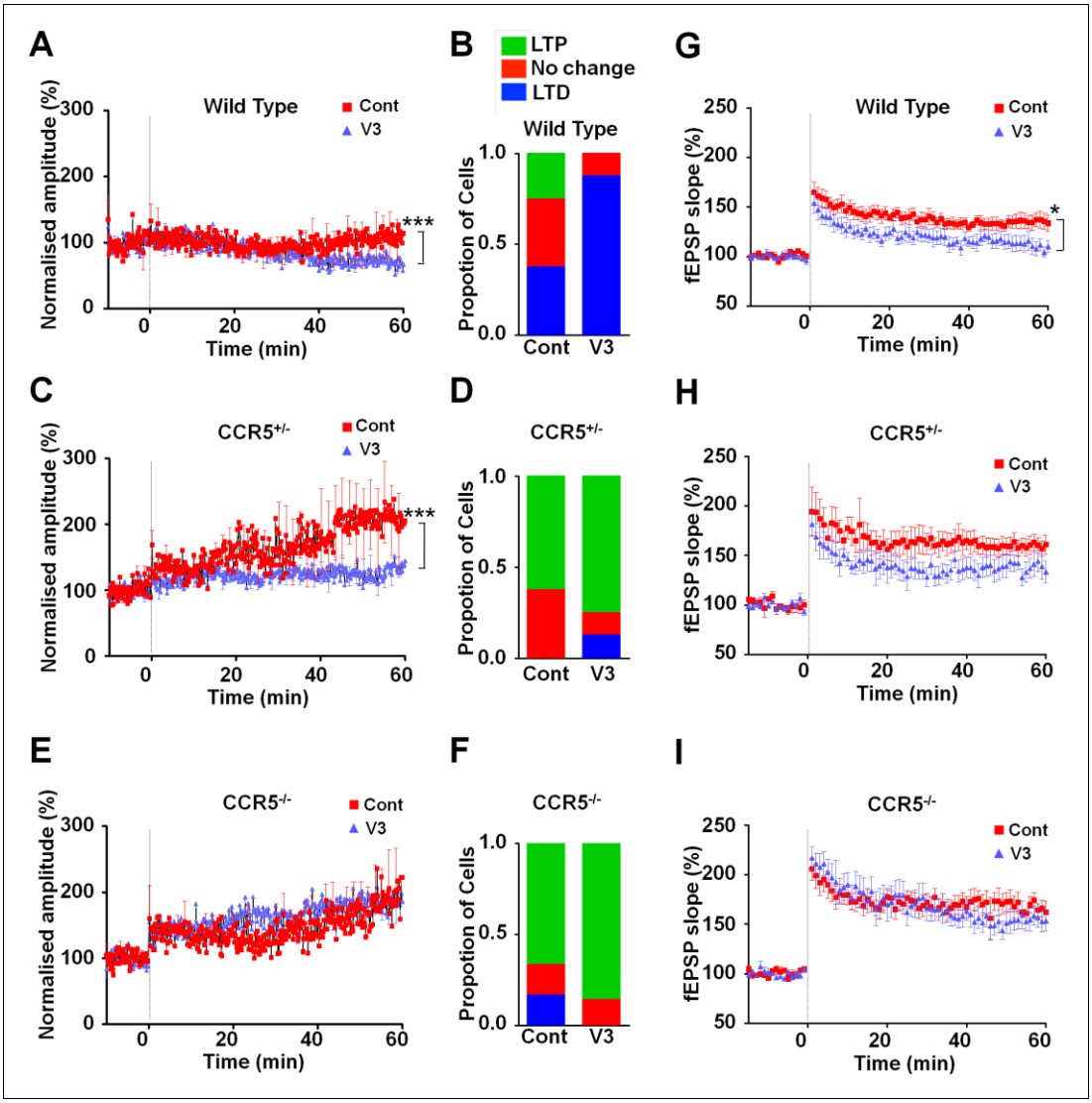

Figure 9. *Ccr5* knockout prevents gp120 V3 peptide induced long-term potentiation deficits both in hippocampus and in barrel cortex. (**A**) Whole-cell patch clamp recordings were made from pyramidal cells in L2/3 of the barrel cortex of WT mice. When LTP was induced with a spike-timing dependent protocol, in control conditions the trace showed no significant potentiation, while V3 peptide treatment caused significant depression (n = 8 for both Control and V3; ***p<0.001, Student's *t*-test). (**B**) WT control cells showed equal proportions of LTP, LTD and no change; In contrast, 7 out of 8 V3-treated cells showed LTD. (**C**) Cells from *Ccr5*$^{+/-}$ mice showed strong LTP under control conditions, while V3-treated cells show significantly reduced LTP (n = 8 for both Control and V3; ***p<0.001, Student's *t*-test). (**D**) Although LTP magnitude was reduced in V3-treated cells, the proportion of cells undergoing potentiation in slices from *Ccr5*$^{+/-}$ mice was similar to control. (**E**, **F**) Both control cells and V3-treated cells from *Ccr5*$^{-/-}$ mice showed strong potentiation, with no significant difference in amplitude and in the probability of LTP (Control n = 6, V3 n = 7; p=0.25). (**G**) Hippocampal CA1 fEPSPs were recorded in hippocampal slices before (baseline) and after 5 TBS (theta bursts stimulation). V3 peptide resulted in LTP deficits in the fEPSP measured during the last 10 min of recordings in hippocampal slices from WT mice (n = 8 for both Control and V3; *p<0.05, Student's *t*-test). (**H**, **I**) V3

Figure 9 continued on next page

Figure 9 continued

peptide treatment had no significant effect on *Ccr5*$^{+/-}$ (control n = 8, V3 n = 7; p=0.105, Student's *t*-test) and *Ccr5*$^{-/-}$ mice (control n = 7, V3 n = 7, p=0.340, Student's *t*-test). Error bars indicate SEM.

DOI: 10.7554/eLife.20985.023

hippocampus is sufficient to block V3-induced memory deficit, shRNA-Cont or shRNA-CCR5 AAV was injected to the hippocampus, and two weeks later, V3 peptide was infused into the hippocampus, and mice were trained 30 min after V3 peptide infusion. Similar to the effects in WT mice, V3 peptide caused memory deficits in shRNA-Cont mice. Importantly, these deficits were prevented by hippocampal *Ccr5* knockdown [***Figure 10F***; Two-way ANOVA, overall (shRNA virus × treatment) interaction: $F_{(1,34)}$ = 0.61; Main effect of treatment: $F_{(1,34)}$ = 7.19; Post hoc linear contrast: shRNA-Cont/Cont versus shRNA-Cont/V3, $t_{(34)}$ = 2.45 p<0.05; shRNA-Cont/Cont versus shRNA-CCR5/Cont, $t_{(34)}$ = 2.55 p<0.05; shRNA-Cont/V3 versus shRNA-CCR5/V3, $t_{(34)}$ = 3.50 p<0.01, Bonferroni post-tests], demonstrating that CCR5 is an in vivo target for the V3 peptide-dependent memory deficits.

Since our results indicate that CCR5 regulates MAPK/CREB signaling, we next determined whether an acute injection of the V3 peptide into the dorsal hippocampal CA1 area results in deficits in MAPK or CREB activation after learning (***Figure 11A***). P44/42 pMAPK and pCREB levels in the dorsal hippocampal CA1 subregion (***Lein et al., 2004***) were measured 1 hr or 3 hr after learning, respectively. Compared to controls, V3 peptide resulted in a significant decrease in pMAPK (***Figure 11B***, $t_{(11)}$ = 2.71 p<0.05, Student's *t*-test), but had no effect on pCREB (***Figure 11C***). A similar decrease in pMAPK was observed when the V3 peptide was infused into the hippocampus of mice injected with shRNA-Cont AAV. Importantly, this decrease in pMAPK activation after learning was ameliorated by hippocampal *Ccr5* knockdown [***Figure 11D***; Two-way ANOVA, overall (shRNA virus × treatment) interaction: $F_{(1,28)}$ = 0.35; Main effect of treatment: $F_{(1,28)}$ = 11.8, Post hoc linear contrast: shRNA-Cont/Cont versus shRNA-Cont/V3, $t_{(28)}$ = 2.85 p<0.05; shRNA-Cont/V3 versus shRNA-CCR5/V3, $t_{(28)}$ = 2.48 p<0.05, Bonferroni post-tests]. Interestingly, unlike the *Ccr5*$^{+/-}$ mice, that showed enhanced pMAPK activation after learning (***Figure 2B***), compared to shRNA-Cont mice, mice injected with shRNA-CCR5 AAV did not show enhanced pMAPK, probably because in these mice *Ccr5* was knocked down in only the subset of hippocampal neurons transfected by the AAV virus. Altogether, these results indicate that decreasing CCR5 protects against the acute deficits caused by V3 peptide on hippocampal MAPK signaling, synaptic plasticity, and learning and memory, a result consistent with the idea that CCR5 activation contributes to the cognitive deficits triggered by HIV proteins.

Discussion

CCR5 is a chemokine receptor that plays an important role in inflammatory responses. A learning and memory reverse genetic screen showed that the *Ccr5* knockout results in enhanced learning and memory for contextual fear conditioning. This phenotype was confirmed in other learning and memory tasks including the water maze and social recognition. Importantly, the *Ccr5* knockout did not affect a number of behaviors that could have confounded the learning and memory findings, including anxiety, activity, social interaction, cued conditioning, and shock reactivity. This enhancement in learning and memory is consistent with increases in plasticity at the systems and cellular levels. In the barrel cortex, *Ccr5* knockout results in dramatically accelerated experience-dependent plasticity: *Ccr5*$^{+/-}$ mice showed robust experience-dependent sensory plasticity at a time point (7-days after whisker removal) when WT mice show no evidence of plasticity. Importantly, temporally and spatially restricted knockdown of *Ccr5,* specifically in adult hippocampus or barrel cortex, also resulted in enhancements in learning and memory as well as experience-dependent plasticity, demonstrating that these effects are not due to changes during development.

MAPK and CREB have been implicated in learning and memory (***Bourtchuladze et al., 1994***; ***Roth and Sweatt, 2008***). Our results indicate that the *Ccr5* knockout did not alter MAPK or CREB signaling under baseline conditions. However, *Ccr5* knockout resulted in an increase in MAPK and CREB signaling levels at 1- and 3 hr after training, respectively. Enhanced MAPK or CREB signaling have been associated with enhancements in learning and memory. For example, HRas^{G12V} mice have enhanced MAPK levels following training, and show increases in LTP and sensory plasticity, as

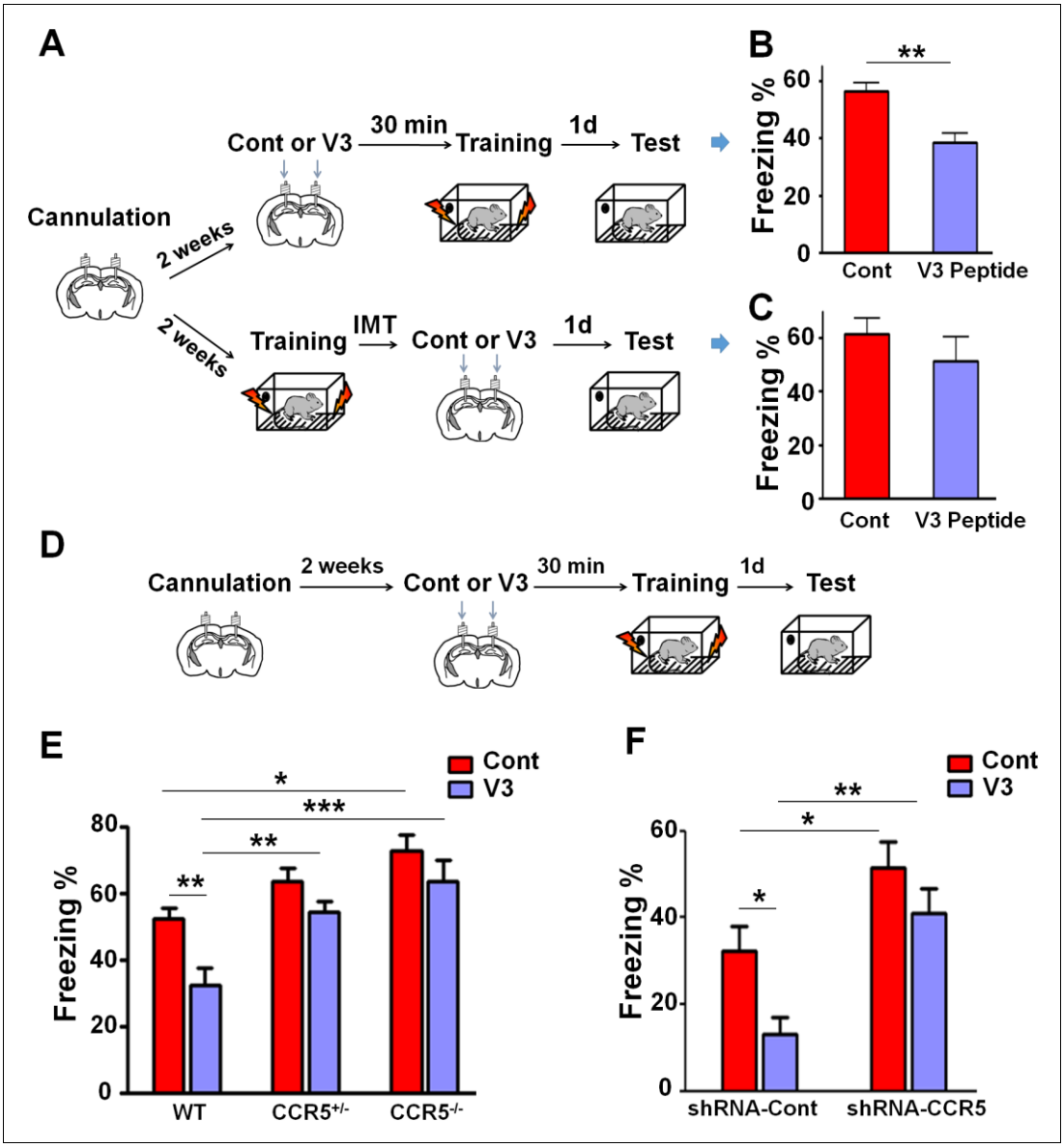

Figure 10. Both *Ccr5* knockout and knockdown protect against gp120 V3 peptide induced memory deficits. (**A**) Schematic of V3 peptide infusion and fear conditioning for the experiments shown in **B** and **C**. (**B**) 30 min after V3 peptide infusion into hippocampus, C57BL/6N mice were trained with fear conditioning. V3 peptide caused contextual memory deficits (Cont n = 6, V3 n = 6; **p<0.01, Student's *t*-test). (**C**) When V3 peptide was infused into hippocampus immediately after fear conditioning training, no difference was observed between the control group and the V3 peptide group (Cont n = 10, V3 n = 10). (**D**) Schematic for experiments shown in **E** and **F**. (**E**) 30 min after V3 peptide infusion into hippocampus, mice were trained with fear conditioning. V3 peptide caused contextual memory deficits in WT mice, but *Ccr5* knockout protected against V3-induced memory deficits (WT/Cont

Figure 10 continued on next page

Figure 10 continued

n = 10, WT/V3 peptide n = 11, *Ccr5*$^{+/-}$/Cont n = 8, *Ccr5*$^{+/-}$/V3 peptide n = 11, *Ccr5*$^{-/-}$/Cont n = 8, *Ccr5*$^{-/-}$/V3 peptide n = 8; *p<0.05, **p<0.01, ***p<0.001, Two-way ANOVA). (**F**) V3 peptide caused contextual fear conditioning memory deficits in mice injected with shRNA-Cont AAV, but hippocampal *Ccr5* knockdown protected against V3-induced memory deficits (shRNA-Cont/Cont n = 10, shRNA-Cont/V3 n = 9, shRNA-CCR5/Cont n = 10, shRNA-CCR5/V3 n = 9; *p<0.05, **p<0.01, Two-way ANOVA). Error bars indicate SEM.

DOI: 10.7554/eLife.20985.024

The following figure supplement is available for figure 10:

Figure supplement 1. V3-HA peptide binds to hippocampal CCR5.

DOI: 10.7554/eLife.20985.025

well as enhancements in learning and memory tested in a number of tasks (***Kaneko et al., 2010***; ***Kushner et al., 2005***); Similarly, enhanced CREB signaling is also associated with memory enhancements in multiple tasks and model systems (***Czajkowski et al., 2014***; ***Kathirvelu and Colombo, 2013***; ***Zhou et al., 2009***) and in barrel cortex plasticity (***Barth et al., 2000***; ***Glazewski et al., 1999***).

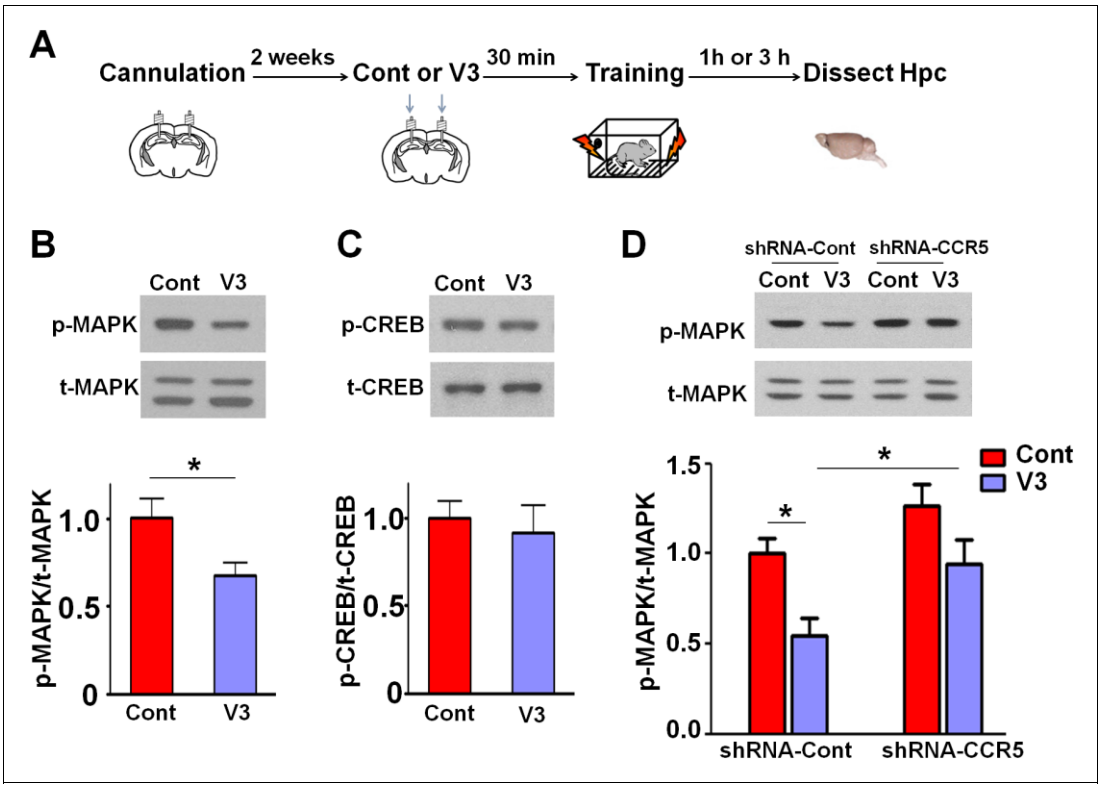

Figure 11. *Ccr5* knockdown ameliorates hippocampal p44/42 MAPK signaling deficits caused by V3 peptide treatment. (**A**) The dorsal hippocampal CA1 subregion was extracted 1 hr after training. V3 peptide reduced p44/42 pMAPK levels at 1 hr after fear conditioning (Cont n = 6, V3 n = 7; *p<0.05, Student's *t*-test). (**B**) V3 peptide had no effect on pCREB when dorsal hippocampal CA1 subregion was extracted 3 hr after fear conditioning (Cont n = 5, V3 n = 6). (**C**) V3 peptide reduced p44/42 pMAPK in the dorsal CA1 of mice injected with shRNA-Cont virus at 1 hr after fear conditioning, but *Ccr5* knockdown ameliorated the decrease in p44/42 pMAPK levels observed after learning (n = 8 for each group; *p<0.05, Two-way ANOVA). Error bars indicate SEM.

DOI: 10.7554/eLife.20985.026

Altogether, these results indicate that increases in MAPK and CREB signaling are integral to the learning and memory enhancements in the *Ccr5* knockout mice.

Ccr5 knockout mice show enhanced long-term synaptic plasticity changes both in hippocampus and barrel cortex. For example, our spike pairing protocol in the cortex induced LTP 20% of the time in WT mice and 70% of the time in the *Ccr5* knockout mice. Our neocortical studies also showed that similar to $HRas^{G12V}$ mice (**Kaneko et al., 2010**; **Kushner et al., 2005**), $Ccr5^{+/-}$ mice also have lower release probability and lower mini-amplitudes. The initial conditions present at the synapses of $Ccr5^{+/-}$ mice thereby create the headroom for greater pre- and post-synaptic potentiation at the synapse, both of which are important components of plasticity (**Dachtler et al., 2011**; **Hardingham and Fox, 2006**). Together with the increased responsiveness of the MAPK/CREB signaling pathway, the naive state of the synapse under CCR5 hypo-function creates a potent mix for increased synaptic potentiation.

In agreement with the enhanced learning and memory with manipulations that decrease CCR5, transgenic mice that overexpress CCR5 in excitatory neurons show learning and memory deficits, demonstrating that CCR5 acts as a suppressor for plasticity and memory. Although a previous study (**Lee et al., 2009**) reported learning and memory deficits in aged CCR5 mutants, this study used aged mice (12–18 month old) and the control mice with a different genetic background. Our CCR5 transgenic results suggested that CCR5 activation by viral proteins, and subsequent plasticity and memory suppression, may contribute to HIV associated impairments in cognition.

A recent study reported that transgenic mice overexpressing an HIV viral protein (gp120) showed neuronal degeneration and subsequent behavioral deficits that could be ameliorated by a *Ccr5* mutation (**Maung et al., 2014**). Similarly, multiple doses of gp120 in rats also resulted in physiological and cognitive deficits (**Tang et al., 2009**). Interestingly, our study shows that acute treatment (one injection 30 min before training) of HIV gp120 V3 loop peptide, which is known to bind and activate CCR5 in the brain (**Chan et al., 1999**; **Shah et al., 2006**; **Sirois et al., 2005**), was sufficient to induce deficits in a key cellular mechanism for learning and memory (LTP) and also in hippocampus-dependent learning and memory in WT mice. Remarkably, these deficits were prevented by either a viral-mediated *Ccr5*-knockdown or by a *Ccr5* knockout mutation. The V3 loop is important for HIV binding to CCR5 or CXCR4, and LTP deficits caused by the V3 loop peptide had been reported to be blocked by a CXCR4 antagonist (**Dong and Xiong, 2006**). Nevertheless, our results show that both in the barrel cortex and in hippocampus, the LTP deficits caused by the V3 peptide are prevented by the homozygous *Ccr5* mutation, demonstrating that CCR5 plays a critical role in the V3-induced deficits in neuroplasticity. CCR5 antagonists and inhibitors have shown efficacy in reduction of viral load in clinical studies (**Fätkenheuer et al., 2005**; **Gulick et al., 2008**). Our findings support the application of brain permeable CCR5 antagonists, not only as a combination drug in antiretroviral (ARV) therapy, but also as a treatment for cognitive deficits caused by HIV coat proteins.

Previous studies showed that the establishment of long-lasting synaptic changes and long-term memory requires the removal of inhibitory constraints on MAPK/CREB signaling (**Abel et al., 1998**). Our findings with *Ccr5* knockout, region-specific viral knockdown, and neuronal CCR5 over-expression demonstrate that CCR5 functions as a plasticity and memory suppressor by acting on the MAPK/CREB signaling pathway. Our results also suggest that the inappropriate activation of this suppressor by HIV coat proteins contributes to cognitive deficits. Since decreasing CCR5 function leads to robust increases in plasticity and memory, CCR5 provides a novel target for cognitive enhancement, and for the development of treatments for cognitive deficits.

Materials and methods

Subjects

3-month old C57BL/6N and *Ccr5* knockout ($Ccr5^{-/-}$) mice were purchased from Taconic Farms (Germantown, NY) and tested in a reverse genetic screen (**Figure 1—figure supplement 1**). $Ccr5^{-/-}$ mice were then bred with C57BL/6N mice to generate $Ccr5^{+/-}$. Experimental WT, $Ccr5^{+/-}$, and $Ccr5^{-/-}$ mice (3 to 5 months old) were generated by intercrossing $Ccr5^{+/-}$ mice. Littermates were used for all experiments (except the initial reverse genetic screen). Experimental *Ccr5*-overexpressing transgenic mice were generated and maintained in the C57BL/6N background. $Yfp^{+}/Ccr5^{+/-}$ mice were

generated by breeding male Thy1-YFP mice with female *Ccr5*$^{+/-}$ mice, and 3 to 6 months old Yfp^{+}/*Ccr5*$^{+/-}$ mice and their littermates Yfp^{+}/*Ccr5*$^{+/+}$ (Yfp^{+}/WT) mice were used for the spine density experiment. 10-week-old male C57BL/6N mice were purchased from Taconic Farms (Germantown, NY) for shRNA-cont or shRNA-CCR5 AAV injections and for the V3 loop peptide experiments. Mice were group housed with free access to food and water, and maintained on a 12:12 hr light:dark cycle. All experiments were performed during the light phase of the cycle. All studies were approved by the Animal Research Committee at UCLA and University of Cardiff and carried out in compliance with the United Kingdom's Animals (Scientific Procedures) Act 1986 where applicable.

Fear conditioning

For the reverse genetic screen for remote memory phenotypes, mice were subjected to a training session with a total time of 8 min. The mice were allowed to explore the training chamber for 2 min, and then 3 tone-shock pairs (2 s 0.75 mA shock co-terminated with 30 s tone) were delivered and the 3 tones started at 2, 3 and 4 min. Two weeks after training, the mice were first returned to chambers (context B) which were different from the training chambers (context A) for the cued memory test (tone test), and 90 min later mice were returned to the training chamber for a 5 min test to assess contextual memory. Standard Z scores were used to present the results of the memory screen, which combine both freezing and suppression of activity ratios (SR) scores from the same mice. Suppression of activity ratios (SR) were calculated as SR=(test activity)/(test activity + baseline activity). Z scores for the entire wild type population were calculated as Z score=(individual-population mean)/standard deviation, and the expected value is a mean of 0 and a standard deviation of 1. Z scores for each mutant were calculated as: Z score= average[(%Freezing individual–%Freezing population mean)/(standard deviation of population), (−1)*(SR individual–SR population mean)/(standard deviation of the population)]. So Z scores reflect alterations in both freezing and activity suppression caused by different genetic mutations, with simplified comparisons and improved reliability (***Matynia et al., 2008***).

To test contextual memory for *Ccr5* knockout or knockdown mice, the mice were subjected to a training session with a total time of 5 min. Mice were allowed to explore the training chamber for 2 min, and then 3 shocks (2 s, 0.75 mA) were delivered at 2, 3 and 4 min. To test contextual memory for CCR5 transgenic mice, the mice were either subjected to a daily weak training for 5 days, or to a context pre-exposure fear-conditioning paradigm. During the daily weak conditioning, the mice were allowed to explore the training chamber for 25 s, and then a 1 s, 0.4 mA shock were delivered and mice were removed for the training box 5 s after the shock. The freezing levels during the 25 s period before the shock were used to measure contextual memory. For the context pre-exposure fear conditioning, the mice were pre-exposed to the training context for 7 min on day 1. The mice were brought back to the same context on day 2, and 10 s later received 3 shocks (0.75 mA) with 5 s interval between the 3 shocks. The mice were removed from the training boxes 40 s after the last shock. On day 3, the mice were tested for 5 min in the same training context.

Morris water maze

In the hidden version of the Morris water maze, mice were trained with two blocks per day for 5 days and each block consisted of two trials with 30 s interval between the trials. In each trial, mice were given 60 s to find the platform. If mice found the platform earlier than 60 s, the trial ended then. If mice failed to find the platform, the trial terminated at 60 s. After each trial, mice were put on the platform for 15 s (*Ccr5*$^{+/-}$ and shRNA-CCR5 mice) or 20 s (CCR5 transgenic mice). Probe tests with a time of 60 s were administered after two days of training (*Ccr5*$^{+/-}$ and shRNA-CCR5 mice and their controls) or after three days of training (CCR5 transgenic mice and their controls). Testing at day 2 maximized our ability to see enhancements, while testing at day 3 maximized our ability to see deficits. To examine whether mice from different groups were able to learn the Morris water maze task with extended training, a second probe test was performed after five days of training. Mice showing floating behavior during training or probe test were excluded from further training or from data analysis. Floating behavior was judged by mouse swimming speed, and mice with a swimming speed lower than (average speed – 2 × SD (standard deviation)) were excluded.

Social recognition

Mice were handled for 3 days (2 min handling each day) before social recognition task. During the 3-day social recognition task, mice were first habituated to the testing chamber for 10 min on day 1. On day 2, mice were placed back into the same chamber and habituated for 5 min, and then were allowed to interact for 7 min with an ovariectomized (OVX) female mouse placed under a wired cylinder (training session). On day 3, mice were placed back into the same chamber and habituated for 5 min, and then were allowed to interact with two OVX females (one familiar and one novel) for 5 min (test session). The time mice spent on exploring (sniffing) the OVX mice were hand scored by experimenters blinded of mouse genotypes and of familiar or novel OVX mice.

Open field

Mice were placed in a novel open field (28 cm × 28 cm × 25 cm), and were allowed to explore it for a period of 20 min. The total distance mice traveled, and percentage time mice spent in the peri- or center region of the open field were analyzed.

Elevated plus maze

Mice were placed on an elevated plus maze and were allowed to explore it for 5 min. The elevated plus maze has two open arms and two close arms (with walls of 16.5 cm height), and each arm is 29 cm long and 8 cm wide. The percentage of time mice spent in the open arms, and open arm entry times were analyzed.

Ccr5 knockdown efficiency measurement

To measure *Ccr5* knockdown efficiency, HEK 293 cells were co-transfected with CCR5-tdTomato plus either shRNA-CCR5 or shRNA-Cont (dsRed) plasmids. HEK293 cells were ordered from ATCC (CRL-1573) and were tested with Mycoplasma Detection Kit (R&D Systems, CUL001B) to make sure there was no contamination. One day after plasmid transfection, cells were imaged to examine the effect of shRNA-CCR5 on CCR5-tdTomato expression. *Ccr5* knockdown efficiency was also tested by measuring *Ccr5* mRNA expression in the hippocampus one month after the injection of AAV containing shRNA-cont or shRNA-CCR5. To measure *Ccr5* mRNA expression, tissue samples were collected from the dorsal hippocampus and total RNA was extracted by RNeasy Mini Kit (Qiagen, Valencia, CA, USA) and treated with DNase (Qiagen). Total RNA was first reverse-transcribed into cDNA using oligo (dT) primers and Superscipt III First-Strand Synthesis System (Invitrogen, Carlsbad, CA, USA), and was then quantified by qPCR. The following primer sequences were used for the *Ccr5* qPCR: 5'GCTGCCTAAACCCTGTCATC 3'(forward) and 5'GTTCTCCTGTGGATCG GGTA3' (reverse). The ribosome protein RPL13A was used as a housekeeping control.

Immunoblotting for hippocampal samples

Dorsal hippocampus was homogenized with RIPA buffer (Sigma, St. Louis, MO, R0278) supplemented with protease inhibitor cocktail (Sigma, P8340), phosphatase inhibitor cocktail 2 (Sigma, P5726), phosphatase inhibitor cocktail 3 (Sigma, P0044), and 0.5% SDS. After measuring protein concentration with the BCA protein assay kit (Pierce, Rockford, IL, 23225), protein samples were loaded to NuPAGE Novex 4–12% Bis-Tris protein gel (ThermoFisher Scientific, Carlsbad, CA, NP0336BOX), and after separation, proteins were transferred onto polyvinylidene difluoride (PVDF) membranes. The PVDF membranes were blocked with 5% nonfat milk at room temperature for 1 hr and then probed with primary antibodies (phospho-CREB, Cell Signaling 9198, 1:4000 dilution; phospho-p44/42 MAPK, Cell Signaling 9101, 1:10,000 dilution) at 4°C overnight. Membranes were then incubated with secondary antibodies for 1 hr and developed with ECL solutions. The phospho-CREB or phospho- p44/42 MAPK primary antibodies was stripped with Restore western blot stripping buffer (ThermoFisher Scientific, 21059). After stripping, the PVDF membranes were blocked with 5% nonfat milk at room temperature for 1 hr and then probed with primary antibodies (CREB, Cell Signaling 9197, 1:1000 dilution; p44/42 MAPK, Cell Signaling 9102, 1:4000 dilution) at 4°C overnight. Membranes were then incubated with secondary antibodies for 1 hr and developed with ECL plus solutions and scanned with Typhoon 9410 imager and quantified with imageJ.

Immunostaining for hippocampal samples

Mice were transcardially perfused with 4% PFA (4% paraformaldehyte in 0.1 M phosphate buffer) and after perfusion brains were extracted and incubated with 4% PFA overnight at 4˚C. Coronal sections were cut at 50 µm on a microtome and transferred to PBS, then blocked in 5% Normal Goat Serum in 0.1 M PBS and 0.1% TritonX-100 for 1 hr. After blocking sections were incubated in a primary antibody mix (in 0.1 M PBS, 0.2% TritonX-100 and 5% Normal Goat Serum) of rabbit anti-GFP (Abcam AB6556, 1:500 dilution), mouse anti-Neun (Chemokon, MAB377, 1:1000), and rabbit anti-GFAP (Dako Z0334, 1:500) or rabbit anti-Iba1 (Wako 019–19741, 1:500) for two days at 4˚C. After 3 × 15 min washes in 0.1 M PBS and 0.1% TritonX-100 the secondary antibodies were applied (in 0.1 M PBS, 0.2% TritonX-100 and 3% Normal Goat Serum): Alexa488 goat anti-rabbit (Invitrogen A-11034, 1:500 dilution), Alexa568 goat anti-rabbit (Invitrogen A-11011, 1:500 dilution), and Alexa647 goat anti-mouse (Invitrogen A-21235, 1:500 dilution). Slices were incubated in the secondary mix for 2 hr at room temperature. After 2 × 15 min washes in 0.1 M PBS and 0.1% TritonX-100, slices were incubated with 4',6-diaminodino-2-phenylindole (DAPI, Life Technologies D-21490, 1:2000) for 15 min, and then were further washed with 0.1 M PBS and 0.1% TritonX-100 for 15 min before mounted onto slides with ProLong Gold antifade mounting media (Life Technologies, P36934). All immunostaining images were acquired with a Nikon A1 Laser Scanning Confocal Microscope (LSCM).

Immunostaining for cortical samples

Candidate mice were transcardially perfused, as described in the in vivo electrophysiology section, three weeks after injection of AAV. Fixed brains were removed and stored whole in 20% sucrose PBS after 24 hr postfix in 4% formaldehyde/20% sucrose PBS. Coronal sections were cut at 40 µm on a freezing microtome and transferred to PBS, then blocked in 5% Normal Goat Serum in 0.1 M PBS and 0.1% TritonX-100 for 1 hr. After blocking sections were incubated in a primary antibody mix (in 0.1 M PBS, 0.1% TritonX-100 and 3% Normal Goat Serum) of chicken polyclonal anti-GFP (Abcam AB13970, 1:500 dilution) and mouse monoclonal anti-NeuN (Millipore MAB377, 1:100 dilution) for 2 hr at room temperature, 18 hr overnight at 4˚C and a further 2 hr at room temperature. After 3 × 30 min washes in 0.1 M PBS and 0.1% TritonX-100 the secondary antibodies were applied (in 0.1 M PBS, 0.1% TritonX-100 and 3% Normal Goat Serum): Alexa488 goat anti-chicken (Life Technologies A11039, 1:200 dilution) and Alexa594 goat anti-mouse (Life Technologies A11032, 1:200 dilution). Slices were incubated in the secondary mix for 3.5 hr at room temperature, and then after a further 3 × 20 min washes in 0.1 M PBS and 0.1% TritonX-100 were mounted in Vectashield DAPI hardset (Vector H1500). The same protocol was applied to tangential slices alternating with slices stained for cytochrome oxidase to localise viral spread across barrels. Coronal sections were visualized using a Leica TCS SP2 confocal microscope and tangential sections were visualized with an Olympus BX61 microscope in both epifluorescent and transmissive brightfield modes. Colocalisation of staining in confocal images was automatically quantified with Imaris F1 7.7.2 (Bitplane, Zurich, Switzerland).

Hippocampal viral injection surgery

To knockdown *Ccr5* in pyramidal fields of the hippocampus, high titers of Adeno-associated virus (AAV) engineered to knock-down *Ccr5* with an shRNA approach (shRNA-Cont or shRNA-CCR5 viruses, 0.7 µl, 1 × 10^{13} unit/ml) were stereotaxically injected into the hippocampal CA1 sub region of 3 months old C57Bl/6Tac mice through a 30-gauge Hamilton microsyringe at four sites at the following coordinates relative to bregma (mm): AP: −1.8, ML: ±0.8, DV: −1.6; or AP: −2.5, ML: ±2, DV: −1.6). After infusion, the microsyringe was left in place for an additional 5 min to ensure full virus diffusion. After surgery, mice were treated with antibiotics and their health was monitored every day for two weeks.

Hippocampal V3 peptide infusion

To infuse V3 loop peptide (CTRPNYNKRKRIHIGPGRAFYTTKNIIGTIRQAHC, Disulfide Bridge: 1–35) into hippocampus, two cannula were implanted at the following coordinates relative to bregma (mm): AP: −2.1, ML: ±1.7, DV: −1.6. Two weeks after cannulation, either at 30 min before fear conditioning training or immediately after training, mice were anesthetized and saline (control) or V3 peptide (concentration 2 µg/µl) was infused into hippocampus with the infusion speed 0.1 µl/min and 1

µl solution to each hemisphere. After infusion, the injector was left in place for an additional 5 min to ensure full diffusion.

V3-HA peptide immunoprecipitation

V3-HA peptide (CTRPNYNKRKRIHIGPGRAFYTTKNIIGTIRQAHCGYPYDVPDYA, Disulfide Bridge: 1–35, from GenScript) and hippocampal CCR5 binding was detected with Pierce co-Immunoprecipitation (Co-IP) kit. Mouse hippocampal tissue was prepared with IP Lysis/Wash Buffer, and was mixed with anti-HA-agarose (Sigma) and incubated overnight at 4˚C with or without V3-HA peptide. After elution, the samples were detected with CCR5 antibody (Santa Cruz Biotechnology) with western blot.

Cortical viral injection surgery

To knockdown *Ccr5* in the barrel cortex, subjects (C57Bl/6N mice; Taconic Farms, Ry, Denmark) aged 2–3 months at time of surgery were anaesthetized with ketamine/xylazine (80/6 mg/kg) and immobilized in a stereotaxic frame (David Kopf Instruments, Tujunga, CA) with a thermostatically controlled heating blanket (Harvard Instruments). The left parietal cranium was exposed and kept moist with sterile cortex buffer. A dental drill was used to make a small craniotomy over the likely location of the D1/D2 barrel (from bregma: AP: −1.5, ML: ±3), the dura resected with a 30 G hypodermic needle and a pulled sharp bevelled glass pipette attached to a Hamilton syringe (Esslab, Essex, UK) was carefully inserted to a depth of 300 µm (DV: −0.3). After 2–3 min 100 nl of high-titre (1×10^{13} unit/ml) AAV was injected over a 5 min period. Fast green was added to the virus to allow visual confirmation of the injection. The incision was closed with sutures and mice were allowed to recover for three weeks before starting the deprivation protocol.

In vivo electrophysiology

Subjects

Mice aged between P50 and P90 were anesthetized with isoflurane and maintained by urethane (1.5 g/kg body weight i/p) plus a trace amount of acepromazine. Supplemental doses of urethane (10% of the initial dose) were administered as required to maintain anaesthesia depth. Analgesic (lidocaine) was applied to the ears and scalp. Deprived vibrissae were replaced by attaching the corresponding contralateral whisker to the trimmed stub with cyanoacrylate adhesive. Naïve mice had their whiskers acutely cut and re-attached to minimize mechanical differences between cohorts.

Surgery

Mice were immobilized in a stereotaxic frame (Narashige, Japan) and body temperature maintained at 37˚C with a thermostatically controlled heating blanket (Harvard Apparatus, Kent, UK). A 2 × 2 mm section of the left parietal cranium was thinned with a dental drill over the barrel cortex (0–2 mm caudal from bregma and 2–4 mm lateral from midline). Before each penetration a small fleck of bone was removed from the recording site with a 30 G hypodermic needle just large enough to introduce the electrode.

Recordings

Recordings were made from barrels corresponding to the spared whisker and its immediate surrounding deprived barrels using carbon fibre microelectrodes. Action potentials were isolated with a window discriminator to provide single-unit recordings, recorded with a Neurolog system (Digitimer, Welwyn Garden City, UK) and digitised with a CED 1401 and Spike2 software (CED, Cambridge, UK) running on a Windows PC.

Stimulation of whiskers was performed with a 3 × 3 matrix piezo-electric stimulator (Cardiff University Mechanical Engineering Centre) driven by a CED 3901 piezo amplifier (CED, Cambridge, UK). Stimuli were applied as a trapezoidal ramp with 10 ms rise time, 10 ms plateau and 10 ms return time, peak deflection was 300 µm (20˚ whisker deflection). Receptive fields were mapped using pseudorandom sequences in blocks of 10 (9 whiskers and one blank field) at 5 Hz (***Jacob et al., 2010***, ***2012***).

Histology

Recording sites were confirmed by histology. After each penetration a small lesion (1 µA DC for 10 s, tip negative) was made at 350 µm estimated depth. At the end of the experiment the mouse was deeply anaesthetized and transcardially perfused with 0.1 M phosphate-buffered saline, followed by 4% formaldehyde in PBS. The brain was carefully removed after fixation and the cortex flattened between two glass slides as previously described (***Strominger and Woolsey, 1987***). After 24 hr postfix in 4% formaldehyde and 20% sucrose in PBS flattened cortices were transferred to 20% sucrose in PBS until sectioning. Tangential sections (35 µm) were cut on a freezing microtome and reacted with diaminobenzidine and cytochrome C to stain for cytochrome oxidase activity (***Wong-Riley, 1979***). This procedure allows for clear identification of the barrels and confirmation of the recording site.

In vitro electrophysiology

Slicing procedure

Mice aged between P50 and P60 were killed by cervical dislocation, decapitated and the brain quickly removed and cooled in ice-cold dissection buffer (in mM: 108 choline-Cl, 3 KCl, 26 $NaHCO_3$, 1.25 NaH_2, PO_4, 25 D-glucose, 3 Na-pyruvate, 1 $CaCl_2$, 6 $MgSO_4$, 285 mOsm) bubbled with 95% O_2/5% CO_2. Coronal slices (350 µm thick) were cut on a vibrating microtome (Microm HM650V, Thermo Fisher, Cheshire, UK) and transferred to a holding chamber containing normal artificial CSF (in mM: 119 NaCl, 3.5 KCl, 1 NaH_2PO_4, 10 D-glucose, 2 $CaCl_2$, 1 $MgSO_4$, 300 mOsm) bubbled with 95% O_2/5% CO_2. Slices were incubated at 32˚C for 45 min after slicing, then returned to room temperature until recording.

Recordings

Whole cell recordings were performed at 35–37˚C. Barrels were identified in slices under bright field illumination using an Olympus BX50WI microscope. Pyramidal neurons were identified using DIC optics. Recording pipettes (4–10 MΩ) were pulled from borosilicate glass (Clark GC150-F10, Harvard Apparatus, UK) and filled with a potassium gluconate-based recording solution (in mM: 110 K-gluconate, 10 KCl, 2 $MgCl_2$, 2 Na_2ATP, 0.03 Na_2GTP, 10 HEPES, pH 7.3, 270 mOsm). LII/III pyramidal cells were selected for their characteristic regular spiking behavior under depolarizing current. Recordings were aborted if Vm deviated spontaneously by more than 5 mV, or access resistance deviated by more than 20% during the recording. An Axon Multiclamp 700 B (Molecular Devices, Sunnyvale, CA) in current clamp mode was used as the patch amplifier and signals were telegraphed to and digitised by a CED 1401 with Signal software (CED, Cambridge, UK) running on a Windows PC.

LTP experiments

A tungsten monopolar stimulating electrode was placed centrally to a selected barrel in layer IV and suitable pyramidal neurons were identified in the area vertically above the stimulating electrode. Once a whole cell recording was established extracellular stimulus was applied at 0.1 Hz, consisting of a pairs of pulses at 20 Hz. The stimulus was of 0.2 ms duration and 1–35 V intensity, designed to produce a monosynaptic EPSP of 3–6 mV in the postsynaptic cell. After 10 min of baseline recording, LTP was induced by pairing a suprathreshold 2.5 ms somatic depolarizing pulse with a single presynaptic stimulus (5 ms pre-post interval). Four runs of 50 paired stimuli at 2 Hz were delivered at 0.025 Hz. After LTP induction the stimulus paradigm was switched back the same as in the baseline recording and one hour of post-paring data were acquired. EPSP amplitudes were calculated as the peak response above the preceding baseline voltage. Significant potentiation was calculated by comparing mean EPSP amplitude at 50–60 mins after LTP induction with mean baseline EPSP amplitude using Student's t-test.

Release probability experiments

The position of the recording and stimulating electrodes were identical to those for the LTP experiments. Once the recordings were established the perfusion solution was switched to magnesium-free ACSF and an NMDA-receptor mediated response was isolated by the addition of 20 µM CNQX to the bath solution. Single extracellular stimuli were delivered at 0.1 Hz. After a stable baseline had been established, stimulation was halted and 10 µM MK-801 was washed onto the slice for 10 min.

Stimulation was then resumed as before and at least 100 further stimulus trials were recorded, still in the presence of MK-801 and CNQX in Mg-free ACSF. Single and double-exponential fits of the response amplitude over time were performed with GraphPad Prism 5 and 6 (GraphPad, La Jolla, CA). The rate of decrease in the NMDAr-mediated EPSPs is directly related to the release probability of synapses in the observed pathway.

mEPSP recordings

Recordings were made in layer II/III pyramidal cells. Miniature AMPA receptor-mediated EPSPs were isolated by the bath application of 1 μM tetrodotoxin, 100 μM picrotoxin and 50 μM D-AP5. Action potential blockade was confirmed with the injection of highly-depolarizing square current pulses (0.8–1 nA, 500 ms). 100–500 events were analysed per cell with a template-matching and threshold-crossing method (Axograph X, Berkeley, CA). Well-defined, isolated mEPSPs were identified and used to train a loose-fitting template, with a detection minimum threshold of 2.5 times the RMS baseline noise (***Clements and Bekkers, 1997***). Amplitudes and inter-event intervals were binned and their cumulative distribution compared using a Kolmogorov-Smirnov test.

Statistical analysis

Results are expressed as mean ± s.e.m. Student's *t*-tests were used for statistical comparisons between groups, unless specified (ANOVA analyses, binomial test, Bonferroni post-tests, χ-squared test, Kruskal-Wallis test or K-S test) in the results or figure legends. $p<0.05$ indicates significant difference between groups (significance for comparisons: *$p<0.05$; **$p<0.01$; ***$p<0.001$). Sample sizes were chosen on the basis of previous studies. No statistical methods were used to predetermine the sample size.

Acknowledgements

We thank Ayal Lavi, Adam Frank, Michael Sofroniew, Yan Ao, and Kenta Saito for advice and technical support. We thank Antony Landreth, Anna Matynia, Mika Guzman, Cindy Montes, and Aida Amin for their contribution to the reverse genetic screen. This work was supported by grants from the NIMH (P50-MH0779720) to AJS and KDF, and from the MRC (G0901299) to KDF, and the Dr Miriam and Sheldon G Adelson Medical Research Foundation to AJS.

Additional information

Funding

Funder	Grant reference number	Author
National Institute of Mental Health	P50-MH0779720	Kevin Fox Alcino J Silva
Dr. Miriam and Sheldon G. Adelson Medical Research Foundation		Alcino J Silva
Medical Research Council	G0901299	Kevin Fox

The funders had no role in study design, data collection and interpretation, or the decision to submit the work for publication.

Author contributions

MZ, Conception and design, Acquisition of data, Analysis and interpretation of data, Drafting or revising the article; SG, Conception and design, Acquisition of data, Analysis and interpretation of data, Drafting or revising the article ; SH, YS, SW, YC, MS, Acquisition of data; TKS, Conception and design, Acquisition of data; YN, Contributed unpublished essential data or reagents; DJC, Y-SL, Analysis and interpretation of data; KF, AJS, Conception and design, Analysis and interpretation of data, Drafting or revising the article

Author ORCIDs
Stuart Greenhill, http://orcid.org/0000-0002-5038-5258
Alcino J Silva, http://orcid.org/0000-0002-1587-4558

Ethics

Animal experimentation: All experiments were performed during the light phase of the cycle. All studies were approved by the UCLA Institutional Animal Care and Use Committee, also known as the Chancellor's Animal Research Committee (ARC, protocol# 1998-070), and by University of Cardiff and carried out in compliance with the United Kingdom's Animals (Scientific Procedures) Act 1986 where applicable.

References

Abel T, Martin KC, Bartsch D, Kandel ER. 1998. Memory suppressor genes: inhibitory constraints on the storage of long-term memory. *Science* **279**:338–341. doi: 10.1126/science.279.5349.338, PMID: 9454331

Atkins CM, Selcher JC, Petraitis JJ, Trzaskos JM, Sweatt JD. 1998. The MAPK cascade is required for mammalian associative learning. *Nature Neuroscience* **1**:602–609. doi: 10.1038/2836, PMID: 10196568

Barth AL, McKenna M, Glazewski S, Hill P, Impey S, Storm D, Fox K. 2000. Upregulation of cAMP response element-mediated gene expression during experience-dependent plasticity in adult neocortex. *Journal of Neuroscience* **20**:4206–4216. PMID: 10818156

Bliss TV, Collingridge GL. 1993. A synaptic model of memory: long-term potentiation in the hippocampus. *Nature* **361**:31–39. doi: 10.1038/361031a0, PMID: 8421494

Bourtchuladze R, Frenguelli B, Blendy J, Cioffi D, Schutz G, Silva AJ. 1994. Deficient long-term memory in mice with a targeted mutation of the cAMP-responsive element-binding protein. *Cell* **79**:59–68. doi: 10.1016/0092-8674(94)90400-6, PMID: 7923378

Cartier L, Hartley O, Dubois-Dauphin M, Krause KH. 2005. Chemokine receptors in the central nervous system: role in brain inflammation and neurodegenerative diseases. *Brain Research Reviews* **48**:16–42. doi: 10.1016/j.brainresrev.2004.07.021, PMID: 15708626

Chan SY, Speck RF, Power C, Gaffen SL, Chesebro B, Goldsmith MA. 1999. V3 recombinants indicate a central role for CCR5 as a coreceptor in tissue infection by human immunodeficiency virus type 1. *Journal of Virology* **73**:2350–2358. PMID: 9971818

Chwang WB, O'Riordan KJ, Levenson JM, Sweatt JD. 2006. ERK/MAPK regulates hippocampal histone phosphorylation following contextual fear conditioning. *Learning & Memory* **13**:322–328. doi: 10.1101/lm.152906, PMID: 16741283

Clements JD, Bekkers JM. 1997. Detection of spontaneous synaptic events with an optimally scaled template. *Biophysical Journal* **73**:220–229. doi: 10.1016/S0006-3495(97)78062-7, PMID: 9199786

Cormier EG, Dragic T. 2002. The crown and stem of the V3 loop play distinct roles in human immunodeficiency virus type 1 envelope glycoprotein interactions with the CCR5 coreceptor. *Journal of Virology* **76**:8953–8957. doi: 10.1128/JVI.76.17.8953-8957.2002, PMID: 12163614

Cui Y, Costa RM, Murphy GG, Elgersma Y, Zhu Y, Gutmann DH, Parada LF, Mody I, Silva AJ. 2008. Neurofibromin regulation of ERK signaling modulates GABA release and learning. *Cell* **135**:549–560. doi: 10.1016/j.cell.2008.09.060, PMID: 18984165

Czajkowski R, Jayaprakash B, Wiltgen B, Rogerson T, Guzman-Karlsson MC, Barth AL, Trachtenberg JT, Silva AJ. 2014. Encoding and storage of spatial information in the retrosplenial cortex. *PNAS* **111**:8661–8666. doi: 10.1073/pnas.1313222111, PMID: 24912150

Dachtler J, Hardingham NR, Glazewski S, Wright NF, Blain EJ, Fox K. 2011. Experience-dependent plasticity acts via GluR1 and a novel neuronal nitric oxide synthase-dependent synaptic mechanism in adult cortex. *Journal of Neuroscience* **31**:11220–11230. doi: 10.1523/JNEUROSCI.1590-11.2011, PMID: 21813683

Dash PK, Hochner B, Kandel ER. 1990. Injection of the cAMP-responsive element into the nucleus of aplysia sensory neurons blocks long-term facilitation. *Nature* **345**:718–721. doi: 10.1038/345718a0, PMID: 2141668

Dong J, Xiong H. 2006. Human immunodeficiency virus type 1 gp120 inhibits long-term potentiation via chemokine receptor CXCR4 in rat hippocampal slices. *Journal of Neuroscience Research* **83**:489–496. doi: 10.1002/jnr.20745, PMID: 16400660

Ellis R, Langford D, Masliah E. 2007. HIV and antiretroviral therapy in the brain: neuronal injury and repair. *Nature Reviews Neuroscience* **8**:33–44. doi: 10.1038/nrn2040, PMID: 17180161

Fox K. 1992. A critical period for experience-dependent synaptic plasticity in rat barrel cortex. *Journal of Neuroscience* **12**:1826–1838. PMID: 1578273

Fätkenheuer G, Pozniak AL, Johnson MA, Plettenberg A, Staszewski S, Hoepelman AI, Saag MS, Goebel FD, Rockstroh JK, Dezube BJ, Jenkins TM, Medhurst C, Sullivan JF, Ridgway C, Abel S, James IT, Youle M, van der Ryst E. 2005. Efficacy of short-term monotherapy with Maraviroc, a new CCR5 antagonist, in patients infected with HIV-1. *Nature Medicine* **11**:1170–1172. doi: 10.1038/nm1319, PMID: 16205738

Galanakis PA, Kandias NG, Rizos AK, Morikis D, Krambovitis E, Spyroulias GA. 2009. NMR evidence of charge-dependent interaction between various PND V3 and CCR5 N-terminal peptides. *Biopolymers* **92**:94–109. doi: 10.1002/bip.21127, PMID: 19117029

Galicia O, Sánchez-Alavez M, Méndez Díaz M, Navarro L, Prospero-García O. 2002. [HIV glycoprotein 120: possible etiological agent of AIDS-associated dementia]. *Revista De Investigacion Clinica; Organo Del Hospital De Enfermedades De La Nutricion* **54**:437–452. PMID: 12587419

Glazewski S, Barth AL, Wallace H, McKenna M, Silva A, Fox K. 1999. Impaired experience-dependent plasticity in barrel cortex of mice lacking the alpha and delta isoforms of CREB. *Cerebral Cortex* **9**:249–256. doi: 10.1093/cercor/9.3.249, PMID: 10355905

Glazewski S, Fox K. 1996. Time course of experience-dependent synaptic potentiation and depression in barrel cortex of adolescent rats. *Journal of Neurophysiology* **75**:1714–1729. PMID: 8727408

Gulick RM, Lalezari J, Goodrich J, Clumeck N, DeJesus E, Horban A, Nadler J, Clotet B, Karlsson A, Wohlfeiler M, Montana JB, McHale M, Sullivan J, Ridgway C, Felstead S, Dunne MW, van der Ryst E, Mayer H, MOTIVATE Study Teams. 2008. Maraviroc for previously treated patients with R5 HIV-1 infection. *New England Journal of Medicine* **359**:1429–1441. doi: 10.1056/NEJMoa0803152, PMID: 18832244

Guzowski JF, McGaugh JL. 1997. Antisense oligodeoxynucleotide-mediated disruption of hippocampal cAMP response element binding protein levels impairs consolidation of memory for water maze training. *PNAS* **94**:2693–2698. doi: 10.1073/pnas.94.6.2693, PMID: 9122258

Hall J, Thomas KL, Everitt BJ. 2001. Cellular imaging of zif268 expression in the hippocampus and amygdala during contextual and cued fear memory retrieval: selective activation of hippocampal CA1 neurons during the recall of contextual memories. *Journal of Neuroscience* **21**:2186–2193. PMID: 11245703

Hardingham N, Fox K. 2006. The role of nitric oxide and GluR1 in presynaptic and postsynaptic components of neocortical potentiation. *Journal of Neuroscience* **26**:7395–7404. doi: 10.1523/JNEUROSCI.0652-06.2006, PMID: 16837587

Hessler NA, Shirke AM, Malinow R. 1993. The probability of transmitter release at a mammalian central synapse. *Nature* **366**:569–572. doi: 10.1038/366569a0, PMID: 7902955

Hunt JS, Romanelli F. 2009. Maraviroc, a CCR5 coreceptor antagonist that blocks entry of human immunodeficiency virus type 1. *Pharmacotherapy* **29**:295–304. doi: 10.1592/phco.29.3.295, PMID: 19249948

Jacob V, Estebanez L, Le Cam J, Tiercelin JY, Parra P, Parésys G, Shulz DE. 2010. The matrix: a new tool for probing the whisker-to-barrel system with natural stimuli. *Journal of Neuroscience Methods* **189**:65–74. doi: 10.1016/j.jneumeth.2010.03.020, PMID: 20362614

Jacob V, Petreanu L, Wright N, Svoboda K, Fox K. 2012. Regular spiking and intrinsic bursting pyramidal cells show orthogonal forms of experience-dependent plasticity in layer V of barrel cortex. *Neuron* **73**:391–404. doi: 10.1016/j.neuron.2011.11.034, PMID: 22284191

Kaneko M, Cheetham CE, Lee YS, Silva AJ, Stryker MP, Fox K. 2010. Constitutively active H-ras accelerates multiple forms of plasticity in developing visual cortex. *PNAS* **107**:19026–19031. doi: 10.1073/pnas.1013866107, PMID: 20937865

Kathirvelu B, Colombo PJ. 2013. Effects of lentivirus-mediated CREB expression in the dorsolateral striatum: memory enhancement and evidence for competitive and cooperative interactions with the hippocampus. *Hippocampus* **23**:1066–1074. doi: 10.1002/hipo.22188, PMID: 23939934

Kogan JH, Frankland PW, Silva AJ. 2000. Long-term memory underlying hippocampus-dependent social recognition in mice. *Hippocampus* **10**:47–56. doi: 10.1002/(SICI)1098-1063(2000)10:1<47::AID-HIPO5>3.0.CO;2-6, PMID: 10706216

Kushner SA, Elgersma Y, Murphy GG, Jaarsma D, van Woerden GM, Hojjati MR, Cui Y, LeBoutillier JC, Marrone DF, Choi ES, De Zeeuw CI, Petit TL, Pozzo-Miller L, Silva AJ. 2005. Modulation of presynaptic plasticity and learning by the H-ras/extracellular signal-regulated kinase/synapsin I signaling pathway. *Journal of Neuroscience* **25**:9721–9734. doi: 10.1523/JNEUROSCI.2836-05.2005, PMID: 16237176

Lee YK, Kwak DH, Oh KW, Nam SY, Lee BJ, Yun YW, Kim YB, Han SB, Hong JT. 2009. CCR5 deficiency induces astrocyte activation, Abeta deposit and impaired memory function. *Neurobiology of Learning and Memory* **92**:356–363. doi: 10.1016/j.nlm.2009.04.003, PMID: 19394434

Lee YS, Silva AJ. 2009. The molecular and cellular biology of enhanced cognition. *Nature Reviews Neuroscience* **10**:126–140. doi: 10.1038/nrn2572, PMID: 19153576

Lein ES, Zhao X, Gage FH. 2004. Defining a molecular atlas of the hippocampus using DNA microarrays and high-throughput in situ hybridization. *Journal of Neuroscience* **24**:3879–3889. doi: 10.1523/JNEUROSCI.4710-03.2004, PMID: 15084669

Liang M, Kamata M, Chen KN, Pariente N, An DS, Chen IS. 2010. Inhibition of HIV-1 infection by a unique short hairpin RNA to chemokine receptor 5 delivered into macrophages through hematopoietic progenitor cell transduction. *The Journal of Gene Medicine* **12**:255–265. doi: 10.1002/jgm.1440, PMID: 20186995

Matus-Amat P, Higgins EA, Barrientos RM, Rudy JW. 2004. The role of the dorsal hippocampus in the acquisition and retrieval of context memory representations. *Journal of Neuroscience* **24**:2431–2439. doi: 10.1523/JNEUROSCI.1598-03.2004, PMID: 15014118

Matynia A, Anagnostaras SG, Wiltgen BJ, Lacuesta M, Fanselow MS, Silva AJ. 2008. A high through-put reverse genetic screen identifies two genes involved in remote memory in mice. *PLoS One* **3**:e2121. doi: 10.1371/journal.pone.0002121, PMID: 18464936

Maung R, Hoefer MM, Sanchez AB, Sejbuk NE, Medders KE, Desai MK, Catalan IC, Dowling CC, de Rozieres CM, Garden GA, Russo R, Roberts AJ, Williams R, Kaul M. 2014. CCR5 knockout prevents neuronal injury and behavioral impairment induced in a transgenic mouse model by a CXCR4-using HIV-1 glycoprotein 120. *The Journal of Immunology* **193**:1895–1910. doi: 10.4049/jimmunol.1302915, PMID: 25031461

Mayford M, Bach ME, Huang YY, Wang L, Hawkins RD, Kandel ER. 1996. Control of memory formation through regulated expression of a CaMKII transgene. *Science* **274**:1678–1683. doi: 10.1126/science.274.5293.1678, PMID: 8939850

Meucci O, Fatatis A, Simen AA, Bushell TJ, Gray PW, Miller RJ. 1998. Chemokines regulate hippocampal neuronal signaling and gp120 neurotoxicity. *PNAS* **95**:14500–14505. doi: 10.1073/pnas.95.24.14500, PMID: 9826729

Morikis D, Rizos AK, Spandidos DA, Krambovitis E. 2007. Electrostatic modeling of peptides derived from the V3-loop of HIV-1 gp120: implications of the interaction with chemokine receptor CCR5. *International Journal of Molecular Medicine* **19**:343–351. doi: 10.3892/ijmm.19.3.343, PMID: 17273779

Musante V, Longordo F, Neri E, Pedrazzi M, Kalfas F, Severi P, Raiteri M, Pittaluga A. 2008. RANTES modulates the release of glutamate in human neocortex. *Journal of Neuroscience* **28**:12231–12240. doi: 10.1523/JNEUROSCI.3212-08.2008, PMID: 19020017

Ndhlovu LC, Umaki T, Chew GM, Chow DC, Agsalda M, Kallianpur KJ, Paul R, Zhang G, Ho E, Hanks N, Nakamoto B, Shiramizu BT, Shikuma CM. 2014. Treatment intensification with maraviroc (CCR5 antagonist) leads to declines in CD16-expressing monocytes in cART-suppressed chronic HIV-infected subjects and is associated with improvements in neurocognitive test performance: implications for HIV-associated neurocognitive disease (HAND). *Journal of NeuroVirology* **20**:571–582. doi: 10.1007/s13365-014-0279-x, PMID: 25227930

Paruch S, Heinis M, Lemay J, Hoeffel G, Marañón C, Hosmalin A, Périanin A. 2007. CCR5 signaling through phospholipase D involves p44/42 MAP-kinases and promotes HIV-1 LTR-directed gene expression. *The FASEB Journal* **21**:4038–4046. doi: 10.1096/fj.06-7325com, PMID: 17627030

Riedel G, Micheau J, Lam AG, Roloff EL, Martin SJ, Bridge H, de Hoz L, Poeschel B, McCulloch J, Morris RG. 1999. Reversible neural inactivation reveals hippocampal participation in several memory processes. *Nature Neuroscience* **2**:898–905. doi: 10.1038/13202, PMID: 10491611

Roth TL, Sweatt JD. 2008. Rhythms of memory. *Nature Neuroscience* **11**:993–994. doi: 10.1038/nn0908-993, PMID: 18725902

Schafe GE, Atkins CM, Swank MW, Bauer EP, Sweatt JD, LeDoux JE. 2000. Activation of ERK/MAP kinase in the amygdala is required for memory consolidation of pavlovian fear conditioning. *Journal of Neuroscience* **20**:8177–8187. PMID: 11050141

Shah M, Smit TK, Morgello S, Tourtellotte W, Gelman B, Brew BJ, Saksena NK. 2006. Env gp120 sequence analysis of HIV type 1 strains from diverse areas of the brain shows preponderance of CCR5 usage. *AIDS Research and Human Retroviruses* **22**:177–181. doi: 10.1089/aid.2006.22.177, PMID: 16478400

Shen W, Proost P, Li B, Gong W, Le Y, Sargeant R, Murphy PM, Van Damme J, Wang JM. 2000. Activation of the chemotactic peptide receptor FPRL1 in monocytes phosphorylates the chemokine receptor CCR5 and attenuates cell responses to selected chemokines. *Biochemical and Biophysical Research Communications* **272**:276–283. doi: 10.1006/bbrc.2000.2770, PMID: 10872839

Silva AJ, Kogan JH, Frankland PW, Kida S. 1998. CREB and memory. *Annual Review of Neuroscience* **21**:127–148. doi: 10.1146/annurev.neuro.21.1.127, PMID: 9530494

Sirois S, Sing T, Chou KC. 2005. HIV-1 gp120 V3 loop for structure-based drug design. *Current Protein & Peptide Science* **6**:413–422. doi: 10.2174/138920305774329359, PMID: 16248793

Sorce S, Myburgh R, Krause KH. 2011. The chemokine receptor CCR5 in the central nervous system. *Progress in Neurobiology* **93**:297–311. doi: 10.1016/j.pneurobio.2010.12.003, PMID: 21163326

Stanciu M, Radulovic J, Spiess J. 2001. Phosphorylated cAMP response element binding protein in the mouse brain after fear conditioning: relationship to fos production. *Molecular Brain Research* **94**:15–24. doi: 10.1016/S0169-328X(01)00174-7, PMID: 11597761

Strominger RN, Woolsey TA. 1987. Templates for locating the whisker area in fresh flattened mouse and rat cortex. *Journal of Neuroscience Methods* **22**:113–118. doi: 10.1016/0165-0270(87)90004-5, PMID: 2830438

Tang H, Lu D, Pan R, Qin X, Xiong H, Dong J. 2009. Curcumin improves spatial memory impairment induced by human immunodeficiency virus type 1 glycoprotein 120 V3 loop peptide in rats. *Life Sciences* **85**:1–10. doi: 10.1016/j.lfs.2009.03.013, PMID: 19345695

Torres-Muñoz JE, Van Waveren C, Keegan MG, Bookman RJ, Petito CK. 2004. Gene expression profiles in microdissected neurons from human hippocampal subregions. *Molecular Brain Research* **127**:105–114. doi: 10.1016/j.molbrainres.2004.05.017, PMID: 15306126

Tran PB, Banisadr G, Ren D, Chenn A, Miller RJ. 2007. Chemokine receptor expression by neural progenitor cells in neurogenic regions of mouse brain. *The Journal of Comparative Neurology* **500**:1007–1034. doi: 10.1002/cne.21229, PMID: 17183554

Tyner JW, Uchida O, Kajiwara N, Kim EY, Patel AC, O'Sullivan MP, Walter MJ, Schwendener RA, Cook DN, Danoff TM, Holtzman MJ. 2005. CCL5-CCR5 interaction provides antiapoptotic signals for macrophage survival during viral infection. *Nature Medicine* **11**:1180–1187. doi: 10.1038/nm1303, PMID: 16208318

Westmoreland SV, Alvarez X, deBakker C, Aye P, Wilson ML, Williams KC, Lackner AA. 2002. Developmental expression patterns of CCR5 and CXCR4 in the rhesus macaque brain. *Journal of Neuroimmunology* **122**:146–158. doi: 10.1016/S0165-5728(01)00457-X, PMID: 11777554

Wong-Riley M. 1979. Changes in the visual system of monocularly sutured or enucleated cats demonstrable with cytochrome oxidase histochemistry. *Brain Research* **171**:11–28. doi: 10.1016/0006-8993(79)90728-5, PMID: 223730

Yin JC, Wallach JS, Del Vecchio M, Wilder EL, Zhou H, Quinn WG, Tully T. 1994. Induction of a dominant negative CREB transgene specifically blocks long-term memory in Drosophila. *Cell* **79**:49–58. doi: 10.1016/0092-8674(94)90399-9, PMID: 7923376

Zhou Y, Won J, Karlsson MG, Zhou M, Rogerson T, Balaji J, Neve R, Poirazi P, Silva AJ. 2009. CREB regulates excitability and the allocation of memory to subsets of neurons in the amygdala. *Nature Neuroscience* **12**: 1438–1443. doi: 10.1038/nn.2405, PMID: 19783993

Zhou L, Saksena NK. 2013. HIV associated neurocognitive disorders. *Infectious Disease Reports* **5**:e8. doi: 10.4081/idr.2013.s1.e8

2.2 Methods

Subjects

All experiments were conducted in accordance with the guidelines established by the UCLA Animal Research Committee. Adult (3-8 months old) male and female *Ccr5*$^{+/-}$*; yfp*$^{+}$ double transgenic mice and their WT littermates *Ccr5*$^{+/+}$*; yfp*$^{+}$ mice were used for the spine imaging experiments (*Ccr5*$^{+/-}$ breeders were C57BL/6NTac; Thy1-YFP-H breeders were C57BL/6J). *Ccr5*$^{+/-}$ and WT littermates, with or without Thy1-YFP were used for the behavioral enhancement experiments. C57BL/6NTac (3-4 months old) WT male mice were used for AAV injections. Animals were kept on a 12:12-h light:dark cycle with food and water ad libitum.

AAV Injection Surgery

AAV5 viral vectors containing shRNA-CCR5 or shRNA-DsRed (control), with a fluorescence protein GFP sequence, were engineered to decrease CCR5 expression levels in neurons. Mice were anesthetized with 2% isoflurane, placed in a stereotaxic frame, and kept warm with a monitored heating pad. A piece of skull (1mm width square) right above the center of RSC were thinned by a dental drill and removed bilaterally. AAV viral vectors were stereotaxically injected into the center of RSC bilaterally through a 30-gauge Hamilton microsyringe with a 50 μm wide capillary needle at 2 sites at the following coordinates relative to bregma (mm): AP: -2.3, ML: ±0.7, DV: -0.5. After injection, the microsyringe were left in place for an additional 5 min to ensure full virus diffusion. After surgery, the mice were left for 2 weeks for recovery, followed by being handled for 1 week.

Contextual Fear Conditioning

Following recovery from surgery, mice were handled and habituated to transport cues for 1 weeks. On the first day after handling/habituation mice underwent the first home cage baseline imaging session (Day-3). Two days later (Day0) mice underwent the second baseline imaging session. The following day half the mice were randomly selected to begin contextual fear conditioning using a multi-day paradigm. Animals were placed in conditioning chambers, 45 s later were given one 1.5-sec 0.5mA shock, and 10 s later were given a second shock of the same intensity and duration. Animals were removed from the conditioning chamber 2 min later and placed in their home cage. On day 2 mice were conditioned again as on day 1, except that 90 min after conditioning mice were imaged. Training continued as above for a total of 5 days. Each conditioning chamber (32 cm wide, 25 cm high, 25 cm deep) is equipped with stainless steel grid floor (36 rods, each rod 2-mm diameter, 8-mm center to center; Med-Associates Inc., Georgia, VT) and stainless steel drop-pan. Chambers are scented with 100% isopropyl alcohol to provide a background odor. Each chamber is equipped with an overhead LED light source providing white light. Each chamber is connected to a solid-state scrambler, providing AC constant current shock, controlled via an interface connected to a Windows computer running Video Freeze (Med-Associates Inc., Georgia, VT), a program designed for the automated assessment of freezing, an index of fear memory. *Ccr5*$^{+/-}$ and WT littermates follow the same contextual fear conditioning and imaging protocol. Activity suppression ratio for each day is calculated as average activity during test divided by the sum of activity during baseline (activity on Day1 before 1st shock) plus activity during test.

Morris Water Maze

On the first day after handling/habituation (same as CFC), *Ccr5*$^{+/-}$ and WT littermates underwent the first home cage baseline imaging session (Day-4). 48 hours later (Day-2) and 96 hours later (Day0) mice underwent the second and third baseline imaging session. The following day, all mice with Thy1-YFP were trained with two blocks per day for 5 days to find a hidden platform in Morris Water Maze. Each block consisted of two trials with 30 s interval between the trials. In each trial, mice were given 60 s to find the platform. If mouse found the platform earlier than 60 s in a certain trial, that trial terminated at the time mice finds the platform. If mice failed to find the platform, the trial terminated at 60 s. After each trial, mice were put on the platform for 15 sec. On day 3 and day 5, probe tests with a time of 60 s were administered 1 hour after training. During the probe test, platform was removed from the maze. 1) Percentage of time mouse spent in each quadrant and 2) platform crossing in each quadrant during probe test -which tests the accuracy of positional memory- were analyzed. AAV injected mice followed the same protocol.

Confocal Imaging

Mice were perfused 90 minutes after probe tests on day 5 of training. Brains were extracted and sectioned. Brain slices were incubated with 4', 6-diaminodino-2-phenylindole (DAPI) for 15 min before mounting onto slides. Images were acquired through Nikon A1 Laser Scanning Confocal Microscope.

2.3 Results

2.3.1 *Ccr5*$^{+/-}$ show contextual and spatial memory enhancement

I trained *Ccr5*$^{+/-}$ mice and their wildtype (WT) littermate controls in either contextual fear conditioning (CFC) or Morris Water Maze (MWM) - a spatial learning task - and imaged dendritic spines in RSC in a subset of animals that expressed Thy1-YFP. Consistent with findings shown in Chapter 2.1, I confirmed that the *Ccr5*$^{+/-}$ and Thy1-YFP double-transgenic mice showed superior contextual memory performances in CFC only after one day of training (Fig. 2.1). In addition, *Ccr5*$^{+/-}$ mice also showed enhanced spatial learning and memory in a probe test given after 3 days of training in MWM (Fig. 2.2a-d). In the probe test given after 5 days of training, although both *Ccr5*$^{+/-}$ and WT mice spent significantly more time in the training quadrant than the other three quadrants (Fig. 2.2e), *Ccr5*$^{+/-}$ still showed enhanced accuracy for recall of platform location compared to the WT littermates, as shown by the increased number of crossings of the platform location (Fig. 2.2f).

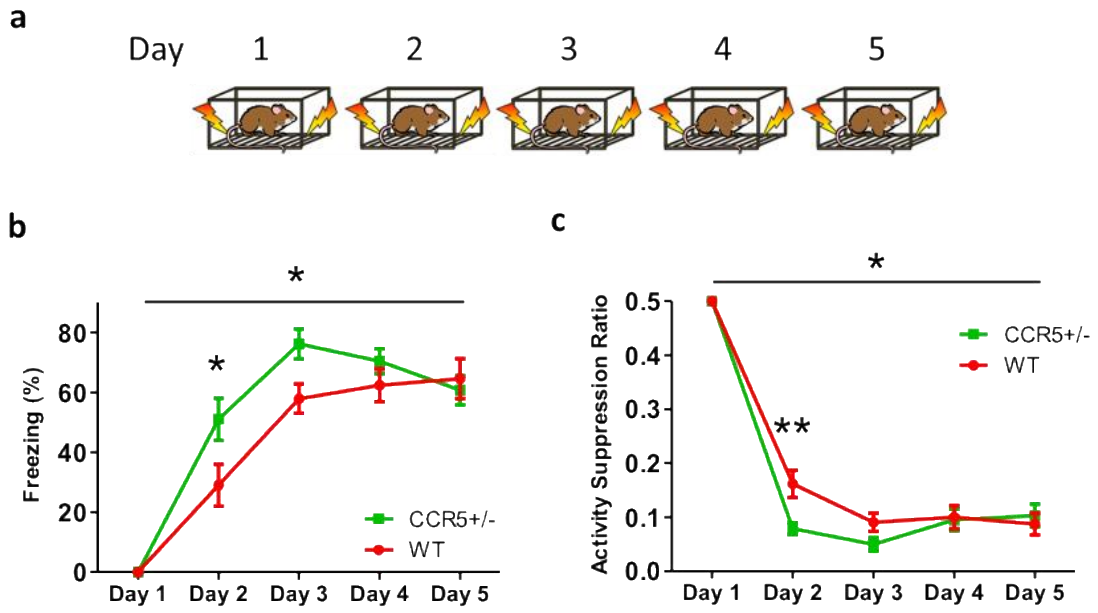

Figure 2.1. *Ccr5*$^{+/-}$ show enhanced memory in contextual fear conditioning. (a) Timeline of CFC training. **(b)** *Ccr5*$^{+/-}$ mice show enhanced contextual learning and memory relative to WT littermates (*Ccr5*$^{+/-}$ n=12, WT n=15; Two-way RM ANOVA, genotype x time interaction: $F_{(4,100)}$=2.60, p=0.0404; Bonferroni post-test for Day2: p<0.05). **(c)** *Ccr5*$^{+/-}$ mice have enhanced activity suppression after one day of training in CFC. Activity suppression ratio is the average activity during testing divided by the sum of baseline activity plus activity during testing (*Ccr5*$^{+/-}$ n=12, WT n=15; Two-way RM ANOVA, genotype x time interaction: $F_{(4,100)}$=2.74, p=0.0329; Bonferroni post-test for Day2: p<0.01). Very low values indicate a high level of fear, 0.5 indicates no fear, and values greater than 0.5 indicate conditioned safety. Data are represented as mean ± s.e.m. **p<0.01, *p<0.05.

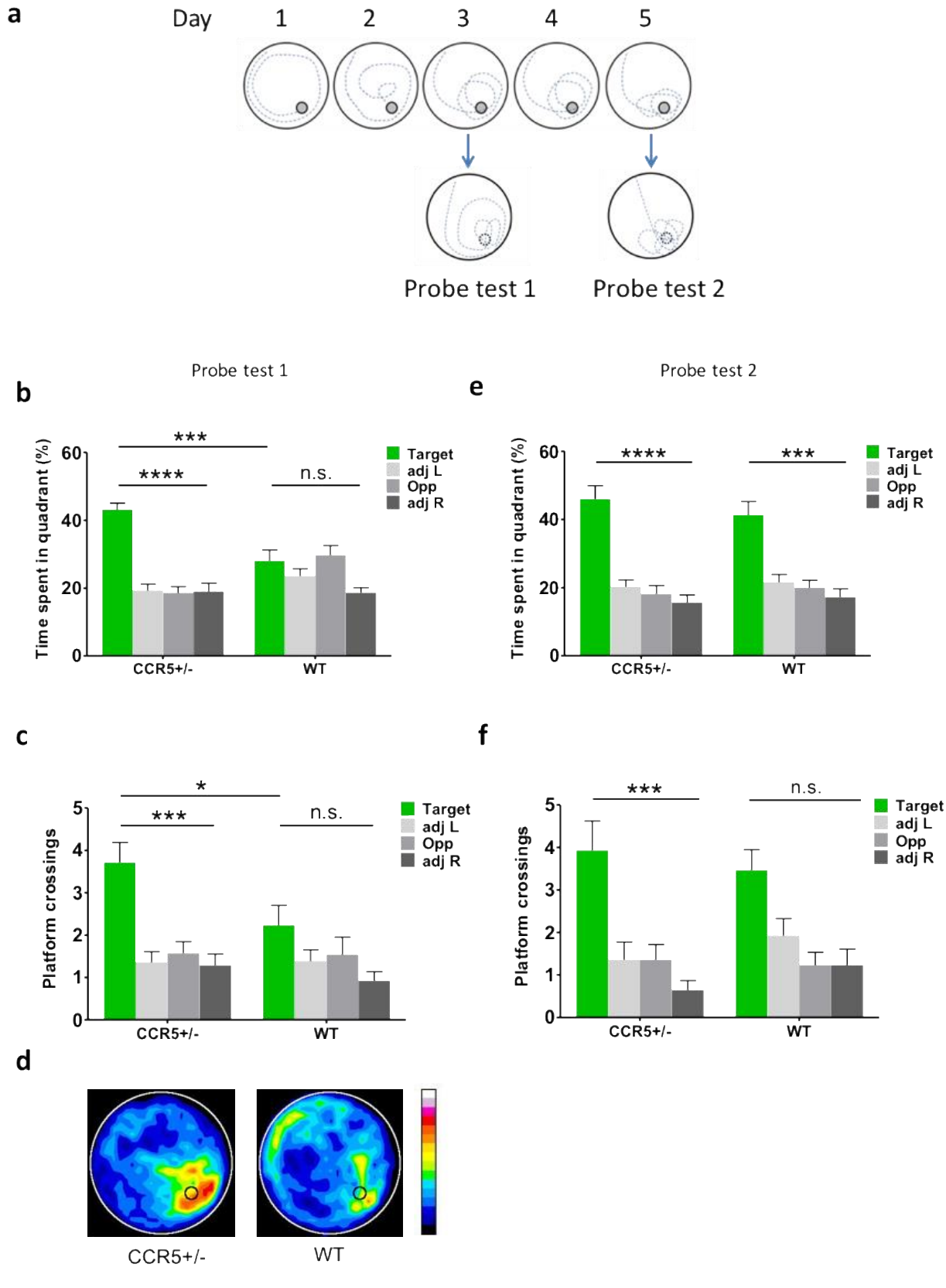
a
Day
1
2
3
4
5
Probe test 1
Probe test 2
b
Probe test 1
Time spent in quadrant (%)
***
****
n.s.
Target
adj L
Opp
adj R
CCR5+/-
WT
e
Probe test 2
****
***
c
Platform crossings
*
f
d
CCR5+/-
WT

Figure 2.2. *Ccr5*$^{+/-}$ show enhanced memory in Morris water maze. (a) Timeline of MWM training. **(b)** In a MWM probe test given after only 3 days of training, *Ccr5*$^{+/-}$ mice spent significantly more time in the target quadrant than in the other three quadrants. In contrast, at this point WT mice did not search selectively for the platform (*Ccr5*$^{+/-}$ n=14, WT n=13; Two-way RM ANOVA, genotype x percentage of time in each quadrant interaction $F_{(3,75)}$=9.11, p<0.0001; Bonferroni post-tests for the target quadrant versus all other quadrants: p<0.0001 for *Ccr5*$^{+/-}$, p>0.05 for WT; Unpaired t-test for the target quadrant, $t_{(25)}$=4.173, p=0.0003). **(c)** In a MWM probe test given after 3 days of training, *Ccr5*$^{+/-}$ mice show enhanced accuracy for recall of platform location compared to the WT littermates, as shown by the increased number of crossings of the platform location (*Ccr5*$^{+/-}$ n=14, WT n=13; Two-way RM ANOVA, genotype x platform crossings in each quadrant interaction $F_{(3,75)}$=2.04, p=0.1153; Bonferroni post-tests for the target quadrant versus all other quadrants: p<0.001 for *Ccr5*$^{+/-}$, p>0.05 for WT; Unpaired t-test for the target quadrant, $t_{(25)}$=2.221, p=0.0356). **(d)** Heat maps show the combined traces of the mice from each group during the probe test. **(e)** In a probe test given after 5 days of training, both groups spent significantly more time in the target quadrant than in the other three quadrants (*Ccr5*$^{+/-}$ n=14, WT n=13; Two-way RM ANOVA, genotype x percentage of time in each quadrant interaction, p=0.7078; Bonferroni post-tests for the target quadrant versus all other quadrants: p<0.0001 for *Ccr5*$^{+/-}$, p<0.001 for WT). **(f)** In a probe test given after 5 days of training, *Ccr5*$^{+/-}$ mice still show enhanced accuracy for recall of platform location compared to the WT littermates, as shown by the increased number of crossings of the platform location (*Ccr5*$^{+/-}$ n=14, WT n=13; Two-way RM ANOVA, genotype x platform crossings in each quadrant interaction, p=0.5693; Bonferroni post-tests for the target quadrant versus all other

quadrants: $p<0.001$ for *Ccr5*$^{+/-}$, $p>0.05$ for WT. Data are represented as mean ± s.e.m. ****$p<0.0001$, ***$p<0.001$, **$p<0.01$, *$p<0.05$; n.s., not significant.

2.3.2 CCR5 knockdown in retrosplenial cortex leads to spatial memory enhancement

After confirming the enhanced learning and memory phenotype by *Ccr5*$^{+/-}$, next I want to ask whether RSC is an important region for the enhancement that I have seen in heterozygous mutant mice. To do so, I injected adeno-associated virus containing shRNA-CCR5 or shRNA-DsRed (shRNA-control) into RSC specifically in adult C57BL/6NTac mice (Fig. 2.3). After 3 week-recovery from surgery, mice were trained in MWM to test the spatial learning and memory performance. I found that, knockdown of CCR5 specifically in RSC dramatically enhanced spatial learning and memory performance in a probe test given after 3 days of training (Fig. 2.4a-d). In the probe test given after 5 days of training, although both CCR5 knockdown and control mice spent significantly more time in the training quadrant than the other three quadrants (Fig. 2.4e), CCR5 knockdown mice still showed enhanced accuracy for recall of platform location compared to the control mice, as shown by the increased number of crossings of the platform location (Fig. 2.4f). This finding indicates that RSC has a fundamental role for CCR5 to take its effect on spatial learning and memory. This result further suggests that spine dynamics in RSC are likely to reflect the performance of spatial learning and memory.

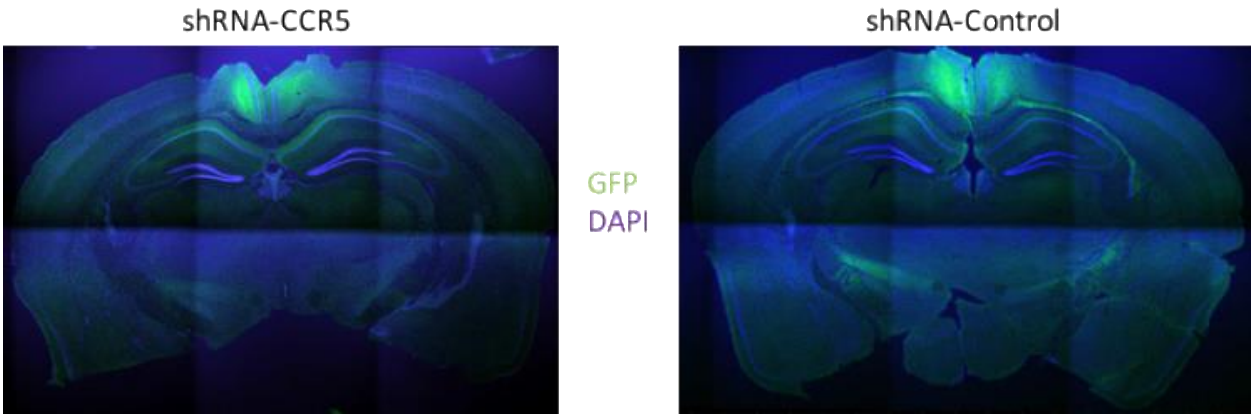

Figure 2.3. AAV containing shRNA-CCR5 or shRNA-Control mainly infect neurons in RSC. One month after virus injection, mice were perfused and brains were extracted and sectioned. Brain slices were stained with DAPI to label cell nuclear. GFP labels AAV-infected neurons.

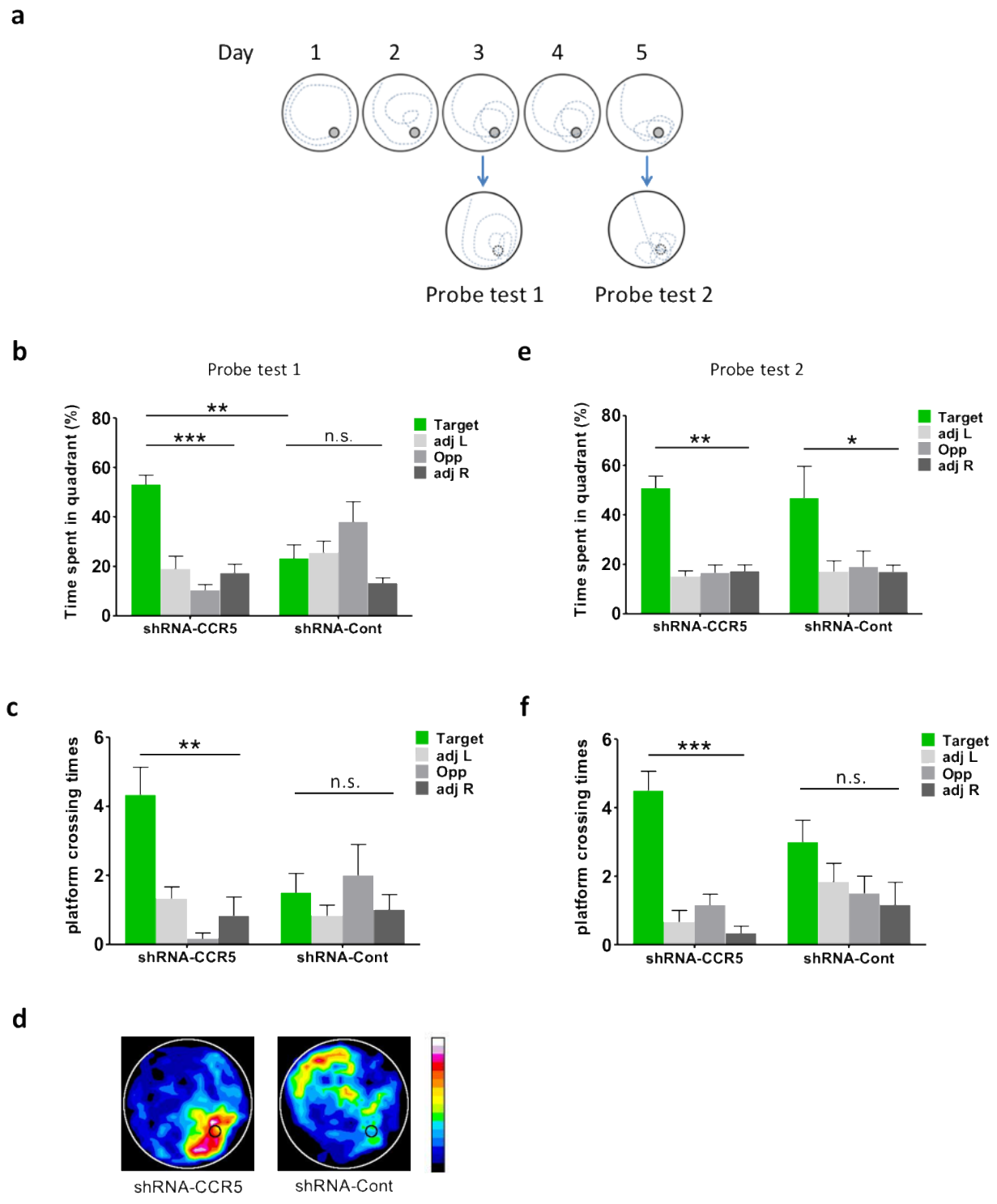

Figure 2.4. CCR5 knockdown in RSC enhances spatial learning and memory in Morris water maze. (a) Timeline of MWM training. **(b)** In a MWM probe test given after only 3 days of

training, mice injected with shRNA-CCR5 spent significantly more time in the target quadrant than in the other three quadrants. In contrast, at this point shRNA-dsRed (shRNA-control) mice did not search selectively for the platform (shRNA-CCR5 n=6, shRNA-control n=6; Two-way RM ANOVA, genotype x percentage of time in each quadrant interaction, p=0.0002; Bonferroni post-tests for the target quadrant versus all other quadrants: p<0.001 for shRNA-CCR5, p>0.05 for shRNA-control; Unpaired t-test for the target quadrant, p<0.01). **(c)** In a MWM probe test given after 3 days of training, shRNA-CCR5 mice show enhanced accuracy for recall of platform location compared to the WT littermates, as shown by the increased number of crossings of the platform location (shRNA-CCR5 n=6, shRNA-control n=6; Two-way RM ANOVA, genotype x platform crossings in each quadrant interaction, p=0.0042; Bonferroni post-tests for the target quadrant versus all other quadrants: p<0.01 for shRNA-CCR5, p>0.05 for shRNA-control). **(d)** Heat maps show the combined traces of the mice from each group during the probe test. **(e)** In a probe test given after 5 days of training, both groups spent significantly more time in the target quadrant than in the other three quadrants (shRNA-CCR5 n=6, shRNA-control n=6; Two-way RM ANOVA, genotype x percentage of time in each quadrant interaction, p=0.9643; Bonferroni post-tests for the target quadrant versus all other quadrants: p<0.01 for shRNA-CCR5, p<0.05 for shRNA-control). **(f)** In a probe test given after 5 days of training, shRNA-CCR5 mice still show enhanced accuracy for recall of platform location compared to the WT littermates, as shown by the increased number of crossings of the platform location (shRNA-CCR5 n=6, shRNA-control n=6; Two-way RM ANOVA, genotype x platform crossings in each quadrant interaction, p=0.0807; Bonferroni post-tests for the target quadrant versus all other quadrants: p<0.001 for shRNA-CCR5, p>0.05 for shRNA-control). Data are represented as mean ± s.e.m. ***p<0.001, **p<0.01, *p<0.05; n.s., not significant.

2.4 Discussion

CCR5 is a chemokine receptor that has an important function in inflammatory responses. Based on the evidence we found through contextual fear conditioning and Morris water maze, CCR5 deficiency results in learning and memory enhancement. This enhancement is consistent with increases in hippocampal plasticity. In the barrel cortex, *Ccr5* knockout mice show accelerated experience-dependent plasticity. Knockdown of CCR5 specifically in adult hippocampus or RSC, both result in enhancement in spatial learning and memory, and same procedure in adult barrel cortex results in enhanced experience dependent plasticity, demonstrating that the effect of CCR5 is not due to changes during development.

Importantly, MAPK and CREB signaling, which have been implicated in learning and memory (Bourtchuladze et al., 1994; Roth and Sweatt, 2008), are found to be enhanced in *Ccr5* knockout mice only after learning, not during baseline (MAPK: 1h, CREB: 3h after training). This finding provides molecular evidence that CCR5 regulate plasticity and learning and memory through the enhanced MAPK and CREB signaling. Enhanced CREB signaling in RSC leads to spatial memory enhancement (Czajkowski et al., 2014), as well as knockdown of CCR5 in RSC causes spatial memory enhancement, suggesting that $Ccr5^{+/-}$ mice can be used as a gain of function manipulation of learning and memory to explore the relationship between spine dynamics in RSC and contextual and spatial learning and memory.

Chapter 3 *Ccr5*$^{+/-}$ mice have enhanced pre-learning dendritic spine turnover

3.1 Introduction

Dendritic spines are dynamic structures whose formation and elimination is postulated to expand memory storage capacity beyond that permissible solely from synaptic weight changes of existing synapses (Chklovskii et al., 2004; Kandel et al., 2014; Poirazi and Mel, 2001). A variety of studies in varying preparations and organisms have shown that spine turnover is modified by electrical activity, sensory experience, and learning (Fu et al., 2012; Holtmaat and Svoboda, 2009; Lai et al., 2012; Toni et al., 1999; Xu et al., 2009; Yang et al., 2009). Additionally, results from juvenile zebra finch show that endogenously higher levels of spine turnover before tutoring correlate with a greater capacity for subsequent song learning during the critical period (Roberts et al., 2010). Adam Frank, a previous graduate student from our lab found that the dendritic spine turnover in RSC happened before training was predictive of future contextual memory, as indicated by context freezing levels (Fig. 3.1). Therefore, I am interested to test the hypothesis that *Ccr5*$^{+/-}$ mice, which show enhanced learning and memory in CFC and MWM, may also have enhanced dendritic spine turnover during baseline.

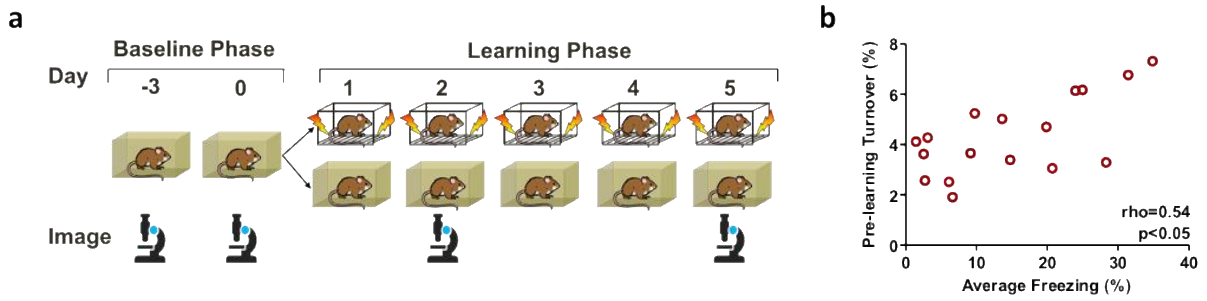

Figure 3.1. Pre-training dendritic spine turnover correlates with contextual learning. (a) Timeline of contextual learning and imaging. One group of mice underwent CFC training every day for 5 days. Control group of mice stayed in home cage. **(b)** Dendritic spine turnover ratio before training (Day-3 to Day0) correlates with future contextual learning. Scatter plot shows the relationship between dendritic spine turnover prior to training and average freezing in the contextual conditioning task measured from Day2 to Day5 (n=17 mice*; Spearman's rho*=0.54, p=0.0255).

3.2 Methods

Subjects

All experiments were conducted in accordance with the guidelines established by the UCLA Animal Research Committee. Adult (3-8 months old) male and female *Ccr5*$^{+/-}$*; yfp*$^{+}$ double transgenic mice and their WT littermates *Ccr5*$^{+/+}$*; yfp*$^{+}$ mice were used for the spine imaging experiments (*Ccr5*$^{+/-}$ breeders were C57BL/6NTac; Thy1-YFP-H breeders were C57BL/6J). *Ccr5*$^{+/-}$ and WT littermates, with or without Thy1-YFP were used for the behavioral

enhancement experiments. Animals were kept on a 12:12-h light:dark cycle with food and water ad libitum. For MK801 experiments, *Ccr5*$^{+/-}$*; yfp*$^{+}$ double transgenic mice and their WT littermates *Ccr5*$^{+/+}$*; yfp*$^{+}$ mice were used for the spine imaging and trained with CFC task. Intraperitoneal injections of MK801 were performed twice daily (0.25 mg/kg dissolved in saline). Injections started at 4 days before the first imaging day, and continued for 13 days until the last imaging was done.

Cranial window implantation

The procedure we utilized for window implantation has been described in detail (Holtmaat et al., 2009); briefly, mice were anesthetized with isoflurane, placed in a stereotaxic frame, and kept warm with a monitored heating pad. Custom cut coverslips (square, 2x2mm) were cleaned in ethanol and sterilized. A square region of skull 2mm in width was marked using stereotactic coordinates (RSC: center at bregma -2.5 mm AP). The skull was thinned with a dental drill and removed. After cleaning the surgical site with saline, the coverslip was placed on the dural surface and fastened with adhesive and dental acrylics to expose a square window of approximately 2 mm. Next, an aluminum bar with a threaded hole was attached to stabilize the mice during imaging sessions. Finally, mice were maintained on antibiotics during recovery and also given daily injections of carprofen and dexamethasone for 1 week to reduce inflammation. Mice were allowed to recover for three weeks before the first imaging session.

2-Photon imaging

A custom-built two-photon laser scanning microscope was paired with a Spectra-Physics 2-photon laser tuned to 920nm. A 40x 1.0 NA water immersion objective (Zeiss) was used to

acquire images 90 minutes after each behavioral session. Mice were lightly anesthetized with isoflurane and attached to the head mount using a small screw. During the first imaging session, segments of apical dendrites from Layer V pyramidal cells were imaged. These segments were acquired within 200 μm from the cortical surface, likely representing dendrites located in layers I and II/III. Imaged segments were generally oriented in the x,y plane of imaging with minimal z-projection. 512x512 pixel images were acquired at 0.5 μm intervals to fully capture the segment of dendrite, and image stacks generally consisted of 20-30 slices. If a segment of dendrite was larger than could be acquired in one 512x512 stack, additional image stacks were sequentially acquired through the x,y,z plane of the dendrite in question so that its extent could be visualized. The same segments were repeatedly imaged across experimental days by locating their position via a coordinate system established during the first imaging session.

Image and data analysis

Dendritic spines were analyzed and counted by established criteria (Holtmaat et al., 2009). Specifically, the Spine Analysis software included in ScanImage was used to open all imaging days for a given segment of dendrite. A segment is classified as the entire visible length of a piece of dendrite; and segments were often followed across several images. The presence, gain, and loss of spines were quantified across days for each segment, and all segments were examined for a given animal. Importantly, all images were coded following completion of the experiment so that the experimenter was blind to training status and genotype of all mice while analyzing and counting spines. A subset of the images was counted by two experimenters independently to confirm the results.

Statistics

5 and 3 separate replicates of imaging in RSC during CFC and MWM were run, respectively. The data from all replicates were pooled. Results for motor cortex CFC and imaging were collected from a single experiment. The size of each replicate was chosen to include approximately equal numbers of mice for group comparison, and to maximize the number of animals able to be imaged in one replicate cycle (~8-12 hours). On the first day of training, every other cage was taken for behavior. Cage placement on the rack was random, choice of animals for CFC was as well. All available *Ccr5*$^{+/-}$ and their wildtype littermates at the age between 3 to 8 months were used for experiments. Correlations were calculated as Spearman's rho to compensate for the non-normality of the data. Similarly, the Mann-Whitney U test was used for all other group comparisons, except where indicated. All p-values represent results from two-sided tests. Animals with behavioral data outside two standard deviations of the mean were excluded for the statistic tests. Animals with less than 5 spines gained during the learning phase were excluded for the statistic tests. Turnover ratio equals sum of number of gained and lost spines between two time points divided by sum of total number of spines on each time point.

3.3 Results

Baseline spine images were taken on Day -3 and 0 for CFC group, while on Day -4, -2 and 0 for MWM group (Fig. 3.2a, c). Pre-learning turnover of the first two imaging sessions were used for following analysis (CFC: Day-3 to Day 0; MWM: Day -4 to Day -2). As expected, we found that pre-training spine turnover of RSC was enhanced in *Ccr5*$^{+/-}$ mice in both groups that trained for CFC (Fig. 3.2b) and MWM (Fig. 3.2d).

Chronic blockade of NMDA (*N*-methyl-D-aspartate) receptors with the antagonist MK801 prevented this increased spine turnover in *Ccr5*$^{+/-}$ mice, while having no effect on their wildtype littermates (Fig. 3.3), suggesting that the enhancement of pre-learning spine turnover observed in *Ccr5* mutants is due to plasticity-related mechanisms.

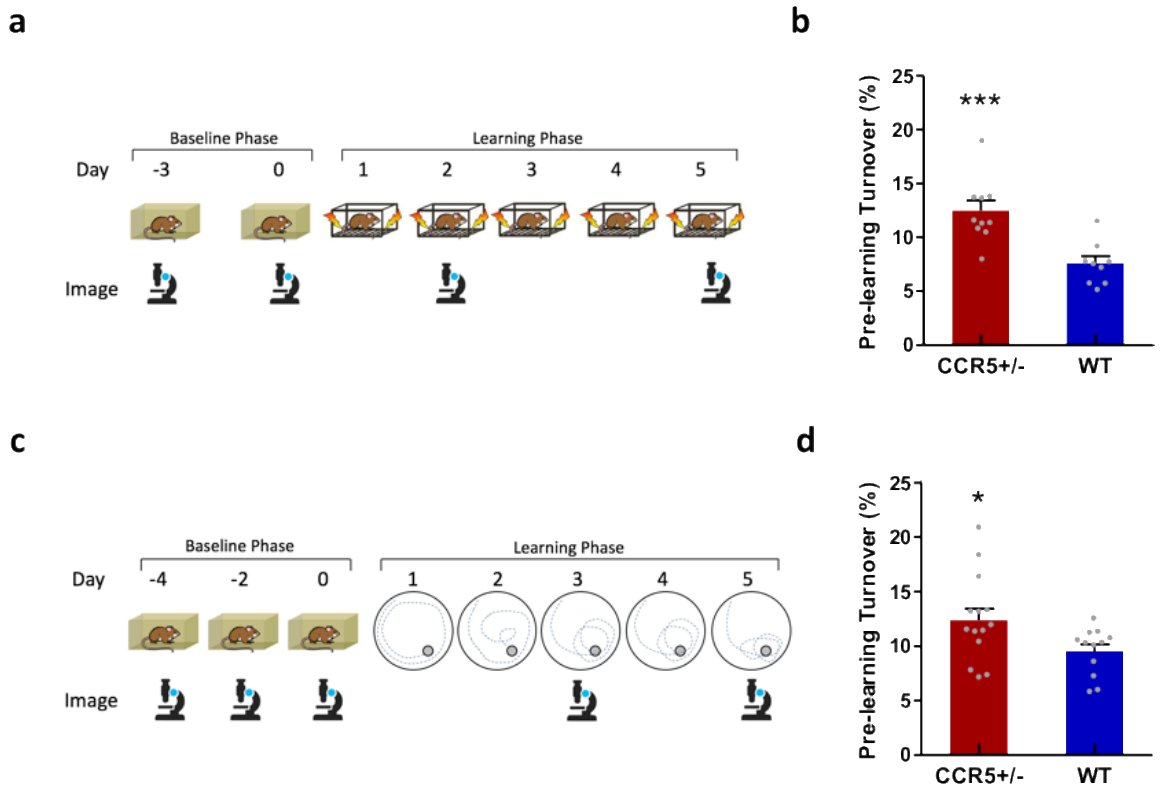

Figure 3.2. Pre-training dendritic spine turnover is enhanced in *Ccr5*$^{+/-}$ mice. (a) Timeline of contextual learning and imaging. **(b)** *Ccr5*$^{+/-}$ mice have increased baseline spine turnover prior to CFC (Day-3 to Day0) relative to WT littermates (*Ccr5*$^{+/-}$ n=10, WT n=9; U=6.00, p=0.0006). **(c)** Timeline of spatial learning and imaging. **(d)** *Ccr5*$^{+/-}$ mice have increased baseline spine turnover prior to MWM (Day-4 to Day-2) compared to WT littermates (*Ccr5*$^{+/-}$ n=14, WT n=12; U=38.00, p=0.0193). Data are represented as mean ± s.e.m. plus individual points. ***p<0.001, *p<0.05.

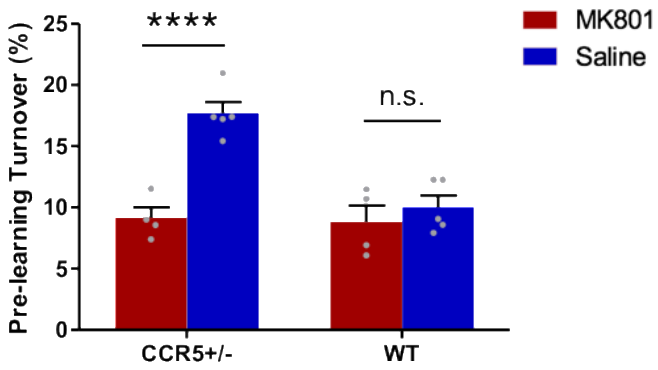

Figure 3.3. Enhanced pre-learning spine turnover of *Ccr5*$^{+/-}$ mice is NMDA receptor activity-dependent. *Ccr5*$^{+/-}$ mice that receive MK801 treatment (0.25 mg/kg, twice daily) no longer have enhanced baseline spine turnover rate, while MK801 does not have a significant effect on their WT littermates (MK801|*Ccr5*$^{+/-}$ n=4, Saline|*Ccr5*$^{+/-}$ n=5, MK801|WT n=4, Saline|WT n=5, Two-way ANOVA, genotype x treatment interaction: $F_{(1,14)}$=13.00, p=0.0029; Bonferroni post-test for *Ccr5*$^{+/-}$: p<0.0001, WT: p>0.05). ****p<0.0001; n.s., not significant.

3.4 Discussion

Adam Frank in our lab has found that there is a significant positive correlation between baseline spine turnover and future contextual learning. Also, spine turnover night before song tutoring correlates with song learning performance on the next day in juvenile zebra finches (Roberts et al., 2010). These findings are further extended by a genetic manipulation of enhanced learning and memory. *Ccr5*$^{+/-}$ mice not only have enhanced performance in contextual and spatial learning tasks, but also have enhanced baseline spine turnover. These convergent evidences

suggest that spine turnover before learning is a determinant of future learning performance. Intrinsic basal spine turnover may allow neurons to efficiently sample synaptic space. Further, the increases in pre-learning spine turnover by *Ccr5* mutation is prevented by NMDA receptor antagonist, suggesting that the enhancement is due to plasticity-dependent mechanisms mediated by NMDA receptors. Given this increased basal turnover, as well as enhanced contextual and spatial memory performance, I posit that learning-related spine clustering in *Ccr5*$^{+/-}$ mice is also enhanced.

Chapter 4 *Ccr5*$^{+/-}$ mice have enhanced clustered spine formation

4.1 Introduction

Data shown indicate that baseline spine turnover is an important determinant of future learning and memory performance. However, long-term memories are thought to be stored in stable synapses. Excessive spine turnover may lead to rapid loss of acquired information. Therefore, a stabilizing mechanism of newly formed synapses is required. To determine whether contextual learning affects spine dynamics, Adam Frank split mice into two groups: one group underwent CFC while the second remained in their home cages. Both groups were imaged on the same schedule: in the early stages of learning and again at the end of day 5 of training (Fig. 4.1a).

Trained animals showed a striking increase in the number of new spines that were clustered (two or more spines within 5 µm of each other; Fig. 4.1b, c) in RSC. In contrast, in primary motor cortex (not known to be involved in CFC), animals trained in CFC and home cage control animals had similar levels of clustering (Fig. 4.1d) suggesting that the changes observed in RSC are specific to structures involved in contextual learning and memory. A 5 µm window was chosen for the analyses as a number of biochemical, electrophysiological, and structural studies suggest that a 5-10 µm distance between spines facilitates sharing of resources, spine co-activation, and learning induced structural plasticity (Govindarajan et al., 2011; Harvey and Svoboda, 2007; Harvey et al., 2008; McBride et al., 2008; Murakoshi et al., 2011; Takahashi et al., 2012; Wilson et al., 2016). Further, measurements of the nearest neighbor distances (the distance between a new spine to its closest new spine neighbor) for spines gained during learning were consistent with the results of the 5 µm analyses: in trained animals, the distribution of the nearest neighbor distances was significantly shifted towards smaller values (Fig. 4.1e). Furthermore, resampling analysis of the data from trained animals revealed that clustering within 5 µm would occur randomly for only 22.2% of newly added spines – consistent with the amount of clustering observed in control animals and in motor cortex – while an average of 42.0% of new spines were clustered in RSC of trained animals (Fig. 4.1f).

Mice that have higher rates of learning-related spine clustering in RSC exhibited more contextual freezing (Fig. 4.1g). This linear relationship between spine clustering and contextual learning and memory highlights the potential role of clustered plasticity as a mechanism for cortical information storage. Consistent with the idea of sparse encoding, clustered spines gained during learning in RSC are on average only 2.5% of the total population of spines. Further supporting the hypothesis that clustered spine addition contributes to long-term memory storage, spines

added in clusters in RSC during training have a higher survival rate compared to non-clustered spines (added during training) when examined 4-6 weeks after training (Fig. 4.1h).

Next, given the increased basal turnover in *Ccr5*$^{+/-}$, as well as enhanced contextual and spatial memory performance, I posit that learning-related spine clustering would also be enhanced in *Ccr5*$^{+/-}$.

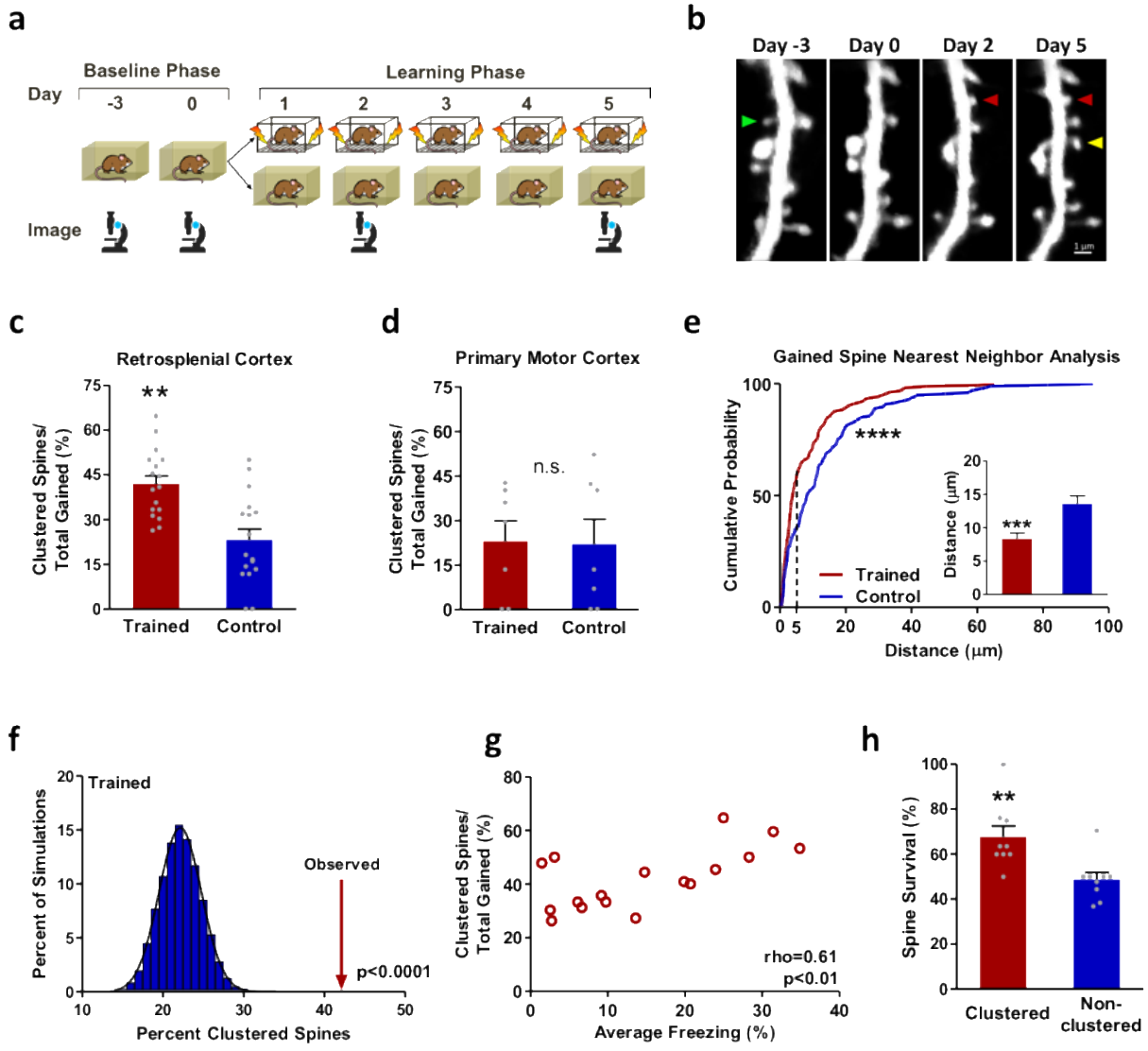

Figure 4.1. Contextual learning induces clustered spine formation in RSC. (a) Timeline of contextual learning and imaging. **(b)** Representative example of longitudinal imaging of a dendritic segment. One spine is lost following the first baseline imaging session (green). One new spines is added by Day 2 of training and persists to Day 5 (red). Another new spine (yellow) is added by Day 5 of training and within 5 μm of the new persistent spine (red), forming a cluster. Scale bar indicates 1 μm. **(c)** Trained mice have a higher percentage of newly added spines that occur in clusters (≤5 μm) in RSC than home cage controls (42.0% vs 23.2%, n=17 mice per group; *Mann-Whitney* U=51.00, p=0.0014). **(d)** Contextual learning does not induce clustered spine addition in primary motor cortex relative to home cage controls (23.0% vs 22.0%, n=7 mice per group; U=24.00, p=1.00). **(e)** The cumulative probability distribution of nearest neighbor measurements for spines formed during CFC in RSC shows that training significantly shifts these distances towards smaller values (Trained, n=155 distance measurements; Control, n=173 distance measurements; *Two-sample Kolmogorov-Smirnov*, D=0.2610, p=2.1006e-05). Inset is mean ± s.e.m. of values in distribution (8.3% vs 13.6%, *Mann-Whitney* U=10294, p=0.0003). **(f)** The percentage of clustered new spines is significantly greater than chance. Shown is a histogram of 10,000 simulations of randomized new spine positions, where the percent of new spines within 5 μm of each other was calculated. The arrow represents the actual percentage of clustered spines observed from the data, black line is Gaussian fit of data (mean of Gaussian fit = 22.1%, observed = 42.0%, n=17 mice; p<0.0001, as no simulated values were as or more extreme than the observed value). **(g)** Clustered spine formation is linearly correlated with freezing averaged from Day2 to Day5 (n=17 mice; *Spearman's rho*=0.61, p=0.0088). **(h)** Clustered spines imaged at the end of training (Day5) have a higher survival rate than non-clustered spines 4-6 weeks after training (67.6% vs 49.0%, n=9 mice; *Mann-Whitney* U=8.000,

p=0.0042). Data are represented as mean ± s.e.m. for **c, d** inset of **e,** and **h**. ****p<0.0001, ***p<0.001, **p<0.01; n.s. not significant.

4.2 Methods

Same subjects and procedures as in Chapter 3.

Statistics

Clustering ratio equals the number of clustered spines divided by total number of new spines gained after Day 0 and stable at Day 5. Clustered spines are defined as a new spine that has a distance less than 5μm with another new spine. For the resampling analysis of clustering, the segment length and number of new spines were collected for each segment of dendrite. For each resampling, the new spines were randomly distributed along the length of each dendritic segment. The average percentage of these repositioned spines within 5 μm of each other was calculated. This process was repeated 10,000 times for each method of analysis and the resulting mean values across all animals were compared to the observed mean value.

4.3 Results

I trained *Ccr5*$^{+/-}$ mice and their wildtype (WT) littermate controls in either CFC or Morris Water Maze (MWM) -a spatial learning task- and imaged dendritic spines in RSC in a subset of animals

that expressed Thy1-YFP (Fig. 4.2a, d). I have confirmed that the *Ccr5*$^{+/-}$ mice showed superior performances in both CFC (Fig. 2.1) and MWM (Fig. 2.2). Training in MWM also induced clustered spine formation in RSC (Fig. 4.3); and clustering is significantly greater than chance (Fig. 4.4). Remarkably, contextual and spatial learning-related spine clustering were enhanced in the RSC of *Ccr5*$^{+/-}$ mice (Fig. 4.2b, e); and, clustered spines added during training (CFC or MWM) were significantly more stable than non-clustered spines at 4 weeks post-training for both *Ccr5*$^{+/-}$ and WT animals (Fig. 4.2c, f). Importantly, at 4 weeks post-training, the percentage of clustered spine survival correlated with remote memory performance (Fig. 4.5), again suggesting a role for clustered spines in long-term cortical information storage.

Chronic treatment with MK801 impaired clustered spine formation in both *Ccr5*$^{+/-}$ and WT mice (Fig. 4.6), further demonstrating that spine clustering is a plasticity-dependent mechanism of learning and memory.

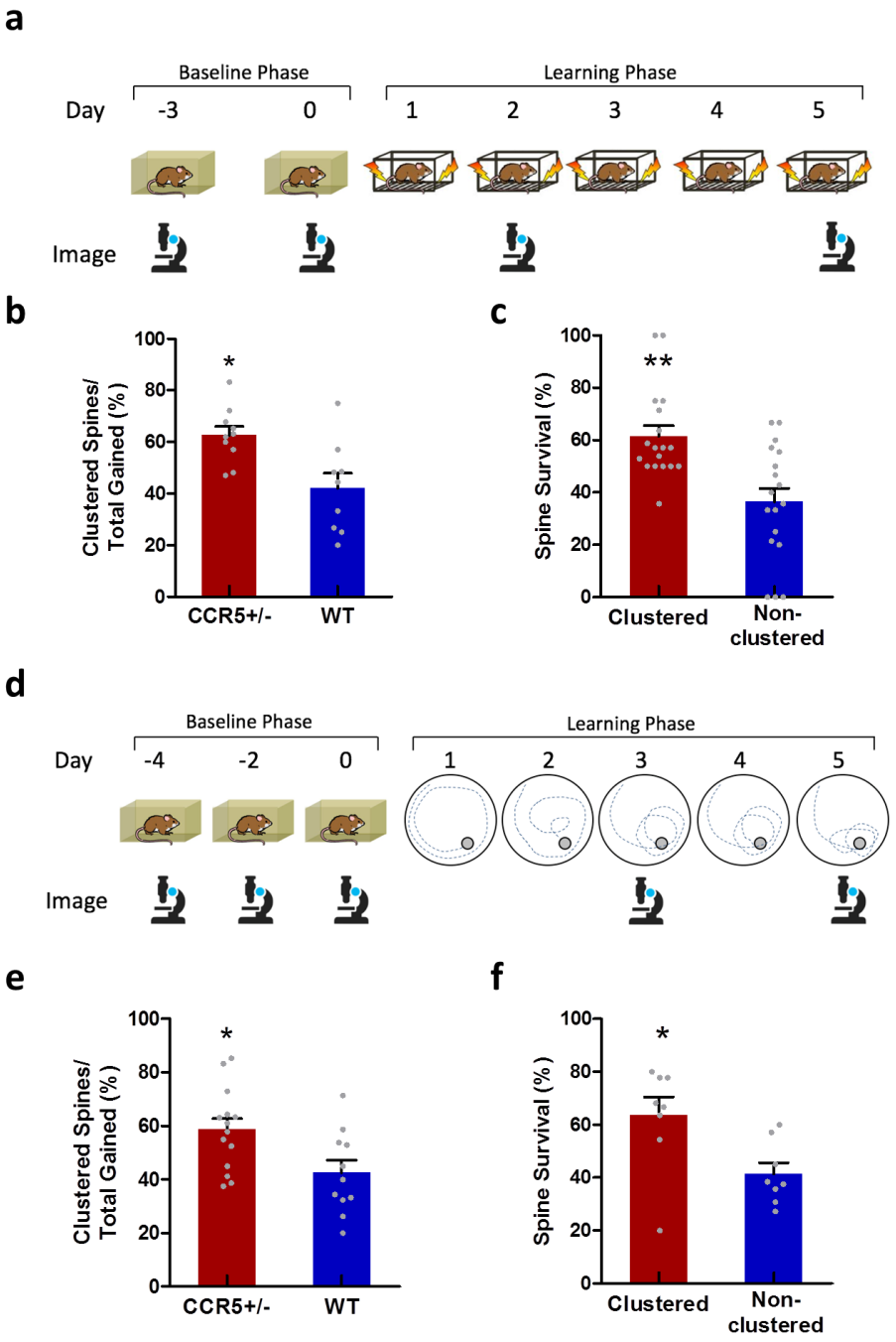

Figure 4.2. *Ccr5* heterozygous null mutation (*Ccr5*$^{+/-}$) augments learning-related spine clustering in RSC. **(a)** Timeline of CFC training and imaging. **(b)** The percentage of new spines added in clusters during CFC is significantly greater for *Ccr5*$^{+/-}$ than WT littermates (*Ccr5*$^{+/-}$

n=10, WT *n*=9; *U*=15.50, *p*=0.0178). **(c)** Clustered spines added during CFC are more stable at 4 weeks post-training than non-clustered spines added at the same time (*n*=18 mice with combined *Ccr5*$^{+/-}$ and WT; *U*=62.50, *p*=0.0017). **(d)** Timeline of MWM training and imaging. **(e)** The percentage of new spines added in clusters during MWM training is significantly greater for *Ccr5*$^{+/-}$ than WT littermates (*Ccr5*$^{+/-}$ *n*=14, WT *n*=11; *U*=33.50, *p*=0.0186). **(f)** Clustered spines added during MWM are significantly more stable at 4 weeks post-training than non-clustered spines added at the same time (*n*=8 mice with combined *Ccr5*$^{+/-}$ and WT; *U*=10.00, *p*=0.0207). Data are represented as mean ± s.e.m. ***p*<0.01, **p*<0.05; n.s., not significant.

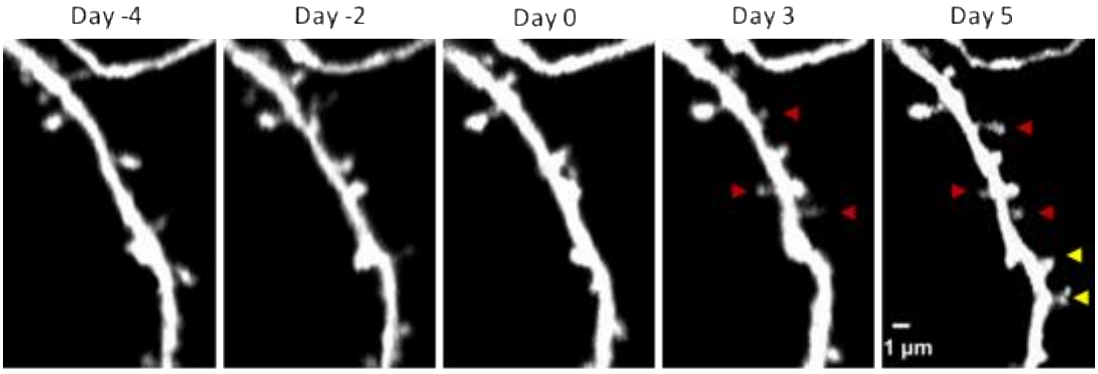

Figure 4.3. Representative example of longitudinal imaging of a dendritic segment during spatial learning. Three new spines were added by Day 3 of MWM training within 5 µm of each other (red arrowhead). Two new spines were added between Day 3 and 5 of training within 5 µm of each other (yellow arrowhead). There are total five learning-related clustered spines in this example.

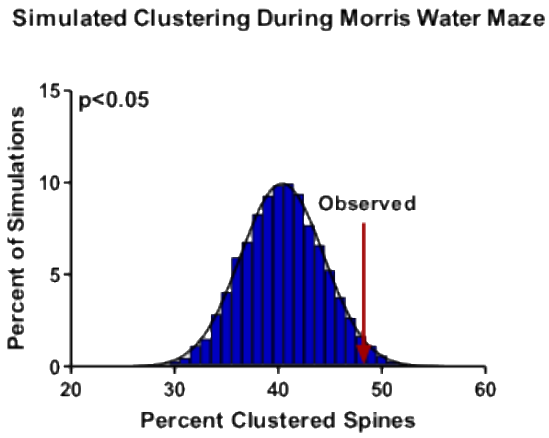

Figure 4.4. Resampling analysis indicates that the percentage of clustered new spines during spatial learning is significantly greater than chance. Shown is a histogram of 10,000 simulations of randomized new spine positions, where the percent of new spines within 5 μm of each other was calculated and averaged across animals. The arrow represents the actual averaged percentage of clustered spines observed from the data, black line is Gaussian fit of data (mean of Gaussian fit = 40.4%, observed= 48.8%, *n*=7 mice; *p*=0.0185, one tailed).

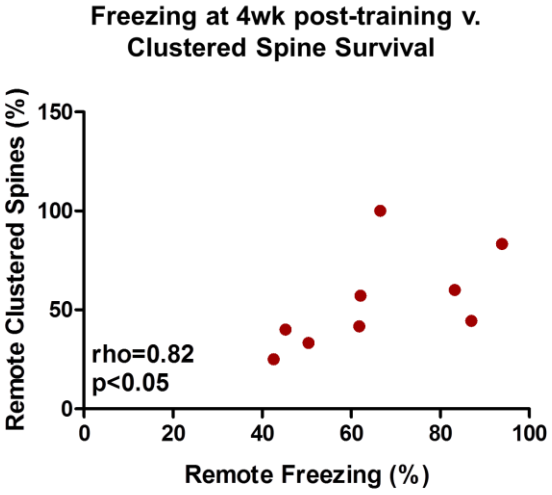

Figure 4.5. The percentage of persistent learning-related clustered spines is correlated with remote memory. Wild type mice were tested for their memory of the training context four

weeks after contextual training ended. Animals were re-imaged at this time point and the stability of both clustered and non-clustered spines gained during learning was assessed. The number of surviving clustered spines was divided by the total number of surviving spines gained during learning and multiplied by 100% to calculate the percentage of remote clustered spines. This percentage is linearly correlated with the freezing levels at 4 weeks post-training (*n*=9 WT mice; *p*=0.0108). Spearman's rho is indicated on graph.

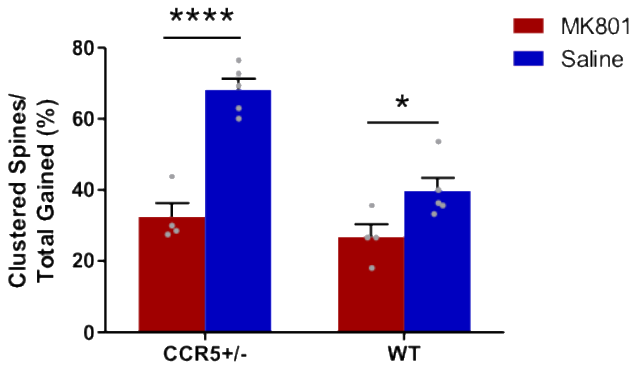

Figure 4.6. Learning-related spine clustering is NMDA receptor activity-dependent. MK801 treatment significantly reduce clustered spine formation in both *Ccr5*$^{+/-}$ and WT littermates (MK801|*Ccr5*$^{+/-}$ *n*=4, Saline|*Ccr5*$^{+/-}$ *n*=5, MK801|WT *n*=4, Saline|WT *n*=5, Two-way ANOVA, genotype x treatment interaction: $F_{(1,14)}$=10.51, *p*=0.0059; Bonferroni post-test for *Ccr5*$^{+/-}$: *p*<0.0001, WT: *p*<0.05). Data are represented as mean ± s.e.m. ****p<0.0001, *p<0.05.

4.4 Discussion

Together, these results indicate that clustered plasticity is a general information storage mechanism, not only for procedural memory in motor cortex (Fu et al., 2012), but also for episodic-like memory in RSC. My findings extend the clustered plasticity hypothesis by demonstrating that clustered spines are likely to be the storage sites of episodic-like memory. My findings include two different memory systems: contextual memory by CFC and spatial memory by MWM. Both of learning tasks induce clustered spine formation, which are more stable than the non-clustered spines. Importantly, memory at a remote time point (4 weeks after training ends) is reflected by the percentage of clustered spines that survived at the remote point, further suggesting that clustered spines facilitate long-term memory storage. *Ccr5*$^{+/-}$ results demonstrate that mice with enhancements of contextual and spatial learning and memory, also have enhancements in spine clustering. Spine clustering is driven by plasticity-dependent mechanisms, as antagonist of NMDA (*N*-methyl-D-aspartate) receptor prevent spine clustering after learning. Taken together, these results demonstrate that enhancements to spine turnover and spine clustering are reflected in enhancements in contextual and spatial learning and memory. This first evidence of 'gain-of-function' manipulation dramatically add to the links between spine turnover, spine clustering, and learning and memory.

Chapter 5 Spines of distinct memories do not tend to form clusters

5.1 Introduction

Memories stored in different dendritic branches are thought to be a mechanism of memory specificity (Cichon and Gan, 2015). Clustered plasticity hypothesis suggest that clustered spines tend to be co-active, thus they should be in the same or related memory circuit (Kleindienst et al., 2011; Takahashi et al., 2012; Wilms and Hausser, 2015). If this hypothesis is true, spines added at a later time point of learning should be added closer to spines gained during the early learning stage, instead of being randomly distributed, or being added next to spines from unrelated memory. Therefore, I hypothesize that the spines gained at an earlier stage of learning serve as an attraction site for later spines to cluster with. To do this, mice were trained with CFC for 5 days. Spine images were taken on Day2 (early stage) and Day5 (late stage). As a control, mice were trained in a dual-learning task, with 5 days of MWM followed by 5 days of CFC. Images were taken on Day5 (end of MWM) and Day10 (end of CFC). The interval between two tasks is 24 hours. The timeline of behavior training and imaging is shown in Fig. 5.1.

5.2 Methods

Resampling analysis of cross-clustering

Resampling method is shown in Fig. 5.2. The positions of all spines identified during imaging were determined for each segment of dendrite. 1st task spines indicate spines that do not exist on

Day0, but gained by Day5. 2nd task spines indicate spines that do not exist on Day5, but gained by Day10. Early spines indicate spines that do not exist on Day0, but gained by Day2. Late spines indicate spines that do not exist on Day2, but gained by Day5.

For each permutation, the number of 2nd task (or late) spines present on a given segment was counted and this number was used to randomly re-assign the "2nd task (or late) spine" identity to all possible spine positions on that segment. The 1st task (or early) spines were kept in the observed position. The average percentage of these repositioned 2nd task (or late) spines that were within 5 μm to the 1st task (or early) spines was calculated. This process was repeated 10,000 times and the resulting mean values across all animals were compared to the observed mean value.

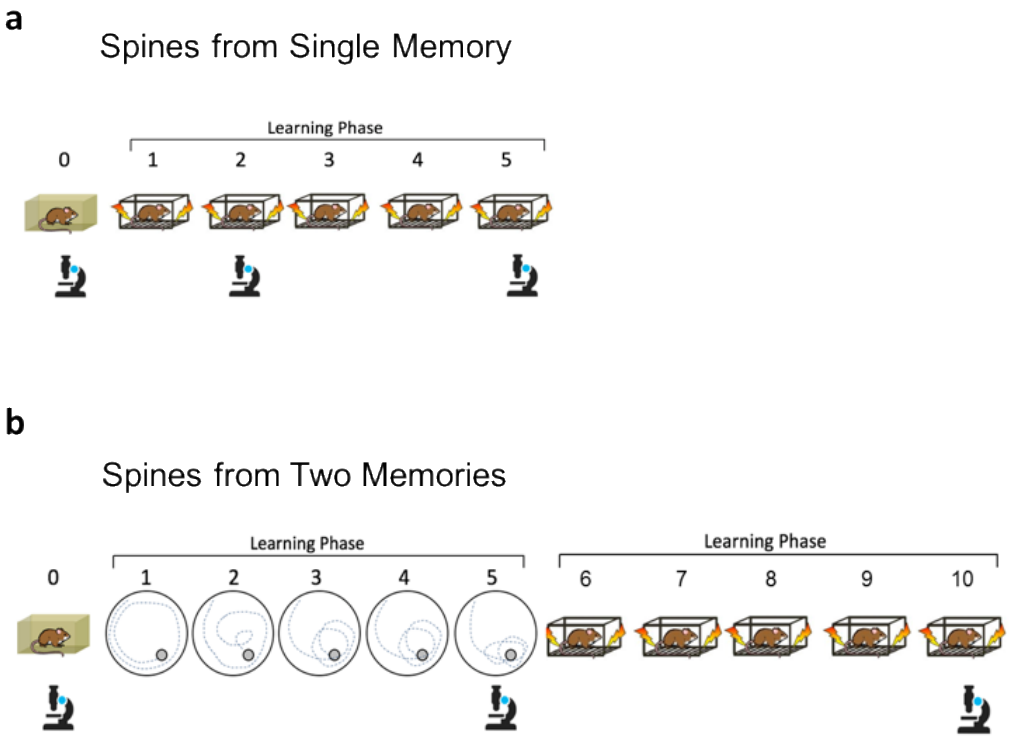

Figure 5.1. Timeline of training and imaging. (a) Timeline for CFC training only. **(b)** Timeline for MWM-CFC dual task training.

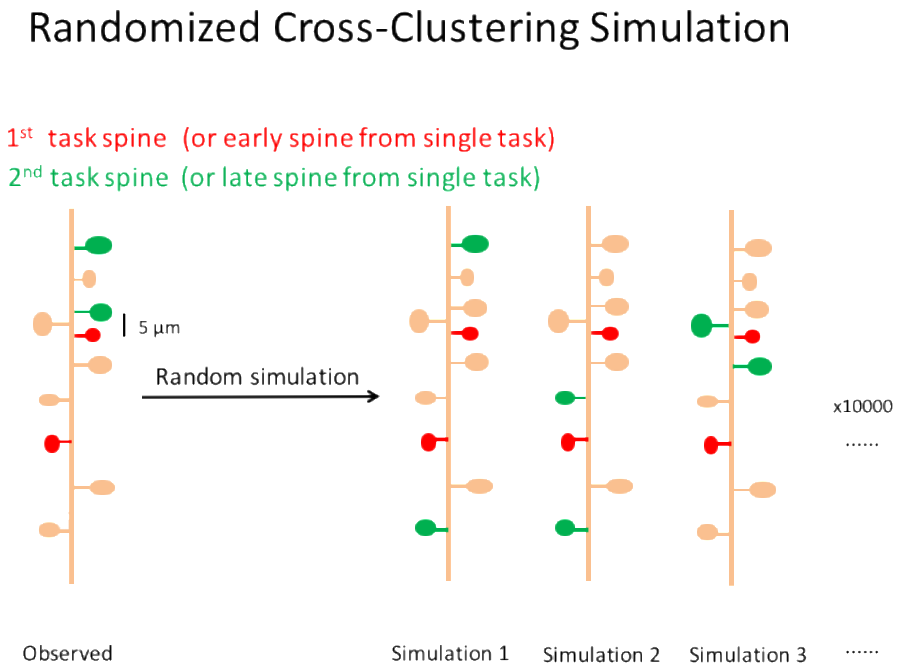

Figure 5.2. Method of randomized cross-clustering simulation. Spines gained during 1st task (or early stage) were kept at the observed position, while the 2nd task (or late stage) spine identities were randomly assigned based on the number of 2nd task (or late stage) spines. Simulation were repeated 10,000 times. Randomized spines were simulated within dendritic branches.

5.3 Results

I analyzed the cross-clustering ratio with resampling bootstrap method described in Fig 5.2. In mice trained with single task, the percentage of Day5 spines that cluster with Day2 spines is significantly above chance level (Fig. 5.3a), suggesting that the spines formed during early stages

serve as attraction sites for later spines to cluster with. In contrast, in mice trained with dual-learning task, the dual-task cross clustering ratio (27.8%) observed from the experiment falls into the median of randomly simulated values (Fig. 5.3b), suggesting that MWM and CFC spines ensembles are independent from each other. In *Ccr5*$^{+/-}$ mice, the result is consistent with WT. Two distinct tasks-induced spines do not tend to form clusters (Fig. 5.4). This finding further support the clustered plasticity hypothesis that clustered spines are involved in same or related circuit.

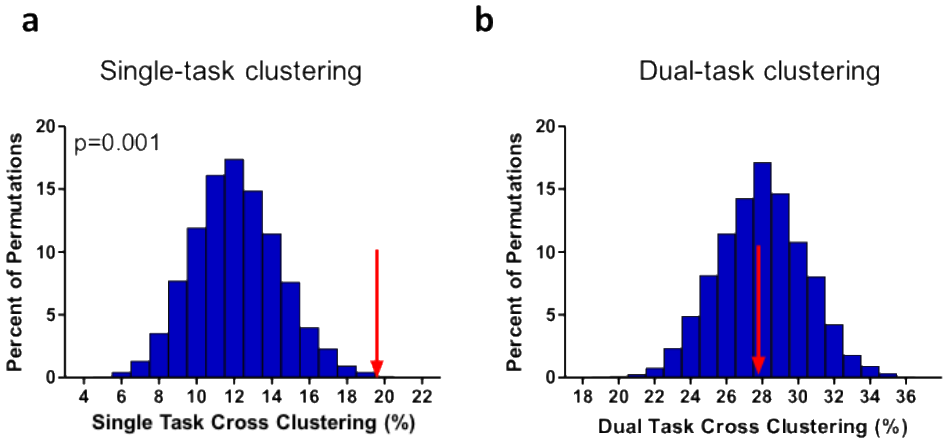

Figure 5.3. Resampling analysis of cross clustering. (a) Spines from the same memory circuit tend to form clusters. Shown is a histogram of 10,000 permutations of Day5 new spine identity, where the percent of Day5 new spines that are clustered with Day2 new spines (within 5 μm of each other) is calculated. The arrow represents the actual percentage of Day5-Day2 clustered spines observed from the data (n=17 wildtype mice; Permutation test, p=0.001). **(b)** The probability for distinct memories-induced new spines to form clusters is at the chance level. Shown is a histogram of 10,000 permutations of CFC new spine identity, where the percent of CFC new spines that are clustered with MWM new spines (within 5 μm of each other) is

calculated. The arrow represents the actual percentage of CFC-MWM clustered spines observed from the data (n=7 wildtype mice; Permutation test, p>0.05).

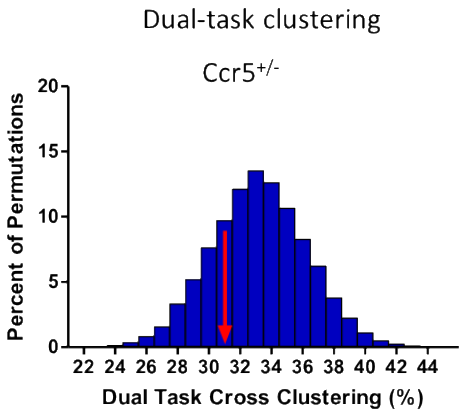

Figure 5.4. Resampling analysis of cross clustering in *Ccr5*$^{+/-}$ mice. The probability for distinct memories-induced new spines to form clusters is at the chance level. Shown is a histogram of 10,000 permutations of CFC new spine identity, where the percent of CFC new spines that are clustered with MWM new spines (within 5 μm of each other) is calculated. The arrow represents the actual percentage of CFC-MWM clustered spines observed from the data (n=6 *Ccr5*$^{+/-}$ mice; Permutation test, p>0.05).

5.4 Discussion

The above finding is consistent with clustered plasticity hypothesis that the clustered spines are usually coactive, thus they are likely to be involved in the same or related memory circuit (Kleindienst et al., 2011; Lu and Zuo, 2017). MWM and CFC are considered as two different memories, with limited similarity. The above finding suggests that spines gained during two

different tasks do not tend to cross cluster with each other. This may add to the mechanisms of memory specificity: memories are still different even when they are encoded on the same dendritic branch, so that we usually do not recall unrelated memories. In contrast, spines gained from one repetitive task prefer to form cluster with each other. This clustered distribution of spines from same or related memories is both timely and spatially efficient. Events from the same memory or related memories can be integrated by coactivation of clustered spines. The shared local protein resource may help clustered spines to stabilize. In addition, this clustered distribution of spines may guide the pre-synaptic axons that are from the same or related memory circuit to a targeted dendritic space. Therefore, memory of related events may be represented by a bundle of circuits which are spatially close to each other.

Chapter 6 Hotspots of dendritic spine turnover facilitate spine clustering

6.1 Introduction

I have found that pre-learning spine turnover and learning-related spine clustering both correlate with contextual learning and memory. *Ccr5*$^{+/-}$ mice have enhanced pre-learning spine turnover, also show enhanced spine clustering after learning. Next, it is interesting to explore the relationship between pre-learning spine turnover and learning-related spine clustering, and ask

whether these two spine measurements have a positive relation with each other. I hypothesize that pre-learning spine turnover serves as a method for neurons to sample their surrounding synaptic space. With an increased turnover rate, neurons are able to more efficiently sample this space and thus are more likely to make connections with presynaptic partners during learning. Clustering then serves as a mechanism to stabilize these new synapses. To do this, correlation analyses are done at both mouse level and dendritic segment level. Next, a nearest neighbor distance simulation is performed to investigate whether the observed distance between a clustered spine to its nearest pre-learning turnover spine is different from chance level.

6.2 Methods

Same subjects were used as previous chapters.

Resampling analysis of nearest neighbor distance

The distance of each clustered spine to its nearest neighbor pre-learning turnover spine was measured. These values were averaged for each animal and then all animals averaged together. For each permutation, the number of pre-learning turnover spines present on a given segment was counted and this number was used to randomly re-assign the "turnover spine" identity to all possible spine positions on that segment. The clustered spines were kept in the observed position. The distance of each clustered spine to its nearest "simulated turnover spine" was measured. These values were averaged for each animal and then all animals averaged together for each permutation, with the process repeated a total of 10,000 times.

Resampling analysis of distribution of segments

For resampling analysis of distribution of segments with different levels of pre-learning turnover and post-learning clustering, the null hypothesis simulation is done by permuting the number of clustered spines on each dendritic segment within each animal and recalculating the percentages of segments of the 4 categories. For example, a mouse has 10 segments and each segment has 2 numbers: number of clustered spines, and number of turnover spines. We simulate the null hypothesis by permuting the number of clustered spines on the 10 segments, without changing the original number of turnover spines. This will yield a random distribution of clustered spines on dendritic segments that is independent of pre-learning turnover. The permutation was repeated for 10,000 times.

6.3 Results

As expected, I found a significant positive correlation between pre-learning spine turnover and learning-related spine clustering at mouse level (Fig. 6.1a). To further explore the spatial relationship between the two, I examined turnover and clustering at the level of dendritic segments and normalized by segment length. The results show that segments with greater amounts of pre-learning turnover also have increased levels of learning-related clustering (Fig. 6.1b). Accordingly, I analyzed the average nearest-neighbor distance between learning-related clustered spines and spines having undergone pre-learning turnover and found this value to be significantly smaller than random chance (Fig. 6.1c), revealing the presence of hotspots of turnover and clustering in dendrites. In *Ccr5*$^{+/-}$ mice, pre-learning spine turnover and learning-

related spine clustering are also correlated at mouse level (Fig. 6.2a) and dendritic segment level (Fig. 6.2b). Next, I analyzed the distribution of dendritic segments regarding levels of pre-learning turnover and learning related clustering. I found that the percentage of segments with concordant turnover and clustering (segments having both clustering and turnover or segments with neither) was higher than random chance, while the percentage of segments with discordant turnover and clustering (segments with only one of the two) was lower than chance level (Fig. 6.3).

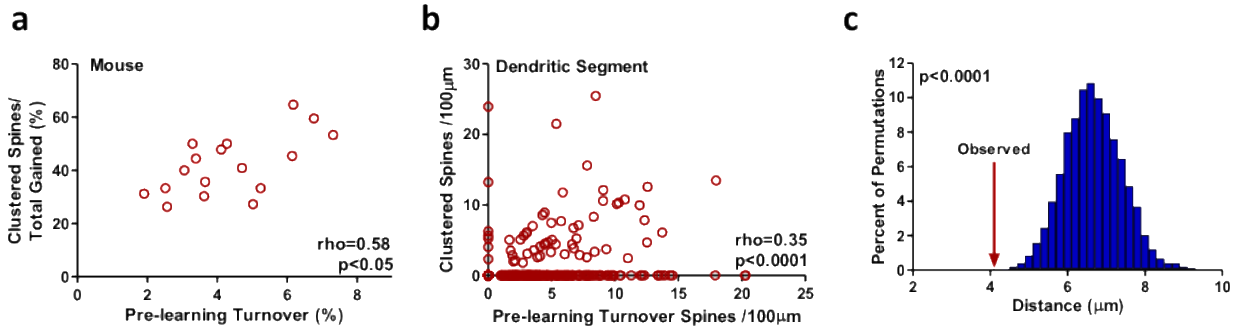

Figure 6.1. Learning-related spine clustering occurs within segments of increased pre-learning spine turnover in wild type mice. (a) There is a positive correlation between the percent of pre-learning spine turnover and the percent of learning-related spine clustering within individual animals (*n*=17 WT mice; *p*=0.0154). **(b)** There is a positive correlation between the density of spines undergoing pre-learning turnover and the density of learning-related clustered spines on each segment of dendrite (*n*=577 segments across 17 WT mice; *p*<0.0001). Segments are defined as the entire length of each branch of dendrite identifiable as unique during imaging. **(c)** The average nearest neighbor distance from each learning-related clustered spine to its closest

neighboring pre-learning turnover spine is significantly smaller than chance. 10,000 permutations of pre-learning turnover spine identity were run, with nearest neighbor distance to clustered spines measured and averaged in each (n=577 segments; Permutation test, p<0.0001, as no permutation values were as or more extreme than our observed value). Spearman's rho is indicated in **a** and **b**.

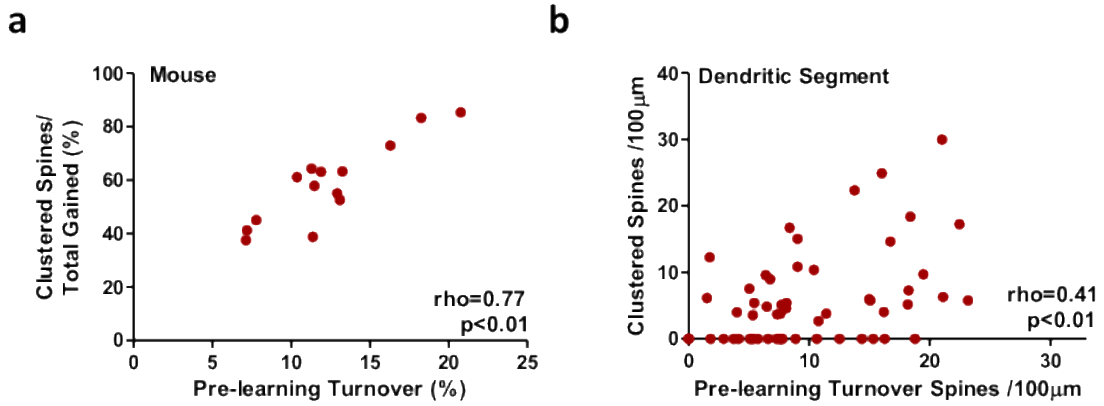

Figure 6.2. Pre-learning turnover and learning-related spine clustering are correlated in *Ccr5*$^{+/-}$ mice. (a) A significant positive correlation exists between the percent of pre-learning spine turnover and the percent of learning-related spine clustering within individual *Ccr5*$^{+/-}$ animals (n=14 *Ccr5*$^{+/-}$ mice; p=0.0014). **(b)** A significant positive correlation exists between the density of spines undergoing pre-learning turnover and the density of learning-related clustered spines on each segment of dendrite (n=57 segments over 6 *Ccr5*$^{+/-}$ mice; p=0.0018). Clustering and turnover were normalized to the length of dendrite for each mouse so that comparisons across mice could be accomplished. Spearman's rho is indicated in **a** and **b**.

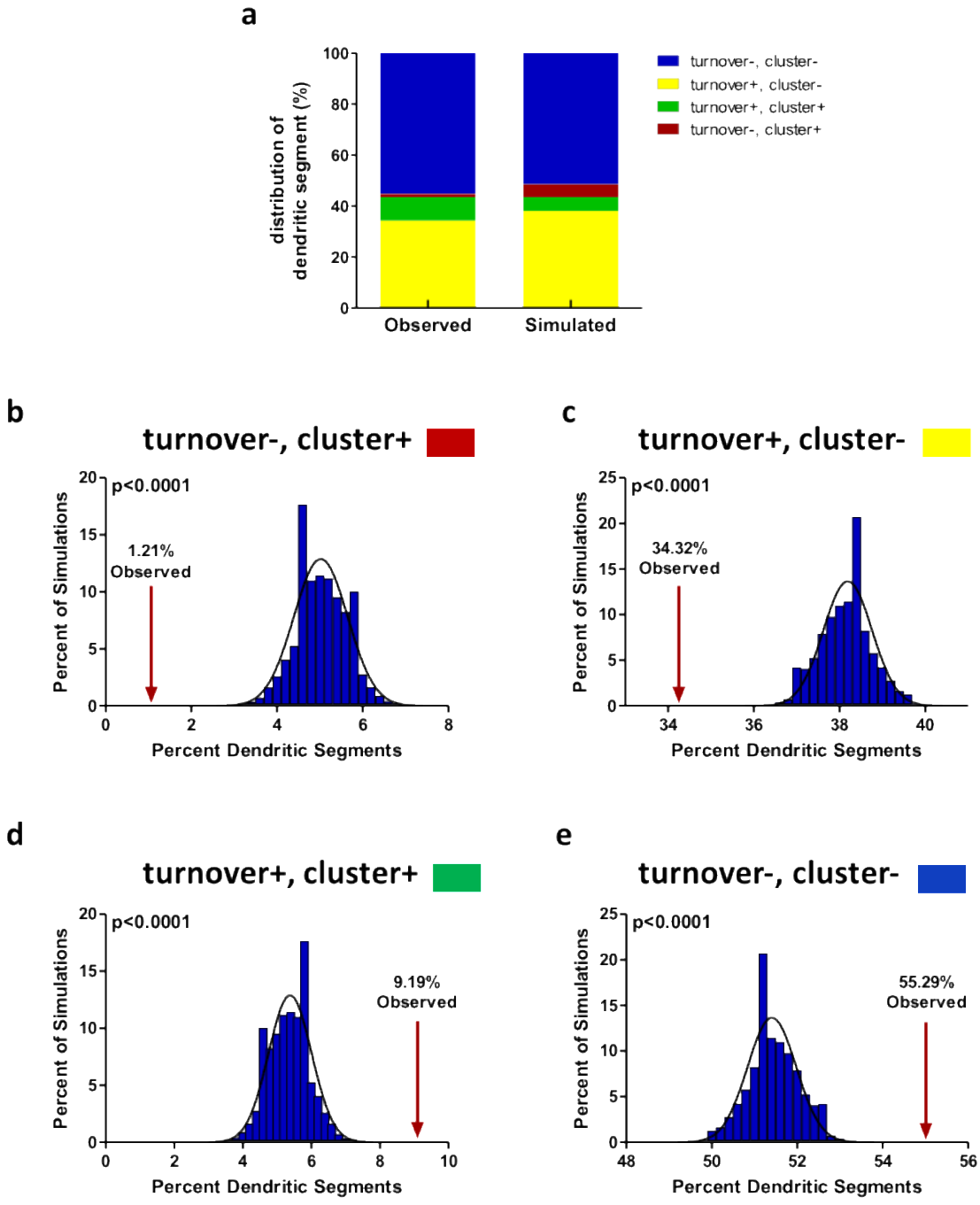

Figure 6.3. Resampling analysis indicates that the distribution of dendritic segments with concordant pre-learning turnover and post-learning clustering observed in data is greater than chance. (a) Observed distribution of dendritic segments that fall into the four categories: i.

segments with no pre-learning turnover spines or clustered spines (blue); ii. segments with pre-learning turnover, but without clustered spines after learning (yellow); iii. segments with both pre-learning turnover and clustered spines (green); iv. segments without pre-learning turnover spines, but gain clustered spines after learning (red). Each observed percentage of the 4 categories is shown individually in the following graphs. The distribution of segments in the same 4 categories are calculated using simulated values, which is done by permuting the number of clustered spines on each dendritic segment within each subject and recalculating the percentages of segments of the 4 categories. Simulated distribution is the average of simulated values of 17 trained mice. **(b, c)** Percentage of segments without turnover, but gain clusters (b) and segments with turnover but do not gain clusters (c) are both lower than chance level. **(d, e)** Percentage of segments with both turnover and clusters (d) and segments without any turnover or clusters (e) are both higher than chance level. Shown in **b, c, d** and **e** is a histogram of 10,000 permutations. The arrow represents the actual percentage of dendritic segments in indicated category observed from data, black line is Gaussian fit of data (mean of Gaussian fit = 5.0%, 38.2%, 5.4% and 51.4% in **b, c, d** and **e** respectively; observed values are indicated in graphs; *n*=17 trained mice).

6.4 Discussion

Based on above evidence, I posit a model where pre-learning spine turnover serves as a method for neurons to sample their surrounding synaptic space. With an increased turnover rate, neurons are able to more frequently sample this space and thus are more likely to make connections with presynaptic partners during learning. Clustering then serves as a mechanism to stabilize these

new synapses. The dendrites with frequent spine turnover before learning become hotspots of memory encoding and storage, because they are likely to have new spines form in clusters on those hotspots.

Chapter 7 Conclusions

7.1 Summary of results

By using transcranial two-photon microscopy to track spine dynamics, I examined the relation between basal spine turnover, contextual or spatial learning and memory, and subsequent spine clustering in the mouse retrosplenial cortex (RSC) - a neocortical structure critical for spatial and contextual learning and memory (Corcoran et al., 2011; Cowansage et al., 2014; Czajkowski et al., 2014; Keene and Bucci, 2008; Robinson et al., 2012). I found that pre-learning spine turnover predicts both learning and memory performance and learning and memory-related spine clustering. Accordingly, *Ccr5*$^{+/-}$ as a genetic manipulation that enhances pre-learning spine turnover also enhances clustering and learning and memory. Spines formed during one learning task do not form cluster with spines induced by an unrelated learning task. Further, I found that pre-learning spine turnover and learning-related clustering are related processes that themselves exhibit spatial clustering within the dendritic tree. According to these findings, I posit a hotspot model of spine formation in which higher rates of pre-learning spine turnover facilitate the

formation of learning and memory-related clustered spines near regions of turnover, and that clustering serves as a means to stabilize structural plasticity (Fig 7.1).

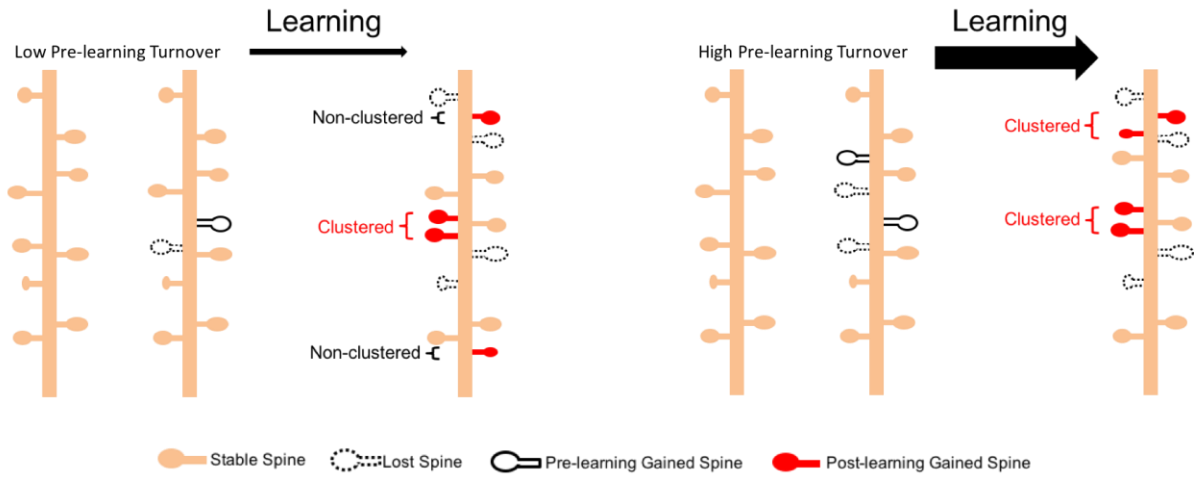

Figure 7.1. Model of hotspots of spine turnover and clustering. Dendrites with higher rates of pre-learning spine turnover may allow neurons to more efficiently sample the surrounding synaptic space and subsequently establish more clustered connections after learning. Clustered spine addition within a small spatial window allows for stabilization of the encoded information.

7.2 Discussion

Our understanding of how information is stored and memories formed within the brain has seen remarkable advancements in the last several decades (Dudai and Morris, 2013; Kandel et al., 2014). For example, it is now generally accepted that information processing and storage occurs across physiological and morphological levels from neurons to dendrites to individual dendritic

spines (Bailey and Kandel, 1993; Holtmaat and Caroni, 2016; Kandel et al., 2014; Kastellakis et al., 2015). For instance, a recent study demonstrated that light-activated shrinkage of new or recently potentiated dendritic spines was sufficient to weaken memory strength (Hayashi-Takagi et al., 2015). Outstanding, though, is a unifying framework for how subcellular processes, such as dendritic spine addition, affect cellular and network properties during learning and information storage.

An emerging theory, known as the clustered plasticity hypothesis, proposes that plastic events occur in a clustered fashion within the dendritic tree (DeBello et al., 2014; Govindarajan et al., 2006; Kastellakis et al., 2015; Poirazi and Mel, 2001). In agreement with clustered plasticity hypothesis, several studies have shown that long-term potentiation (LTP) induces biochemical interactions between clustered spines that alter the threshold for induction of LTP (Harvey and Svoboda, 2007; Harvey et al., 2008; Murakoshi et al., 2011). Further, facilitation of LTP between clustered spines is also due to the sharing of protein synthesis products (Govindarajan et al., 2011). Studies of structural plasticity have additionally shown that learning drives clustered addition of new dendritic spines (Fu et al., 2012; McBride et al., 2008). From a functional perspective, recent data demonstrates enhanced orientation selectivity due to clustered synaptic inputs (Wilson et al., 2016). Interestingly, studies in sensory cortices also suggest that clustered spines may serve to integrate different inputs, as synapses on nearby spines appear to code for distinct visual orientations, sound frequencies, or whisker combinations (Chen et al., 2011; Jia et al., 2010; Varga et al., 2011). However, the principles that govern where and to what extent clustered plasticity operates within dendrites, as well as how these subcellular events impact network dynamics have remained unclear.

My *in vivo* imaging study suggests answers to these outstanding questions. First, animals have individual variability in their baseline rate of spine turnover, and that higher rates of this pre-learning spine turnover correlate with future levels of learning and memory. While similar findings of pre-learning spine turnover predicting future learning have been previously demonstrated in zebra finch during the critical period for song learning (Roberts et al., 2010), my results are important in extending these findings to adult mammalian learning and memory. Critical period plasticity is generally regarded as unique during brain development (Hensch, 2005), however this work shows that structural mechanisms of plasticity important during this juvenile period of learning also operate in adult mammals. Further, the results show that spine dynamics are an important component of neuronal plasticity, learning & memory, and that this spans both classes within the phylum Chordata as well as very different memory systems.

I also show that learning of contextual and spatial tasks increases clustered addition of dendritic spines in RSC. Spine clustering in association with learning has been demonstrated in primary motor cortex during motor learning tasks (Fu et al., 2012) and in barn owl vestibular systems during prism adaptation (McBride et al., 2008). This dissertation add to this body of evidence in support of the clustered plasticity model by showing that spine clustering also occurs in association with episodic-like learning and is moreover positively correlated with learning and memory. Importantly, I show that the *Ccr5*$^{+/-}$ mutation alters spine dynamics and causes enhancements in learning and memory. Moreover, *Ccr5*$^{+/-}$ results show that a genetic manipulation that increases spine turnover also causes an increase in clustering. While other studies have shown that shrinkage of spines (Hayashi-Takagi et al., 2015) negatively impacts memory, this first evidence of positive manipulation of spine dynamics adds a critical line of convergent evidence in support to the clustered plasticity model.

The increases in pre-learning spine turnover and clustering by *Ccr5*$^{+/-}$ mutation is prevented by NMDA receptor antagonist, suggesting that both events are due to plasticity-dependent mechanisms mediated by NMDA receptors. In contrast, NMDA receptor antagonists did not affect the increased rates of spine turnover in *Fmr1* knockout mice, a mouse model of autistic spectrum disorder (Nagaoka et al., 2016), demonstrating that they are not due to plasticity mechanisms mediated by NMDA receptors. In addition, the *Ccr5*$^{+/-}$ mutation also causes increased clustered spine formation after learning. I show that clustered spines are more stable and therefore they may facilitate long-term information storage. As such, although *Ccr5* knockout mice and *Fmr1* knockout mice both show enhanced spine turnover (Cruz-Martin et al., 2010; Nagaoka et al., 2016; Padmashri et al., 2013; Pan et al., 2010), the two mutations result in opposite effects on learning and memory: while the *Ccr5* mutation causes learning and memory enhancement (Zhou et al., 2016), the *Fmr1* mutation causes learning and memory deficits (Bolduc et al., 2008; Dolen et al., 2007; Koekkoek et al., 2005; Krueger et al., 2011; Zhao et al., 2005).

This dissertation also show that spines gained during two different tasks do not tend to cross cluster with each other. This may add to the mechanisms of memory specificity: memories are still different even when they are encoded on the same dendritic branch. In contrast, spines gained from one repetitive task prefer to form cluster with each other. This clustered distribution of spines from same or related memories is both timely and spatially efficient. Events from the same memory or related memories can be integrated by coactivation of clustered spines. The shared local protein resource may help clustered spines to stabilize. In addition, this clustered distribution of spines may guide the pre-synaptic axons that are from the same or related memory

circuit to a targeted dendritic space. Therefore, memory of related events may be represented by a bundle of circuits which are spatially close to each other.

Given my finding that increases in turnover occur in association with increased spine clustering and learning, I explored a possible structural relation between these phenomena. I find that learning-related clustering preferentially occurs on segments of dendrites that have undergone pre-learning turnover. Strikingly, I also found that clustered spine addition preferentially occurs near areas of spine turnover on these dendritic segments. These data suggest that pre-learning turnover facilitates the process of clustering and thus generates hotspots of structural plasticity. Therefore, I propose that increased baseline turnover allows neurons to efficiently sample their synaptic space, such that they can optimize synaptic connectivity during learning. When new connections do occur, clustering then integrates and stabilizes the acquired information.

7.3 References

Aggleton, J.P., and Vann, S.D. (2004). Testing the importance of the retrosplenial navigation system: lesion size but not strain matters: a reply to Harker and Whishaw. Neurosci Biobehav Rev *28*, 525-531.

Bailey, C.H., and Kandel, E.R. (1993). Structural changes accompanying memory storage. Annu Rev Physiol *55*, 397-426.

Bolduc, F.V., Bell, K., Cox, H., Broadie, K.S., and Tully, T. (2008). Excess protein synthesis in Drosophila fragile X mutants impairs long-term memory. Nat Neurosci *11*, 1143-1145.

Bourtchuladze, R., Frenguelli, B., Blendy, J., Cioffi, D., Schutz, G., and Silva, A.J. (1994). Deficient long-term memory in mice with a targeted mutation of the cAMP-responsive element-binding protein. Cell *79*, 59-68.

Branco, T., and Hausser, M. (2010). The single dendritic branch as a fundamental functional unit in the nervous system. Curr Opin Neurobiol *20*, 494-502.

Cai, D.J., Aharoni, D., Shuman, T., Shobe, J., Biane, J., Song, W., Wei, B., Veshkini, M., La-Vu, M., Lou, J., *et al.* (2016). A shared neural ensemble links distinct contextual memories encoded close in time. Nature *534*, 115-118.

Chen, X., Leischner, U., Rochefort, N.L., Nelken, I., and Konnerth, A. (2011). Functional mapping of single spines in cortical neurons in vivo. Nature *475*, 501-505.

Chklovskii, D.B., Mel, B.W., and Svoboda, K. (2004). Cortical rewiring and information storage. Nature *431*, 782-788.

Cichon, J., and Gan, W.B. (2015). Branch-specific dendritic Ca(2+) spikes cause persistent synaptic plasticity. Nature *520*, 180-185.

Corcoran, K.A., Donnan, M.D., Tronson, N.C., Guzman, Y.F., Gao, C., Jovasevic, V., Guedea, A.L., and Radulovic, J. (2011). NMDA receptors in retrosplenial cortex are necessary for retrieval of recent and remote context fear memory. J Neurosci *31*, 11655-11659.

Cowansage, K.K., Shuman, T., Dillingham, B.C., Chang, A., Golshani, P., and Mayford, M. (2014). Direct reactivation of a coherent neocortical memory of context. Neuron *84*, 432-441.

Cruz-Martin, A., Crespo, M., and Portera-Cailliau, C. (2010). Delayed stabilization of dendritic spines in fragile X mice. J Neurosci *30*, 7793-7803.

Czajkowski, R., Jayaprakash, B., Wiltgen, B., Rogerson, T., Guzman-Karlsson, M.C., Barth, A.L., Trachtenberg, J.T., and Silva, A.J. (2014). Encoding and storage of spatial information in the retrosplenial cortex. Proc Natl Acad Sci U S A *111*, 8661-8666.

De Roo, M., Klauser, P., and Muller, D. (2008). LTP promotes a selective long-term stabilization and clustering of dendritic spines. PLoS Biol *6*, e219.

DeBello, W.M., McBride, T.J., Nichols, G.S., Pannoni, K.E., Sanculi, D., and Totten, D.J. (2014). Input clustering and the microscale structure of local circuits. Front Neural Circuits *8*, 112.

Dolen, G., Osterweil, E., Rao, B.S., Smith, G.B., Auerbach, B.D., Chattarji, S., and Bear, M.F. (2007). Correction of fragile X syndrome in mice. Neuron *56*, 955-962.

Dudai, Y., and Morris, R.G. (2013). Memorable trends. Neuron *80*, 742-750.

Epstein, R.A. (2008). Parahippocampal and retrosplenial contributions to human spatial navigation. Trends Cogn Sci *12*, 388-396.

Frey, U., and Morris, R.G. (1997). Synaptic tagging and long-term potentiation. Nature *385*, 533-536.

Fu, M., Yu, X., Lu, J., and Zuo, Y. (2012). Repetitive motor learning induces coordinated formation of clustered dendritic spines in vivo. Nature *483*, 92-95.

Govindarajan, A., Israely, I., Huang, S.Y., and Tonegawa, S. (2011). The dendritic branch is the preferred integrative unit for protein synthesis-dependent LTP. Neuron *69*, 132-146.

Govindarajan, A., Kelleher, R.J., and Tonegawa, S. (2006). A clustered plasticity model of long-term memory engrams. Nat Rev Neurosci *7*, 575-583.

Han, J.H., Kushner, S.A., Yiu, A.P., Cole, C.J., Matynia, A., Brown, R.A., Neve, R.L., Guzowski, J.F., Silva, A.J., and Josselyn, S.A. (2007). Neuronal competition and selection during memory formation. Science *316*, 457-460.

Harker, K.T., and Whishaw, I.Q. (2004). A reaffirmation of the retrosplenial contribution to rodent navigation: reviewing the influences of lesion, strain, and task. Neurosci Biobehav Rev *28*, 485-496.

Harvey, C.D., and Svoboda, K. (2007). Locally dynamic synaptic learning rules in pyramidal neuron dendrites. Nature *450*, 1195-1200.

Harvey, C.D., Yasuda, R., Zhong, H., and Svoboda, K. (2008). The spread of Ras activity triggered by activation of a single dendritic spine. Science *321*, 136-140.

Hausser, M., and Mel, B. (2003). Dendrites: bug or feature? Curr Opin Neurobiol *13*, 372-383.

Hayashi-Takagi, A., Yagishita, S., Nakamura, M., Shirai, F., Wu, Y.I., Loshbaugh, A.L., Kuhlman, B., Hahn, K.M., and Kasai, H. (2015). Labelling and optical erasure of synaptic memory traces in the motor cortex. Nature *525*, 333-338.

Hensch, T.K. (2005). Critical period plasticity in local cortical circuits. Nat Rev Neurosci *6*, 877-888.

Holtmaat, A., Bonhoeffer, T., Chow, D.K., Chuckowree, J., De Paola, V., Hofer, S.B., Hubener, M., Keck, T., Knott, G., Lee, W.C., *et al.* (2009). Long-term, high-resolution imaging in the mouse neocortex through a chronic cranial window. Nat Protoc *4*, 1128-1144.

Holtmaat, A., and Caroni, P. (2016). Functional and structural underpinnings of neuronal assembly formation in learning. Nat Neurosci *19*, 1553-1562.

Holtmaat, A., and Svoboda, K. (2009). Experience-dependent structural synaptic plasticity in the mammalian brain. Nat Rev Neurosci *10*, 647-658.

Jia, H., Rochefort, N.L., Chen, X., and Konnerth, A. (2010). Dendritic organization of sensory input to cortical neurons in vivo. Nature *464*, 1307-1312.

Kandel, E.R., Dudai, Y., and Mayford, M.R. (2014). The molecular and systems biology of memory. Cell *157*, 163-186.

Kastellakis, G., Cai, D.J., Mednick, S.C., Silva, A.J., and Poirazi, P. (2015). Synaptic clustering within dendrites: an emerging theory of memory formation. Prog Neurobiol *126*, 19-35.

Keene, C.S., and Bucci, D.J. (2008). Contributions of the retrosplenial and posterior parietal cortices to cue-specific and contextual fear conditioning. Behav Neurosci *122*, 89-97.

Kleindienst, T., Winnubst, J., Roth-Alpermann, C., Bonhoeffer, T., and Lohmann, C. (2011). Activity-dependent clustering of functional synaptic inputs on developing hippocampal dendrites. Neuron *72*, 1012-1024.

Koekkoek, S.K., Yamaguchi, K., Milojkovic, B.A., Dortland, B.R., Ruigrok, T.J., Maex, R., De Graaf, W., Smit, A.E., VanderWerf, F., Bakker, C.E., *et al.* (2005). Deletion of FMR1 in Purkinje cells enhances parallel fiber LTD, enlarges spines, and attenuates cerebellar eyelid conditioning in Fragile X syndrome. Neuron *47*, 339-352.

Krueger, D.D., Osterweil, E.K., Chen, S.P., Tye, L.D., and Bear, M.F. (2011). Cognitive dysfunction and prefrontal synaptic abnormalities in a mouse model of fragile X syndrome. Proc Natl Acad Sci U S A *108*, 2587-2592.

Lai, C.S., Franke, T.F., and Gan, W.B. (2012). Opposite effects of fear conditioning and extinction on dendritic spine remodelling. Nature *483*, 87-91.

Lanahan, A., and Worley, P. (1998). Immediate-early genes and synaptic function. Neurobiol Learn Mem *70*, 37-43.

Larkum, M.E., and Nevian, T. (2008). Synaptic clustering by dendritic signalling mechanisms. Curr Opin Neurobiol *18*, 321-331.

Losonczy, A., and Magee, J.C. (2006). Integrative properties of radial oblique dendrites in hippocampal CA1 pyramidal neurons. Neuron *50*, 291-307.

Lu, J., and Zuo, Y. (2017). Clustered structural and functional plasticity of dendritic spines. Brain Res Bull *129*, 18-22.

Maguire, E.A. (2001). The retrosplenial contribution to human navigation: a review of lesion and neuroimaging findings. Scand J Psychol *42*, 225-238.

Martin, K.C., and Kosik, K.S. (2002). Synaptic tagging -- who's it? Nat Rev Neurosci *3*, 813-820.

McBride, T.J., Rodriguez-Contreras, A., Trinh, A., Bailey, R., and Debello, W.M. (2008). Learning drives differential clustering of axodendritic contacts in the barn owl auditory system. J Neurosci *28*, 6960-6973.

McKay, B.M., Matthews, E.A., Oliveira, F.A., and Disterhoft, J.F. (2009). Intrinsic neuronal excitability is reversibly altered by a single experience in fear conditioning. J Neurophysiol *102*, 2763-2770.

Miyashita, T., Kubik, S., Lewandowski, G., and Guzowski, J.F. (2008). Networks of neurons, networks of genes: an integrated view of memory consolidation. Neurobiol Learn Mem *89*, 269-284.

Moyer, J.R., Jr., Thompson, L.T., and Disterhoft, J.F. (1996). Trace eyeblink conditioning increases CA1 excitability in a transient and learning-specific manner. J Neurosci *16*, 5536-5546.

Murakoshi, H., Wang, H., and Yasuda, R. (2011). Local, persistent activation of Rho GTPases during plasticity of single dendritic spines. Nature *472*, 100-104.

Nagaoka, A., Takehara, H., Hayashi-Takagi, A., Noguchi, J., Ishii, K., Shirai, F., Yagishita, S., Akagi, T., Ichiki, T., and Kasai, H. (2016). Abnormal intrinsic dynamics of dendritic spines in a fragile X syndrome mouse model in vivo. Sci Rep *6*, 26651.

Oh, M.M., Oliveira, F.A., and Disterhoft, J.F. (2010). Learning and aging related changes in intrinsic neuronal excitability. Front Aging Neurosci *2*, 2.

Oh, W.C., Parajuli, L.K., and Zito, K. (2015). Heterosynaptic structural plasticity on local dendritic segments of hippocampal CA1 neurons. Cell Rep *10*, 162-169.

Padmashri, R., Reiner, B.C., Suresh, A., Spartz, E., and Dunaevsky, A. (2013). Altered structural and functional synaptic plasticity with motor skill learning in a mouse model of fragile X syndrome. J Neurosci *33*, 19715-19723.

Pan, F., Aldridge, G.M., Greenough, W.T., and Gan, W.B. (2010). Dendritic spine instability and insensitivity to modulation by sensory experience in a mouse model of fragile X syndrome. Proc Natl Acad Sci U S A *107*, 17768-17773.

Poirazi, P., and Mel, B.W. (2001). Impact of active dendrites and structural plasticity on the memory capacity of neural tissue. Neuron *29*, 779-796.

Polsky, A., Mel, B.W., and Schiller, J. (2004). Computational subunits in thin dendrites of pyramidal cells. Nat Neurosci *7*, 621-627.

Redondo, R.L., and Morris, R.G. (2011). Making memories last: the synaptic tagging and capture hypothesis. Nat Rev Neurosci *12*, 17-30.

Roberts, T.F., Tschida, K.A., Klein, M.E., and Mooney, R. (2010). Rapid spine stabilization and synaptic enhancement at the onset of behavioural learning. Nature *463*, 948-952.

Robinson, S., Poorman, C.E., Marder, T.J., and Bucci, D.J. (2012). Identification of functional circuitry between retrosplenial and postrhinal cortices during fear conditioning. J Neurosci *32*, 12076-12086.

Roth, T.L., and Sweatt, J.D. (2008). Rhythms of memory. Nat Neurosci *11*, 993-994.

Sano, Y., Shobe, J.L., Zhou, M., Huang, S., Shuman, T., Cai, D.J., Golshani, P., Kamata, M., and Silva, A.J. (2014). CREB regulates memory allocation in the insular cortex. Curr Biol *24*, 2833-2837.

Silva, A.J., Kogan, J.H., Frankland, P.W., and Kida, S. (1998). CREB and memory. Annu Rev Neurosci *21*, 127-148.

Silva, A.J., Zhou, Y., Rogerson, T., Shobe, J., and Balaji, J. (2009). Molecular and cellular approaches to memory allocation in neural circuits. Science *326*, 391-395.

Spruston, N. (2008). Pyramidal neurons: dendritic structure and synaptic integration. Nat Rev Neurosci *9*, 206-221.

Steward, O., and Schuman, E.M. (2001). Protein synthesis at synaptic sites on dendrites. Annu Rev Neurosci *24*, 299-325.

Takahashi, N., Kitamura, K., Matsuo, N., Mayford, M., Kano, M., Matsuki, N., and Ikegaya, Y. (2012). Locally synchronized synaptic inputs. Science *335*, 353-356.

Toni, N., Buchs, P.A., Nikonenko, I., Bron, C.R., and Muller, D. (1999). LTP promotes formation of multiple spine synapses between a single axon terminal and a dendrite. Nature *402*, 421-425.

Trachtenberg, J.T., Chen, B.E., Knott, G.W., Feng, G., Sanes, J.R., Welker, E., and Svoboda, K. (2002). Long-term in vivo imaging of experience-dependent synaptic plasticity in adult cortex. Nature *420*, 788-794.

Vann, S.D., Aggleton, J.P., and Maguire, E.A. (2009). What does the retrosplenial cortex do? Nat Rev Neurosci *10*, 792-802.

Varga, Z., Jia, H., Sakmann, B., and Konnerth, A. (2011). Dendritic coding of multiple sensory inputs in single cortical neurons in vivo. Proc Natl Acad Sci U S A *108*, 15420-15425.

Wilms, C.D., and Hausser, M. (2015). Reading out a spatiotemporal population code by imaging neighbouring parallel fibre axons in vivo. Nat Commun *6*, 6464.

Wilson, D.E., Whitney, D.E., Scholl, B., and Fitzpatrick, D. (2016). Orientation selectivity and the functional clustering of synaptic inputs in primary visual cortex. Nat Neurosci *19*, 1003-1009.

Xu, T., Yu, X., Perlik, A.J., Tobin, W.F., Zweig, J.A., Tennant, K., Jones, T., and Zuo, Y. (2009). Rapid formation and selective stabilization of synapses for enduring motor memories. Nature *462*, 915-919.

Yang, G., Pan, F., and Gan, W.B. (2009). Stably maintained dendritic spines are associated with lifelong memories. Nature *462*, 920-924.

Yang, Y., Liu, D.Q., Huang, W., Deng, J., Sun, Y., Zuo, Y., and Poo, M.M. (2016). Selective synaptic remodeling of amygdalocortical connections associated with fear memory. Nat Neurosci *19*, 1348-1355.

Zhao, M.G., Toyoda, H., Ko, S.W., Ding, H.K., Wu, L.J., and Zhuo, M. (2005). Deficits in trace fear memory and long-term potentiation in a mouse model for fragile X syndrome. J Neurosci *25*, 7385-7392.

Zhou, M., Greenhill, S., Huang, S., Silva, T.K., Sano, Y., Wu, S., Cai, Y., Nagaoka, Y., Sehgal, M., Cai, D.J., *et al.* (2016). CCR5 is a suppressor for cortical plasticity and hippocampal learning and memory. Elife *5*.

Zhou, Y., Won, J., Karlsson, M.G., Zhou, M., Rogerson, T., Balaji, J., Neve, R., Poirazi, P., and Silva, A.J. (2009). CREB regulates excitability and the allocation of memory to subsets of neurons in the amygdala. Nat Neurosci *12*, 1438-1443.